

1
ESL-TR-88-28

AD-A203 461

IONIC PRECURSORS OF SOOT — A COMBINED EXPERIMENTAL-THEORETICAL APPROACH

J. EYLER, M. ZERNER, F. WISEMAN

UNIVERSITY OF FLORIDA
CHEMISTRY AND PHYSICS DEPARTMENTS
GAINESVILLE, FL 32611

JUNE 1988

FINAL REPORT

NOVEMBER 1985 — SEPTEMBER 1987



APPROVED FOR PUBLIC RELEASE: DISTRIBUTION UNLIMITED



ENGINEERING & SERVICES LABORATORY
AIR FORCE ENGINEERING & SERVICES CENTER
TYNDALL AIR FORCE BASE, FLORIDA 32403

89 3 31 071

NOTICE

PLEASE DO NOT REQUEST COPIES OF THIS REPORT FROM
HQ AFESC/RD (ENGINEERING AND SERVICES LABORATORY),
ADDITIONAL COPIES MAY BE PURCHASED FROM:

NATIONAL TECHNICAL INFORMATION SERVICE
5285 PORT ROYAL ROAD
SPRINGFIELD, VIRGINIA 22161

FEDERAL GOVERNMENT AGENCIES AND THEIR CONTRACTORS
REGISTERED WITH DEFENSE TECHNICAL INFORMATION CENTER
SHOULD DIRECT REQUESTS FOR COPIES OF THIS REPORT TO:

DEFENSE TECHNICAL INFORMATION CENTER
CAMERON STATION
ALEXANDRIA, VIRGINIA 22314

REPORT DOCUMENTATION PAGE												
1a. REPORT SECURITY CLASSIFICATION Unclassified		1b. RESTRICTIVE MARKINGS										
2a. SECURITY CLASSIFICATION AUTHORITY		3. DISTRIBUTION/AVAILABILITY OF REPORT Approved for Public Release Distribution Unlimited										
2b. DECLASSIFICATION / DOWNGRADING SCHEDULE												
4. PERFORMING ORGANIZATION REPORT NUMBER(S)		5. MONITORING ORGANIZATION REPORT NUMBER(S) ESL-TR-88-28										
6a. NAME OF PERFORMING ORGANIZATION Chemistry and Physics Departments	6b. OFFICE SYMBOL (If applicable)	7a. NAME OF MONITORING ORGANIZATION Air Force Engineering and Services Center										
6c. ADDRESS (City, State, and ZIP Code) University of Florida Gainesville FL 32611		7b. ADDRESS (City, State, and ZIP Code) HQ AFESC/RDVS Tyndall AFB FL 32403-6001										
8a. NAME OF FUNDING/SPONSORING ORGANIZATION AEESC	8b. OFFICE SYMBOL (If applicable) RDV	9. PROCUREMENT INSTRUMENT IDENTIFICATION NUMBER FO8635-83-C-0136										
8c. ADDRESS (City, State, and ZIP Code) HQ AFESC/RDVS Tyndall AFB FL 32403-6001		10. SOURCE OF FUNDING NUMBERS										
		PROGRAM ELEMENT NO. 6.1	PROJECT NO. 0100									
		TASK NO. 8315	WORK UNIT ACCESSION NO.									
11. TITLE (Include Security Classification) Ionic Precursors of Soot - A Combined Experimental-Theoretical Approach Unclassified												
12. PERSONAL AUTHOR(S) John Eyler, Mike Zerner, and Floyd Wiseman												
13a. TYPE OF REPORT Final	13b. TIME COVERED FROM Nov 85 TO Sep 87	14. DATE OF REPORT (Year, Month, Day) 88 June	15. PAGE COUNT									
16. SUPPLEMENTARY NOTATION Availability of this report is specified on reverse of front cover												
17. COSATI CODES <table border="1"><tr><th>FIELD</th><th>GROUP</th><th>SUB-GROUP</th></tr><tr><td>21</td><td>02</td><td></td></tr><tr><td></td><td></td><td></td></tr></table>	FIELD	GROUP	SUB-GROUP	21	02					18. SUBJECT TERMS (Continue on reverse if necessary and identify by block number) Cyclopropenylum Cation Acetylene Propargylum Cation Diacetylene Encounter Complex Kinetic Modeling		
FIELD	GROUP	SUB-GROUP										
21	02											
19. ABSTRACT (Continue on reverse if necessary and identify by block number) Results of quantum mechanical calculations and ion cyclotron resonance mass spectrometric (ICRMS) studies on hydrocarbon cations proposed to be important mechanistic precursors of soot particles in flames are presented in this technical report. Of these cations, $C_3H_3^+$ is the most abundant in sooting flames. Quantum mechanical calculations give relative energy levels of the various isomers of the cations, energy barriers for certain important reactions, and ultraviolet and infrared spectral lines for some of the isomers. Experimental studies using ICRMS yield data on the rates of reactions of some of these hydrocarbon cations with certain neutral molecules, particularly acetylene (C_2H_2) and diacetylene (C_4H_2) which are both found in sooting flames.												
Quantum mechanical energy calculations show the two most stable isomers of $C_3H_3^+$ to be a cyclic form and a linear form, which is calculated to be 27.7 kcal·mol ⁻¹ higher in energy than the cyclic form. Calculations show												
20. DISTRIBUTION/AVAILABILITY OF ABSTRACT <input checked="" type="checkbox"/> UNCLASSIFIED/UNLIMITED <input type="checkbox"/> SAME AS RPT. <input type="checkbox"/> DTIC USERS		21. ABSTRACT SECURITY CLASSIFICATION Unclassified										
22a. NAME OF RESPONSIBLE INDIVIDUAL Capt Floyd L. Wiseman		22b. TELEPHONE (Include Area Code) (904) 283-4234	22c. OFFICE SYMBOL HQ AFESC/RDVS									

UNCLASSIFIED
SECURITY CLASSIFICATION OF THIS PAGE

the linear form reacts with C_2H_2 , but the cyclic form is unreactive. Calculations also show that the energy barrier to intramolecular conversion from the linear to the cyclic form is prohibitively high. The linear form can react with C_2H_2 to yield four possible isomers of $C_5H_5^+$.

The section on theoretical studies, which includes results of quantum mechanical calculations, also presents a new algorithm for the geometry optimization searches. The algorithm is designed to reduce the number of iterations required to find the lowest-energy geometry for a stable molecule and for transition-state structures in chemical reactions. This algorithm is used in the energy calculations presented in this report.

Quantum mechanical calculations to determine ultraviolet and infrared spectral line positions are presented for some isomers. These calculations, were done to determine which laser frequencies are required to fragment the various isomers. Laser studies to determine which isomers might be present, using the results of these calculations, were done. However, these studies did not successfully determine which isomers of the various cations were present in the ICR reaction chamber.

ICRMS studies reveal that linear $C_3H_3^+$ reacts with C_4H_2 to yield higher molecular weight cations, but $C_3H_3^+$ and C_2H_2 do not react to yield detectable levels of higher molecular weight cations. However, linear $C_3H_3^+$ does isomerize to cyclic $C_3H_3^+$ and in the presence of C_2D_2 yields an isotopic mixture of cyclic $C_3H_3^+$. Therefore, some isomer of $C_5H_5^+$ is forming, but apparently falls apart rapidly. The reaction of $C_3H_3^+$ and C_4H_2 leads to the formation of $C_5H_3^+$, $C_7H_3^+$, $C_9H_5^+$, and $C_{11}H_5^+$, all of which are detected in the reaction chamber.

Kinetic models presented in the report show the mechanistic possibilities for the reactions of linear $C_3H_3^+$ with C_2H_2 , C_2D_2 and C_4H_2 . The model which best fits the data for the reaction of linear $C_3H_3^+$ with C_2D_2 incorporates a kinetic isotope effect factor. This factor indicates there is some bonding rearrangement in the transition-state structure leading to the formation of $C_5H_5^+$. The model which best fits the data for the reaction of linear $C_3H_3^+$ with C_4H_2 incorporates collision-induced stabilization steps for the $C_9H_5^+$ and $C_{11}H_5^+$ cations. These are the only two cations in the scheme showing a build-up in concentrations not followed by an attenuation.

Reactions of C_2H_2 and C_4H_2 with $C_5H_3^+$, $C_5H_5^+$ and $C_7H_7^+$ cations formed from various neutral precursors were also studied as a part of this work. Reactions with C_4H_2 are generally faster than reactions with C_2H_2 . However, the degree of reactivity of the various cations depends upon what the neutral precursors are. Apparently, different proportions of the more reactive isomers are formed from different precursors. Threshold energy curves also lend support to this idea.

Studies presented in this report show that, at low pressures, cationic reactions with C_4H_2 are more important than reactions with C_2H_2 . However, at flame pressures, collision-induced stabilizations may make reactions with C_2H_2 more important.

UNCLASSIFIED
SECURITY CLASSIFICATION OF THIS PAGE

SUMMARY

An understanding of the mechanisms that cause soot formation in flames and other combustion environments could help to eliminate this formation and lead to more efficient fuel consumption, lower atmospheric pollution, and even eliminate plumes seeded through exhaust.

Two soot formation mechanisms have been postulated. One invokes the formation of small radicals, that further react with small hydrocarbons to form the larger particles that make up soot. A second mechanism involves the reaction of small positive ions with neutral hydrocarbons, again leading to soot through condensation and condensation/elimination reactions. This mechanism is postulated due to the observation of high concentrations of $C_3H_3^+$ ions in sooting flames and the precursors of this mechanism have been examined in the work reported here.

The small hydrocarbon ions found in sooting flames have been created in a Fourier Transform Ion Cyclotron Resonance (FTICR) mass spectrometer, and the formation of larger hydrocarbon ions has been examined in a fashion more systematic than can be obtained in flames themselves. It is found that there are at least two forms of $C_3H_3^+$ that might be present in sooting environments, and that one of these forms, probably the cyclic isomer, is not reactive toward either acetylene or diacetylene. Through deuterium exchange studies, at least one form, the linear propargylium cation, has been shown to react with acetylene, as well as diacetylene. Studies of the rates of these reactions have been undertaken to assess their role in actual sooting situations. Reactions of $C_5H_3^+$, $C_5H_5^+$, and $C_7H_7^+$ have also been studied under the terms of this contract, indicating the possible course sooting reactions might follow in the formation of larger molecules responsible for soot.

Quantum chemical methods have been developed for studying these molecules, and calculations have been performed on the lowest energy isomers of $C_3H_3^+$ and $C_5H_5^+$. Four stable structures of $C_3H_3^+$, and nine of $C_5H_5^+$ have been examined in detail, and predictions made of their vibrational and electronic spectra for possible identification in sooting flames and exhausts. Their identification would indeed lend credence to the ionic mechanism of soot

formation. Reactions between the isomers of $C_3H_3^+$ and acetylene have been examined theoretically, and it was found that the cyclic form does not react, whereas the linear form does. In addition, it was found that only one of the reactions between the propargyl ion and acetylene leads to a product thermodynamically stable relative to disproportionation back into the cyclic form of $C_3H_3^+$ and acetylene. These findings are in good agreement with those from the FTICR experiments, and have allowed the mechanisms that might be operative in soot formation to be modeled.

PREFACE

This report was prepared by the Departments of Chemistry and Physics at the University of Florida, Gainesville FL 32611. This work was sponsored by the Air Force Engineering and Services Center, Engineering and Services Laboratory (AFESC/RDVS), Tyndall Air Force Base, Florida 32403-6001.

This report summarizes work done between November 1985 and September 1987 under program element 61101F. AFESC/RDVS project officer was Captain Floyd L. Wiseman.

The authors wish to acknowledge the assistance and contributions of Dr Mehdi Moini and Mrs Feza Ozturk, who worked on this project during their time at the University of Florida.

This report has been reviewed by the Public Affairs Office (PA) and is releasable to the National Technical Information Service (NTIS). At NTIS, it will be available to the general public, including foreign nationals.

This technical report has been reviewed and is approved for publication.

FLOYD L. WISEMAN, Capt, USAF
Project Officer

KENNETH T. DENBLEYKER, Maj, USAF
Chief, Environmental Sciences Branch

THOMAS J. WALKER, Lt Col, USAF, BSC
Chief, Environics Division

LAWRENCE D. HOKANSON, Colonel, USAF
Director, Engineering and Services
Laboratory

Approved For	
NTIS GLAMI <input checked="" type="checkbox"/>	
DISC FTS <input type="checkbox"/>	
Unpublished <input type="checkbox"/>	
Justification _____	
By _____	
Distribution/ _____	
Availability Codes _____	
Dist	Avail and/or Special
A-1	



TABLE OF CONTENTS

Section	Title	Page
I	INTRODUCTION.....	1
	A. OBJECTIVE.....	1
	B. BACKGROUND.....	1
	C. SCOPE/APPROACH.....	7
II	THEORETICAL STUDIES.....	9
	A. INTRODUCTION.....	9
	B. A BROYDEN-FLETCHER-GOLDFARB-SHANNO OPTIMIZATION PROCEDURE FOR SEARCHING QUANTUM MECHANICAL SURFACES FOR MOLECULAR GEOMETRIES.....	10
	C. A SURVEY OF OPTIMIZATION PROCEDURES FOR STABLE STRUCTURES AND TRANSITION STATES.....	21
	D. STRUCTURES AND PROPERTIES OF $C_3H_3^+$ CATIONS.....	32
	E. REACTIONS OF ACETYLENE WITH ISOMERIC FORMS OF THE $C_3H_3^+$ IONS.....	51
	F. STRUCTURES AND PROPERTIES OF $C_5H_5^+$	64
III	EXPERIMENTAL STUDIES.....	81
	A. INTRODUCTION.....	81
	B. EXPERIMENTAL METHODS.....	81
	C. REACTIONS OF $C_3H_3^+$ WITH ACETYLENE AND DIACETYLENE.....	84
	D. REACTIONS OF $C_5H_5^+$ AND $C_5H_3^+$ IONS WITH ACETYLENE AND DIACETYLENE.....	98
	E. REACTIONS OF GASEOUS $C_7H_7^+$ IONS.....	115
IV	KINETIC MODELING OF THE REACTIONS OF $C_3H_3^+$ WITH ACETYLENE, DEUTEROACETYLENE AND DIACETYLENE.....	134
	A. INTRODUCTION.....	134
	B. METHODOLOGY.....	134
	C. THEORY.....	135
	D. RESULTS.....	136
	E. DISCUSSION.....	151

TABLE OF CONTENTS
(CONCLUDED)

Section	Title	Page
V	CONCLUSION AND RECOMMENDATIONS.....	156
	A. CONCLUSIONS.....	156
	B. RECOMMENDATIONS.....	156
	REFERENCES.....	158
	APPENDIX.....	167
	A. FOOTNOTES.....	167
	B. ANALYTICAL EXPRESSIONS FOR KINETIC MODELING.....	169

LIST OF FIGURES

Figure	Title	Page
1	The Calculated Transition State for the Opening of cis 1,2-bromofluorocyclopropane.....	33
2	Optimized Structure (6-31G*) of Cyclopropenylum Cation (I)...	35
3	Optimized Structure (6-31G*) of Propargylium Cation (II).....	38
4	Optimized Structure (6-31G*) of 1-Propynyl Cation (III).....	39
5	Optimized Structure (6-31G*) of Prop-2-en-yl-3-ylidene Cation (IV).....	40
6	Optimized Structure (6-31G*) of Cycloprop-1-yl-2-yliden Cation (V).....	41
7	The Cyclopropenylum Cation.....	53
8	The Propargylium Cation.....	54
9	An Encounter Complex Formed in the Association of C_2H_2 with the Cyclic Form of $C_3H_3^+$	55
10	An Encounter Complex Formed in the Association of C_2H_2 with the Cyclic Form of $C_3H_3^+$	56
11	An Encounter Complex Formed in the Association of C_2H_2 with the Cyclic Form of $C_3H_3^+$	57
12	Four Starting Geometries for the Reaction of Propargylium Cation with Acetylene.....	59
13	A Study of One of the Reactions between Acetylene and the Propargylium Cation.....	60

LIST OF FIGURES

(CONTINUED)

Figure	Title	Page
14	The Final Structures that Result from the Four Initial Conditions as Shown in Figure 12.....	61
15	Structure I.....	67
16	Structure II.....	68
17	Structure III.....	69
18	Structure IV.....	70
19	Structure V.....	71
20	Structure VI.....	72
21	Structure VII.....	73
22	Structure VIII.....	74
23	Structure IX.....	75
24	Isomerization of Linear $C_3H_3^+$ Ions at Different Pressures of C_2H_2	90
25	Isotope Exchange Reactions of $C_3H_3^+$ with C_2D_2	91
26	$C_3H_3^+$ Ion Decay Curves for Reaction with C_3H_3I and C_2D_2	92
27	Reactions of $C_3H_3^+$ with C_4H_2	94
28	$C_3H_3^+$ Decay Curves for the Reactions with C_3H_3I and C_4H_2	95

LIST OF FIGURES

(CONTINUED)

Figure	Title	Page
29	Reactions of $C_5H_3^+$ with C_4H_2 . $C_5H_3^+(\square)$, $C_7H_3^+(+)$, $C_9H_5^+(\diamond)$ and $C_{11}H_5^+(\Delta)$	102
30	$C_5H_5^+$ Ion Decay Curves for Reactions with Cyclo- heptatriene(\square), Cycloheptatriene and Acetylene(+), and Cycloheptatriene and Diacetylene(Δ).....	104
31	$C_5H_5^+$ Ion Decay Curves for Reactions with 1-Penten- 3-yne(\square), 1-Penten-3-yne and Acetylene(+), and 1-Penten-3-yne and Diacetylene(\diamond).....	105
32	Relative Intensities of $C_7H_8^+(+)$ and $C_7H_7^+(\square)$ Ions Produced from Cycloheptatriene as a Function of Electron Impact Energy.....	107
33	Relative Intensities of $C_7H_8^+(+)$ and $C_7H_7^+(\square)$ Ions Produced from Norbornadiene as a Function of Electron Impact Energy.....	108
34	Relative Intensities of $C_5H_6^+(\diamond)$, $C_5H_5^+(+)$, and $C_3H_3^+(\square)$ Ions Produced from Cycloheptatriene as a Function of Electron Impact Energy.....	109
35	Relative Intensities of $C_5H_6^+(\diamond)$, $C_5H_5^+(+)$, and $C_3H_3^+(\square)$ Ions Produced from Norbornadiene as a Function of Electron Impact Energy.....	110
36	Reaction of $C_7H_7^+$ Produced from Toluene by Kr^+ Charge Transfer with its Precursor Neutral.....	118
37	Reaction of $C_7H_7^+$ Produced from Norbornadiene by Xe^+ Charge Transfer with its Precursor Neutral.....	119

LIST OF FIGURES

(CONCLUDED)

Figure	Title	Page
38	Reaction of $C_7H_7^+$ Produced from Cycloheptatriene by Xe^+ Charge Transfer with its Precursor Neutral.....	120
39	Reactions of $C_7H_2^+$ Produced from Toluene by Kr^+ Charge Transfer with Diacetylene.....	125
40	$C_5H_5^+$ and $C_3H_3^+$ Ion Abundances as a Function of Electron Energy.....	127
41	Plot of θ versus $P_{C_2H_2}$ (Equation (122)), Showing Best Fit Line.....	138
42	Model Fit (scheme (123)) to Typical Data Set for $C_3H_3^+$ + C_2D_2 Reactions.....	141
43	A Schematic Diagram of the Reaction of $\ell-C_3H_3^+$ with C_2H_2	144
44	Model Fit (scheme (124)) to Typical Data Set for $C_3H_3^+$ + C_2D_2 Reactions.....	148
45	Data from Ejection Studies ($C_3H_3^+$ + C_2D_2 reaction) and Model Prediction ($C_3HD_2^+$ ejected - A; $C_3H_2D^+$ ejected - B)....	149
46	Model Fit (scheme (125)) to a Typical Data Set for $C_3H_3^+$ + C_4H_2 Reactions.....	152

LIST OF TABLES

Table	Title	Page
1	SOME EXAMPLES COMPARING THE MS AND BFSG UPDATE SCHEMES.....	17
2	RANK 1 UPDATE OPTIMIZATION OF NH ₃ HESSIAN EIGENVALUES (A.U.).....	18
3	BFGS OPTIMIZATION OF NH ₃ HESSIAN EIGENVALUES (A.U.).....	20
4	A COMPARISON OF MS AND BFGS UPDATE METHODS FOR H ₃ CCHCHO.....	21
5	A SUMMARY OF SOME OPTIMIZATIONS.....	30
6	HCN TO CNH TRANSITION STATE SEARCH.....	31
7	CIS 1,2-BROMOFLUOROCYCLOPROPANE TRANSITION STATE SEARCH.....	31
8	RELATIVE STABILITIES OF C ₃ H ₃ ⁺ ISOMERS (A.U.).....	37
9	THE CALCULATED GEOMETRIES (A) OF THE CYCLOPROPYLIUM ION, I, FIGURE 2.....	42
10	THE CALCULATED GEOMETRIES OF THE PROPARGYLIUM ION, II, FIGURE 3.....	42
11	THE CALCULATED GEOMETRIES OF THE 1-PROPYNYL CATION, III, FIGURE 4.....	42
12	THE CALCULATED GEOMETRIES OF THE PROP-2-EN-1-YL-3-YLIDENE CATION, IV, FIGURE 5.....	43
13	THE CALCULATED GEOMETRIES OF THE CYCLOPRO-1-YL 2-YLIDINE CATION, V, FIGURE 6.....	43

LIST OF TABLES
(CONTINUED)

Table	Title	Page
14	CALCULATED VIBRATIONAL FREQUENCIES USING OPTIMIZED STRUCTURES AND WAVEFUNCTIONS.....	47
15	CALCULATED ELECTRONIC SPECTRA OF C_3H_3^+	49
16	THE CALCULATED ENERGIES OF THE REACTION PRODUCTS C_5H_5^+	62
17	CALCULATED VIBRATIONAL FREQUENCIES OF THE REACTION PRODUCTS USING 3-21G OPTIMIZED STRUCTURES AND WAVEFUNCTIONS.....	63
18	THE ENERGIES OF DIFFERENT TAUTOMERS OF C_5H_5^+ , IN HARTREES.....	66
19	CALCULATED VIBRATIONAL FREQUENCIES USING 3-21G OPTIMIZED STRUCTURES AND WAVEFUNCTIONS.....	78
20	CALCULATED ELECTRONIC SPECTRA, USING INDO-CI SPECTROSCOPIC METHOD FOR 6-31G* OPTIMISED GEOMETRIES (1000 cm^{-1}).....	79
21	PRODUCTION OF C_5H_5^+ AND C_5H_3^+ IONS IN MIXTURES OF VARIOUS NEUTRALS AND ACETYLENE.....	87
22	PERCENTAGES OF REACTIVE C_3H_3^+ FOUND FROM VARIOUS PRECURSORS BY VARIOUS IONIZATION TECHNIQUES (MONITORED BY OBSERVING REACTION WITH THE PRECURSOR NEUTRAL).....	88
23	PERCENTAGES OF REACTIVE C_3H_3^+ OBSERVED IN THE REACTION WITH C_4H_2	96
24	CHANGES IN C_3H_3^+ REACTIVITY AT DIFFERENT PRESSURES OF DIACETYLENE.....	96

LIST OF TABLES
(CONCLUDED)

Table	Title	Page
25	PERCENTAGES OF UNREACTIVE $C_5H_5^+$ FOUND FROM VARIOUS PRECURSORS BY CHARGE TRANSFER CHEMICAL IONIZATION MONITORED BY OBSERVING REACTION WITH THE PRECURSOR NEUTRAL.....	106
26	CHANGES IN ION ABUNDANCES AT TWO DIFFERENT IONIZATION ENERGIES FOR NORBORNADIENE.....	106
27	RATE COEFFICIENTS FOR THE REACTION OF $C_5H_5^+$ IONS FROM DIFFERENT PRECURSORS WITH DIACETYLENE.....	112
28	RATE COEFFICIENTS FOR THE REACTION OF $C_5H_5^+$ IONS PRODUCED FROM DIFFERENT PRECURSORS WITH ACETYLENE.....	112
29	PERCENTAGES OF UNREACTIVE $C_7H_7^+$ FOUND FROM VARIOUS PRECURSORS BY DIFFERENT IONIZATION METHODS MONITORED BY OBSERVING REACTION WITH THE PRECURSOR NEUTRAL.....	121
30	RATE COEFFICIENTS FOR DIFFERENT $C_7H_7^+/C_7H_7$ REACTION SYSTEMS.....	123
31	REACTION RATE COEFFICIENTS FOR $C_7H_7^+ + C_4H_2$ REACTION.....	124
32	RESULTS OF FITS OF EQUATION (121) TO KINETIC DATA FOR THE $C_3H_3^+ + C_2H_2$ REACTION.....	137
33	RESULTS OF MODEL FITS (SCHEMES (123) AND (124)) FOR THE SYSTEM $C_3H_3^+ + C_2D_2$ UNDER VARIOUS EXPERIMENTAL CONDITIONS.....	142
34	RESULTS OF MODEL FITS (SCHEME (124)) FOR THE SYSTEM $C_3H_3^+ + C_4H_2$ UNDER VARIOUS EXPERIMENTAL CONDITIONS.....	153

SECTION I

INTRODUCTION

A. OBJECTIVE

The purpose of this research was to provide information about the reactivities, structures, and spectra of gaseous ions. This information allowed an assessment of the proposed ionic mechanism of soot formation, in part, testing its validity when compared to various schemes which rely on free radical mechanisms. A detailed understanding of soot nucleation can guide soot abatement efforts in many combustion systems, leading to improved efficiency in burners and jet engines and to reduced particulate emissions (and thus lowered visibility and signatures) from various combustors.

B. BACKGROUND

1. Ions in Flames

It has long been known that significant concentrations of ions exist in flames. For many years their presence was considered a scientific curiosity. More recently the practical importance of flame ions has been recognized (1). The presence of high ionization levels in jet engine exhausts and rocket plumes can serve both to impede radio communication and to provide unwanted exhaust signatures. Intentionally seeded, conducting flames have a high potential for practical use in MHD reactors. Essentially all hydrocarbon flames are characterized by a predictable and constant level of ions; this fact forms the basis for the nearly universal hydrocarbon flame detector used in modern gas chromatography. There has been a controversy for many years involving the importance of ions in flames to soot formation. Almost equally compelling evidence has been given for the primary importance of radical-molecule reactions and for ion-molecule reactions in the condensation reactions which lead to nucleation and ultimately to soot formation (2).

For these and other reasons there has recently been rapid development years of techniques for the study of ions and electrons in high temperatures

environments. A variety of techniques have been employed. These include microwave absorption and phase shift techniques for measuring electron densities. For more sensitive point source measurements in the relatively thin flame zones Langmuir probes have been extensively used. Stark broadening has been used for measurements of ionization in seeded flames. These techniques are sensitive to local concentrations of charge but provide relatively little information concerning the nature of the ions or their formation or destruction mechanisms.

Combustion products present in flames all have relatively high ionization potentials. Therefore, the presence of high ion concentrations far exceeds that expected from thermochemical equilibrium. It is generally accepted that primary ions are created by chemi-ionization at a very thin reactive zone in flames, undergo extensive secondary reactions and ultimately evolve primarily to H_3O^+ , NO^+ and electrons in the burnt gas region.

At the present time the most sensitive probing of ion concentrations in flames is done with flame-ion mass spectrometers. In this technique microprobes are used to sample gases in the reactive zones of flames (2-10). Typically the pressure is reduced to expand the volume of the reactive zone as an aid in probing. Both positive and negative ion concentrations above 10^7 ions cm^{-3} have been characterized in this way in a variety of flames. A serious potential exists for sampling artifacts when using this technique because of catalyzed reactions in the hot sampling probe and in the mass spectrometer. These effects are discussed extensively by Hayhurst and Kittelson (6).

It is apparent from References 2-10 that positive ion concentrations in flames are significant, with C_3H_3^+ and H_3O^+ reaching concentrations near 10^{10} ions $\cdot\text{cm}^{-3}$ in two torr flames. Concentrations of negative ions are believed to be on the order of 100 times lower, with electrons contributing the remainder of the negative charge required for overall neutrality.

Positive ion concentrations are relatively insensitive to flame temperature (11). This is consistent with the nonthermochemical equilibrium nature of their production mechanism and reflects the probability that

secondary ions are generated from a small number of ionic precursors which are created by chemi-ionization. Studies of the concentration dependence of several positive ions upon fuel-oxidizer stoichiometry (4) give results which again are consistent with chemi-ionization production of one or two primary ions followed by a large number of ion-molecule reactions.

2. Possible Formation Mechanisms

It is generally agreed that primary ions in hydrocarbon flames arise from chemi-ionization rather than from pyrolysis although evidence for a pyrolysis origin continues to surface (5). A score of different chemi-ionization reactions have been proposed and investigated for hydrocarbon flames (2) as potential primary ion formation mechanisms. Most workers are currently in agreement that two radical-molecule reactions are dominantly responsible for creation of primary ions:



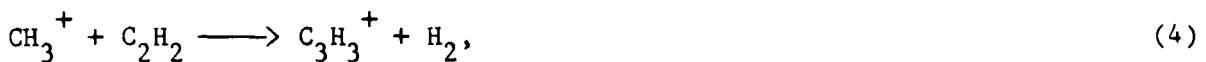
Contrary to what is reported in the older literature, Reaction (1) is currently thought to be slightly exoergic (7). This is consistent with the ion formation process being nearly temperature independent. Considerable controversy abounds concerning the rate of Reaction (1). Values range from 10^{-14} to $10^{-11} \text{ cm}^3 \cdot \text{molecule}^{-1} \cdot \text{sec}^{-1}$. The most recent careful measurement under flow tube conditions by Vinckier (12) gives a value of $k_1 = 2.4 \times 10^{-14} \text{ cm}^3 \cdot \text{molecule}^{-1} \cdot \text{sec}^{-1}$ at room temperature. It is generally concluded that the reaction may be a factor of ten faster at flame temperatures. The rather inefficient channel for ion formation competes with the reaction to produce neutrals:



In laser experiments Filseth (13), et al., have followed the total disappearance rate of $\text{CH}(\text{X}^2\Pi)$ and report a value for $k_3 = 8.8 \times 10^{-11}$

$\text{cm}^3 \cdot \text{molecule}^{-1} \cdot \text{sec}^{-1}$. It is apparent that the branching between Reactions (1) and (3) favors formation of neutrals by $10^3 - 10^4$.

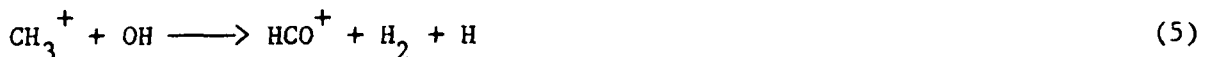
Reaction (2) is about 25 kcal/mole exothermic as written and would therefore be very endothermic for the reaction of ground state $\text{CH}(X^2\Pi)$ to produce C_3H_3^+ . Although the importance of Reaction (2) in flames has been questioned (2), it is currently the only chemi-ionization reaction seriously considered to be responsible for formation of C_3H_3^+ , which precedes the formation of HCO^+ in some flames and therefore is considered as a primary ion. In fact, it has been used as the primary ion formation mechanism in recent crude models of sooting flames (14) although the modelers admit to many unanswered questions about its importance. Of course, C_3H_3^+ can also be produced by secondary reactions, i.e.,



or more complicated schemes (7). C_3H_3^+ appears very early in all of Goodings and Bohme's (7) profiles and the concentration profiles do not show shoulders or secondary peaks.

3. Secondary Ions and Soot Formation

Goodings and Bohme (7) have mapped out a consistent flow picture for the formation of secondary ions in both fuel-rich and lean conditions for methane-oxygen flames. Large numbers of reactions involving HCO^+ with neutrals dominate, which create larger intermediate (usually oxygen containing) ions. The ultimate fate of most of these ions, particularly in fuel-lean conditions, involves formation of HCO^+ , e.g.



followed by conversion to H_3O^+ via the reaction



where the equilibrium lies to the right.

Certain secondary ion-molecule reactions in flames may be important in understanding soot formation. Studies by Prado and Howard (15) and by others (9,10) have demonstrated the presence of large hydrocarbon ions (probably polyaromatic) in sooting flames. Experiments involving the effects of ionic additives (16) and of electric fields (17) on the amount of soot produced in such flames also indirectly point to participation of ions in these processes. Whether these large ions are formed directly from smaller ions by ion-molecule reactions, or whether they are formed by charge, proton, or hydride transfer after large hydrocarbon neutrals have been formed remains unclear. In recent papers discussing ions in flames Hayhurst and Kittelson (6), without much discussion, conclude that the presence of ions like $C_3H_3^+$ and $C_4H_2^+$ indicates the presence of large uncharged hydrocarbon fragments in the burnt gas region. Goodings, Bohme, and Ng (7) argue that both neutral and ion-molecule condensation mechanisms may lead to the larger charged particles important in soot formation, but do not assess the relative importance of the two competing pathways. Bayes and co-workers (18) state rather unequivocally that "the rapid ionic polymerization of acetylene . . . is a probable initiator of soot formation in rich acetylene flames." In his Plenary Lecture (19) on "Soot Formation in Combustion", at the 17th International Combustion Symposium, H. G. Wagner considered the matter still unresolved: "the rapid growth of the large hydrocarbon molecules which are necessary intermediates of soot, indicated that their chemical growth must proceed via fast reactions. These can be either radical reactions or ion reactions, or a combination."

Recent investigations of fuel-rich and sooting ethylene (20), acetylene (9,10,20), and benzene (10) flames have provided evidence which further fuels the ionic versus neutral soot formation controversy. Delfau, Michaud, and Barassin (20) found evidence for two independent ionization regions in fuel-rich ethylene and acetylene flames, the first corresponding to small chemi-ions, and the second to larger ions at the early stages of soot formation. They argue that the large ions can be formed by direct thermoionization of heavy hydrocarbon molecules and young soot particles, which are formed by neutral, and not ionic mechanisms. They further believe that the concentration of high mass ions is too large to be accounted for by an ion-

molecule pathway from the relatively low concentrations of small chemi-ions they observe. The same workers (9) have observed $C_3H_3^+$, $C_5H_3^+$, $C_7H_3^+$, $C_7H_7^+$, $C_9H_3^+$, and large polycyclic aromatic hydrocarbon (PCAH) ions in sooting, premixed acetylene low pressure flames, and have explained the $C_{2n+1}H_3^+$ ($n = 2$, 3, and 4) concentrations in terms of equilibria between these ions, the dominant $C_3H_3^+$ ion, and C_2H_2 and H_2 neutrals present in the flame.

Based on their own measurements (10) and a different interpretation of the above mentioned work, the group at Aerochem Research Laboratories has developed an ionic model for soot formation (14a,b). They also see $C_3H_3^+$ as a major ion in sooting flames, plus relatively high concentrations of $C_5H_3^+$, $C_7H_5^+$, $C_7H_7^+$, $C_{12}H_9^+$, $C_{13}H_9^+$, $C_{15}H_{11}^+$, and $C_{19}H_{11}^+$ ions. They argue for sequential ion-molecule reactions involving the smaller ions and neutrals such as the C_2H_2 fuel as well as C_4H_2 and other carbon rich, hydrogen poor species formed in relatively high abundance in the flame. Even with assumed ion molecule reaction rates of only $2 \times 10^{-11} \text{ cm}^3 \cdot \text{s}^{-1}$ for all relevant reactions, their admittedly crude and incomplete model shows that adequate concentrations of large ions which may be direct soot precursors, as well as reasonable levels of neutrals formed by ion neutralization, can be predicted. However, they repeatedly stress the inadequacy of the input data such as ion-molecule reaction rates, ion structures, and ion thermochemistry used in their model.

4. Recent Developments in Neutral Soot Formation Mechanisms

One of the strongest arguments for an ionic soot nucleation mechanism has been that it is difficult in any of the proposed neutral schemes to produce small cyclic and polycyclic species with a sufficiently high rate to model the quite rapid soot formation seen in flames (14b). Ion/molecule reactions are known to proceed quite rapidly, and to yield cyclic products if those structures are the most stable. Thus ion/molecule reactions seem almost necessary in the early stages of soot nucleation. Recently, however, a neutral/radical soot formation model has been proposed which contains many steps and incorporates quite recently obtained shock tube kinetic data (21). This model is capable of yielding small ring compounds at a higher rate than previously suggested radical mechanisms, although there is some question as to the correct rate constant for one or two of the crucial steps in formation of

the first ring. In comparing an ionic model with this radical scheme, it is quite important to be able to know where the first ionic ring compound is formed. Is a five-membered ring formed as one of the $C_5H_5^+$ isomers, or must the system progress to the C_7 or C_9 size in order to form six-membered or larger rings? One recommendation of a recent workshop on mechanisms of soot formation (22) was that improved data for hydrocarbon ion reactions and structures be obtained so that a more complete ion/molecule model might be developed and compared with the latest neutral/free radical model.

C. SCOPE/APPROACH

This project involved combined experimental and theoretical study of possible ionic precursors of soot in hydrocarbon combustion systems. The reactivities, structures, and spectra of a number of small hydrocarbon ions which have been postulated as important in soot formation were investigated. The ions studied have all been observed in fuel-rich and sooting flames and included $C_3H_3^+$, $C_5H_3^+$, $C_5H_5^+$ and $C_7H_7^+$.

Experimental studies were carried out using Fourier Transform Ion Cyclotron Resonance Mass Spectrometry, and concentrated on kinetic and spectroscopic characterization of the gaseous ions. Rate coefficients for ion/molecule reactions of the ions listed above with a range of neutral molecules found in flames were determined. Measurements were generally made at quite low pressures and near room temperature, but temperatures up to ca. 550 K and pressures up to ca. 5×10^{-5} torr were also investigated. Electronic spectra for $C_5H_5^+$ ions were probed by laser photodissociation techniques, using a Nd:YAG pumped dye laser.

Theoretical studies were carried out by Dr. Zerner and his research group using facilities of the University of Florida Quantum Theory Project. These included a VAX 11/780 computer, a SUN System composed of 3/50 work stations and 3/280 File and Compute servers, and a variety of resident programs for calculating energetics and spectra of chemical species, including gaseous ions. Supercomputer facilities at Florida State University and the University of Pittsburgh were also used. The energies and properties of several isomers of $C_3H_3^+$ and $C_5H_5^+$ were calculated at successively higher levels of

sophistication, and reactivity of $C_3H_3^+$ with C_2H_2 was also followed theoretically. Spectra of the $C_3H_3^+$ and $C_5H_5^+$ ions in both the IR and UV-VIS regions were predicted.

SECTION II

THEORETICAL STUDIES

A. INTRODUCTION

Theoretical studies were performed on the possible precursors of soot and the elementary reactions between small carbocations and acetylene. Quantum mechanical methods of the semiempirical and ab initio types were used, and these are described in some detail in the sections that follow.

In the early stages of this study it was realized that truly effective ways of calculating molecular geometry from an initial configuration of atomic positions and the number of electrons were not available. Methods were designed to accomplish this under the terms of this contract, and these methods are now in widespread use by many groups as a result of our findings. The first two subsections of this section deal with the methods that we have uncovered. They are basically reprints of papers published in part, or in toto. A review paper has also been written on this subject by John Head and Michael Zerner and will soon appear in the *Advances in Quantum Chemistry* (Academic Press), a book which publishes only invited contributions.

Calculations for this contract were performed initially on the Quantum Theory Project's VAX 11/780, augmented with the 3-RA81 disk subsystem bought with funds for this work. As we discovered that only the ab-initio big basis set calculations were really reliable in predicting the relative energies of the species in which we were interested, some of these calculations were performed on the Pittsburgh Supercomputing Center facilities, and some through a separate grant for this purpose on the Florida State University Cyber 205. In addition, supplementary funds obtained during this contract allowed the purchase of a SUN 3/280 computing system, which was totally dedicated to these calculations during the final period of this contract. We had grossly underestimated the amount of computing resources that would be required to lead to definitive results in the relative stabilities of these systems, and to characterizing these systems with respect to their IR and UV-visible spectroscopy. By devoting supercomputer resources to this work, in addition

to the Quantum Theory Project's considerable resources, however, we have obtained state-of-the-art results, and have even shown (Section IIF) that many of our colleagues reporting on these structures in the past have been wrong.

As will be presented in section IIE, we have begun an examination of the actual reaction of acetylene with $C_3H_3^+$. Our results are in agreement with the FT-ICR experimental results presented in Section III. This work will carry on, even in the absence of further funding on this project, for we believe that such studies will lead to a clearer understanding of the possible role that these small carbocations have in the formation of soot particles. Other studies that should be undertaken involve the reactions of $C_3H_3^+$ with diacetylene, and of other small ions with both acetylene and diacetylene.

B. A BROYDEN-FLETCHER-GOLDFARB-SHANNO OPTIMIZATION PROCEDURE FOR SEARCHING QUANTUM MECHANICAL SURFACES FOR MOLECULAR GEOMETRIES

1. Introduction

The use of molecular quantum mechanics to obtain molecular geometry has become reasonably widespread. The structures of molecules as yet unmade and of excited state of molecules present few additional problems. Transition states that can only be inferred from experiments are somewhat more difficult to obtain but utilize the same general techniques.

The most common techniques used to search a molecular energy hypersurface obtained either through semi-empirical or ab initio quantum mechanics require analytic first derivatives of the energy with respect to coordinate displacement, and then proceed to build up curvature information on the surface as they move along it. The most common of these methods used are of the Murtagh Sarrent (MS) (23) type first introduced into quantum chemistry by McIver and Komornicki (24). For small molecules, this method has proven quite successful. For larger molecules, gradients are generally reduced to below 10^{-2} Hartree/Bohr with reasonable efficiency, but a further monotonic decrease of the gradients to an acceptable value is quite slow. It is this reduction difficulty that has prompted us to reexamine the various update procedures that are available and to test their performance, especially with respect to the popular MS method. In

doing this we have found one method, a variant of the Broyden-Fletcher-Goldfarb-Shanno (BFGS) algorithm (25-29) is systematically superior, especially so for large molecules, and does proceed to reduce the gradients in a more or less monotonic fashion. We describe this method here and compare it with our version of the MS method. A more complete report on these methods as well as others we have examined is in progress (30).

2. Quasi-Newton Method

The energy $E(\underline{x}^k)$ and the gradient vector $\underline{g}(\underline{x}^k)$ are expanded in a Taylor series about \underline{x}^k yielding

$$E(\underline{x}^{k+1}) = E(\underline{x}^k) + \underline{g}^k \cdot \underline{s}^k + \frac{1}{2} \underline{s}^k \cdot \underline{H}^k \cdot \underline{s}^k + \dots \quad (7a)$$

$$\underline{g}^{k+1} \equiv \underline{g}(\underline{x}^k) + \underline{H}^k \cdot \underline{s}^k + \dots \quad (7b)$$

with

$$\underline{s}^k = \underline{x}^{k+1} - \underline{x}^k \quad (7c)$$

and where $\underline{H}^k = \underline{H}(\underline{x}^k)$ is the matrix of second derivatives, of the "Hessian" matrix. Extreme points, such as minima saddle points or maxima, are characterized by $\underline{g} = \underline{0}$. Assuming that $\underline{g}^{k+1} \sim \underline{0}$ for large enough k and truncating Eq. (7b) after the second term, yields the familiar Newton equation for the search direction, \underline{s}^k

$$\underline{s}^k = -\underline{H}^{-1} \underline{g}^k \quad (8)$$

For an exact \underline{H} , \underline{s}^k is said to be a true "Newton" step toward the extremum. A sequence of such steps determines a Newton procedure.

Since the calculation of \underline{H} either analytically or numerically is a process many times slower than that for obtaining the energy and gradients. Many methods can be used to approximate \underline{H} the most common of these are the quasi-Newton methods. Since most optimization algorithms repeatedly solve Eq. (8) for \underline{s}^k , the inverse Hessian is usually sought directly. An analogous development for the Hessian itself is easily developed.

The quasi-Newton methods relate the differences of gradients obtained at two different points on the potential energy hypersurface

$$\underline{\gamma}^k = \underline{g}^{k+1} - \underline{g}^k \quad (9)$$

to the differences in the coordinates

$$\underline{\delta}^k = \underline{\alpha}_S^k \underline{x}^k = \underline{x}^{k+1} - \underline{x}^k \quad (10)$$

which, for a quadratic function, should obey the relation

$$\underline{\gamma}^k = \underline{H} \underline{\delta}^k . \quad (11)$$

Quasi-Newton methods are constrained to obey the "Quasi-Newton" condition obtained from rearranging Eq. (11).

$$\underline{G}^{k+1} \underline{\gamma}^k = \underline{\delta}^k \quad (12a)$$

$$\underline{G}^{k+1} \sim (\underline{H}^{k+1})^{-1} \quad (12b)$$

The Murtagh-Sargent method is a Rank 1 method defined by

$$\underline{G}^{k+1} = \underline{G}^k \underline{\varepsilon}^k = \underline{G}^k + a|u\rangle\langle u| \quad (13)$$

where we have used the common Dirac notation and a is a simple scale factor.

Use of the Eq. (12a) yields

$$\underline{G}^k |\gamma^k\rangle + a|u\rangle\langle u|\gamma^k\rangle = |\delta^k\rangle \quad (14)$$

Choosing the constant a in Eq. (14) as $\langle u|\gamma^k\rangle^{-1}$ and substituting into Eq. (13) yields the update equation (25-28)

$$\underline{G}^{k+1} = \underline{G}^k + \frac{(|\delta^k\rangle - \underline{G}^k |\gamma^k\rangle)(\langle \delta^k| - \langle \gamma^k|\underline{G}^k)}{\langle \gamma^k|\delta^k - \underline{G}^k \gamma^k\rangle} \quad (15)$$

that forms the basis of all Rank 1 methods.

The BFGS method is a Rank 2 method

$$\underline{G}^{k+1} = \underline{G}^k + a|u\rangle\langle u| + b|v\rangle\langle v| \quad (16)$$

Various choices of $|u\rangle$ and $|v\rangle$ and of a and b distinguish these methods. The

BFGS choice (29) leads to

$$\begin{aligned} \underline{G}_{\text{BFGS}}^{k+1} = & \underline{G}^k + \frac{(\langle \delta^k | \gamma^k \rangle + \langle \gamma^k | \underline{G}^k | \gamma^k \rangle) |\delta^k\rangle \langle \delta^k|}{|\langle \delta^k | \gamma^k \rangle|^2} \\ & - \frac{|\delta^k\rangle \langle \gamma^k | \underline{G}^k + \underline{G}^k | \gamma^k \rangle \langle \delta^k|}{\langle \delta^k | \gamma^k \rangle} \end{aligned} \quad (17)$$

If cartesian coordinates are used, \underline{G}^1 is usually set to the unit matrix,¹. The first step, \underline{s}^1 , is then in the direction of steepest descent. Subsequent cycles update \underline{G} toward greater accuracy as they move along the surface.

The Rank 1 formula has two principal disadvantages. The positive definiteness of \underline{G}^k may be lost on updating. Secondly, the denominator of Eq. (15) may approach zero sufficiently rapidly as to lead to numerical inaccuracy. Murtagh and Sargent have devised simple methods to detect these problems. There seems to be no really successful solution to either of these problems when they do occur, however, and the inverse Hessian matrix is reset to the unit matrix.

In contrast, the BFGS formula ensures that the Hessian remains positive definite on all updates. A positive definite Hessian is desirable because it always generates a search direction \underline{s}^k , given by Eq. (18) below, which is in the direction of energy decrease. The BFGS formula can even be advantageous over the exact Hessian \underline{H} in regions where the exact Hessian has negative eigenvalues. A search direction will have uphill steps along any normal mode of the molecule which has a negative eigenvalue.

3. Line Searches

With \underline{G}^k updated from either the MS or BFGS formula, a search direction, \underline{s}^k , is determined by

$$\underline{s}^k = -\underline{G}^k \underline{g}^k \quad (18)$$

A line search is then performed to determine how far along this direction a step, $\underline{\delta}^k$, should proceed.

$$\underline{x}^{k+1} = \underline{x}^k + \alpha^k \underline{s}^k \quad (19a)$$

$$\delta^k \equiv \alpha^k \underline{s}^k \quad (19b)$$

A weak line search requires only that $E^{k+1} < E^k$ if searching for a minimum. An exact line search finds that value of α^k for which $E(\underline{x}^k + \alpha^k \underline{s}^k)$ is a minimum. There is thus a competition between the number of energy evaluations that are required to minimize $E(\underline{x}^k + \alpha^k \underline{s}^k)$ along a given \underline{s}^k , or accepting nearly any move along \underline{s}^k that reduces the energy or the gradient norm and then finding a new direction \underline{s}^{k+1} at the new geometry.

We have adopted the following line search strategy (30). In the k -th line search cycle we examine the interval (α_1^k, α_2^k) of acceptable α^k values. Initially $\alpha_1^k = 0$ and α_2^k is determined by

$$|\alpha_2^k \underline{s}^k| \leq \Delta = 0.4 \text{ a.u.}, \quad (20)$$

a condition preventing arbitrarily large coordinate moves. The value of 0.4 a.u. is itself, of course, arbitrary, and larger values might be acceptable for larger molecules. The initial α^k value is set to 1 except for the first cycle where α^1 is set to 0.4. In this first cycle $G^1 = 1$ and the move is along the direction of steepest descent. The value $\alpha^1 = 0.04$ is empirical and nearly always satisfies the line search conditions even for poor starting geometries.

If the initial $\alpha^k > \alpha_2^k$ then α^k is reset to α_2^k . $E^{k+1} = E(\underline{x}^k + \alpha^k \underline{s}^k)$ is evaluated and

$$E^k - E^{k+1} \geq -\rho \alpha^k \langle \underline{s}^k | \underline{g}^k \rangle \quad (21)$$

checked. $\langle \underline{s}^k | \underline{g}^k \rangle$ is the first term in the Taylor series expansion for the energy and is negative for a decrease in energy. From Eq. (7) and Eq. (8) $0 \leq \rho \leq 1/2$, with $\rho = 1/2$ corresponding to an exact line search and any positive value simply leading to a decrease in energy. After considerable numerical testing, we choose $\rho = 0.01$ corresponding to a "weak" search. If this test fails, however, $\alpha^k > \alpha_2^k$ (true). $\alpha_2^k \rightarrow \alpha^k$ (α^k is "replaced" by) and α^k is reduced using the information already available according to

$$\alpha^k \rightarrow \alpha^k + \frac{1}{2}(\alpha^k - \alpha_1^k) \left[1 + \frac{E^k - E^{k+1}}{(\alpha^k - \alpha_1^k) E^1(\alpha_1^k)} \right]^{-1} \quad (22a)$$

$$E^1(\alpha_1^k) = g(x^k + \alpha_1^k s^k) + s^k = \left(\frac{\partial E}{\partial \alpha} \right)_{\alpha=\alpha_1^k} \quad (22b)$$

The energy $E^{k+1} \rightarrow E(x^k + \alpha^k s^k)$ is now computed and the right test of Eq. (21) repeated until the test is obeyed.

The gradient $\underline{g}^{k+1} = g(x^k + \alpha^k s^k)$ is now evaluated and a left extreme test applied

$$|\langle \underline{g}^{k+1} | s^k \rangle| \leq -\sigma \langle \underline{g}^k | s^k \rangle, \quad 0 \leq \sigma \leq 1 . \quad (23)$$

For an exact line search $\langle \underline{g}^{k+1} | s^k \rangle = 0$ (the gradient is perpendicular to the search direction) corresponding to $\sigma = 0$. The value $\sigma = 1$ only requires a reduction of the scalar product $\langle \underline{g}^{k+1} | s^k \rangle$. For the test of Eq. (23) we choose $\sigma = 0.9$, again corresponding to a weak line search. If the left test fails, however, α^k is too small, and a new value is estimated from

$$\alpha^k(\text{new}) = \alpha^k + \frac{(\alpha^k - \alpha_1^k) E^1(\alpha^k)}{E^1(\alpha_1^k) - E^1(\alpha^k)} \quad (24)$$

The energy $E^k \rightarrow E(x^k + \alpha^k(\text{new}) s^k)$ is evaluated and both right and left line test repeated with $\alpha_1^k \rightarrow \alpha^k$ and $\alpha^k \rightarrow \alpha^k(\text{new})$. When both tests have been successfully passed, the partial line search is finished and a new search direction is sought.

In the MS procedure the test for a positive definite Hessian may fail. If so \underline{G}^k is reset to the unit matrix and the line search is conducted as if this were once again the first cycle.

4. Optimization Algorithms

An initial geometry x_1 is chosen. E^1 and \underline{g}^1 are calculated. Then

- (i) A search direction s^k is chosen through Eq. (18). Then
- (ii) A line search is performed to determine how far along this direction to move as described in previous section. Then

- (iii) A test for convergence is made. If convergence is satisfactory, the procedure is complete. If not,
- (iv) Estimate a new Hessian or its inverse and repeat the procedure.

The success of a procedure is measured in the number of such cycles that are required to find the extreme point sought. The fewer energy evaluations, the better the method.

5. Results and Discussion

Table 1 summarizes results of geometry optimizations comparing the MS and BFGS methods. The notation $x(y,z)$ that we use indicates that x line searches, y energy evaluations and z gradient evaluations were required, starting with geometries ranging from quite good to very poor. An indication of the quality of the starting geometry is given by the maximum value of the gradient. Values greater than 0.1 Hartree/Bohr (1 Hartree = 627.5 kcal/mol) usually indicate one or more bond lengths are displaced by more than 0.1 Å. Two of the larger molecules of this study were not successfully optimized by the MS procedure. After fifty cycles, for example, the largest gradient of $[(\text{CH}_3)_2\text{P}(0)\text{O}]^-$ is still larger than 2×10^{-3} a.u./Bohr and that for CH_2CHCHO greater than 7×10^{-3} a.u./Bohr. The former case is difficult as the two methyl groups are rotating relative to one another in an eclipsed conformation along two very soft modes.

Table 2 shows how an optimization proceeds for the Rank 1 update using the line search described. Line 4 of the Hessian eigenvalues indicates that a negative eigenvalue of the Hessian has been detected. This negative eigenvalue

causes the step s^4 to go uphill on the energy surface even though $\langle g|s \rangle$ is negative. There are, as a consequence, repeated failures of the right extreme line search test Eq. (21) and after the eighth energy evaluation the line search terminates without a proper α value. At this stage another Hessian update is taken using the gradients evaluated at the coordinates \underline{x}^4 and \underline{x}^8 and fortunately the new Hessian generated is positive definite. In the remaining cycles the Hessian remains positive definite and the NH_3 geometry optimizes smoothly. We note that even after all gradients have been reduced below 10^{-4} a.u./Bohr, the approximate Hessian eigenvalues are still not accurate.

TABLE 1. SOME EXAMPLES COMPARING THE MS AND BFGS UPDATE SCHEMES.

	max g _i ^b	MS	BFGS
NH ₃ ^c	0.112	7(9,8)	7(8,8)
NH ₃ ^d	0.198	7(11,8)	7(8,8)
H ₂ O ₂	0.024	5(5,5)	6(6,6)
C ₂ H ₆	0.193	17(19,18)	19(20,20)
H ₂ CO	0.264	9(11,10)	11(12,12)
H ₂ CCHCHO	0.105	NO ^e	24(27,26)
[(CH ₃) ₂ P(O)O] ⁻	0.119	NO ^e	43(44,44)
Pyrimidine C ₄ N ₂ H ₄	0.127	11(14,13)	10(11,11)
[2,2'] para cyclophane C ₁₆ H ₁₆	0.050	16(20,18) ^f	10(11,11)

^aThe notation x(y,z) refers to x line searches, y energy evaluations and z gradient evaluations.

^bThe largest initial gradient in a.u./Bohr giving a measure of the "poorness" of the initial geometry. Convergence is assumed when $\max |g_i| < 10^{-4}$ a.u./Bohr, except for $[(CH_3)_2P(O)O]^-$, pyrimidine and [2,2'] paracyclophane where $\max |g_i| < 10^{-3}$ a.u./Bohr.

^cDisplaced 0.05 a.u. along each normal mode.

^dDisplaced 0.08 a.u. along each normal mode.

^eNot optimized after 50 energy evaluations.

^fFor paracyclophane $\max |g^k| < 10^{-3}$ a.u./Bohr at 14(16,15) but the subsequent cycle has an increase in gradient above this threshold even though the energy monotonically decreases.

TABLE 2. RANK 1 (MS) UPDATE OPTIMIZATION OF NH₃-HESSIAN EIGENVALUES (A.U.).

1	1.000D+00	1.000D+00	1.000D+00	1.000D+00	1.000D+00	1.000D+00
2	2.724D+00	1.000D+00	1.000D+00	1.000D+00	1.000D+00	1.000D+00
3	3.227D+00	2.714D+00	1.000D+00	1.000D+00	1.000D+00	1.000D+00
4	-2.354D-02	2.717D+00	1.802D+00	1.000D+00	1.000D+00	1.000D+00
8	2.719D+00	2.331D+00	1.458D+00	1.000D+00	1.000D+00	1.689D-01
9	2.587D+00	2.303D+00	1.456D+00	1.000D+00	9.994D-01	1.581D-01
10	2.370D+00	2.267D+00	1.438D+00	9.999D-01	9.862D-01	1.552D-01
11	2.359D+00	2.262D+00	1.435D+00	9.997D-01	5.302D-01	1.506D-01
Exact						
	2.2744D+00	2.2744D+00	1.4519D+00	1.5998D-01	1.5430D-01	1.5430D-01

Eval. No.		Energy	g	Max g ₁	a
E	G				
1	1	-12.499372	0.358164	0.198326	0.00000D+00
2	2	-12.521284	0.050917	0.031968	4.00000D-01
3	3	-12.522080	0.028010	0.017822	1.00000D+00
4	4	-12.522281	0.019552	0.012914	1.00000D+00
5		-12.476193			8.67976D-01
6		-12.520752			8.01833D-02
7		-12.522073			1.55110D-02 ~
8	5	-12.522235	0.020010	0.012987	3.67105D-03
9	6	-12.523207	0.004431	0.002909	1.00000D+00
10	7	-12.523216	0.000612	0.000343	1.00000D+00
11	8	-12.523216	0.000086	0.000049	1.00000D+00

The MS procedure would detect the negative eigenvalue at cycle 4 and reset the Hessian matrix to the unit matrix and $\alpha^4 = 0.4$. In spite of the loss of all previous Hessian information by the MS procedure, one less cycle is required to complete the optimization. In $\{(\text{CH}_3)_2\text{P}(0)\text{O}\}^-$ the Hessian is reset 17 times in 50 cycles, and there seems to be no more successful procedure for controlling the Rank 1 update than that suggested by Murtagh and Sargent. A somewhat more successful procedure of the MS type, however, does result by setting the right hand extreme, $\alpha_2 = 1$; that is, never permitting an α^k value greater than 1.

Table 3 examines this same situation for the BFGS method. As expected all the eigenvalues of the approximate Hessian remain positive on update, and the optimization proceeds rather smoothly. At the second cycle two eigenvalues of the Hessian are updated, a characteristic of the Rank 2 nature of this method, to be compared to the one value updated in the Rank 1 schemes. In spite of this, at convergence the Hessian eigenvalues obtained from the BFGS scheme are no better than those obtained from the MS procedure.

For larger molecules both the MS and the BFGS method seem equally able to reduce the gradients to below about 10^{-2} a.u./Bohr, usually corresponding to bond lengths to within ± 0.02 Å and bond angles $\pm 2^\circ$ - 3° of their final values. Dihedral angles, however, usually to do with soft torsional or umbrella-like modes, are not accurate with this level of convergence. The BFGS method is superior, as indicated in Table 4 for H_2CCHCHO . MS1 is the procedure described in this work. MS2 is a Murtagh Sargent procedure in which $\alpha_2 = 1$ briefly discussed above. This table is typical in showing the erratic behavior of the gradient norm $|g|$ with the cycling for the MS procedure. To cycle 10 the methods have reasonably similar behavior. However, after that, the BFGS method is clearly superior. At cycle 20 the BFGS method is 10^{-4} a.u. above the converged energy, whereas both MS algorithms are greater than 10^{-4} a.u. from energy convergence after 50 energy evaluations.

In summary, for small molecules, the MS and BFGS methods, as we have described them, have similar behavior. For all the larger molecules examined, those reported here and very many others, the BFGS method is superior. Both the MS and BFGS methods seem equally able to reduce the cartesian gradients to below 0.01 a.u./Bohr, but the MS method often has erratic behavior for larger systems after this point. The BFGS method nearly always reduces the gradient norm in a

TABLE 3. BFGS OPTIMIZATION OF NH₃-HESSIAN EIGENVALUES (A.U.).

1	1.000D+00	1.000D+00	1.000D+00	1.000D+00	1.000D+00	1.000D+00
2	2.723D+00	1.000D+00	1.000D+00	1.000D+00	1.000D+00	9.784D-01
3	3.719D+00	1.755D+00	1.000D+00	1.000D+00	1.000D+00	6.725D-01
4	2.836D+00	2.378D+00	1.032D+00	1.000D+00	1.000D+00	2.641D-01
5	2.785D+00	2.377D+00	1.527D+00	1.000D+00	1.000D+00	1.618D-01
6	2.577D+00	2.364D+00	1.514D+00	1.000D+00	9.994D-01	1.541D-01
7	2.423D+00	2.265D+00	1.476D+00	1.000D+00	9.952D-01	1.627D-01
9	2.434D+00	2.347D+00	1.472D+00	1.000D+00	9.254D-01	1.586D-01

Exact

2.2744D+00	2.2744D+00	1.4519D+00	1.5998D-01	1.5430D-01	1.5430D-01
------------	------------	------------	------------	------------	------------

Eval. No.

E	G	Energy	g	Max g ₁	α
1	1	-12.499372	0.358164	0.198326	0.00000D+00
2	2	-12.521284	0.050917	0.031968	4.00000D-01
3	3	-12.522072	0.028891	0.018206	1.00000D+00
4	4	-12.522491	0.019688	0.015225	1.00000D+00
5	5	-12.523027	0.016294	0.010447	1.00000D+00
6	6	-12.523199	0.007948	0.005281	1.00000D+00
7	7	-12.523215	0.000941	0.000621	1.00000D+00
8	8	-12.523216	0.000101	0.000059	1.00000D+00

TABLE 4. A COMPARISON OF MS AND BFGS UPDATE METHODS FOR H₃CCHCHO^a.

Cycle	MS1		MS2		BFGS ^b	
	ΔE	$ g $	ΔE	$ g $	ΔE	$ g $
1	0.0123	0.195	0.0123	0.195	0.0123	0.195
5	2.6D-3	0.058	2.8D-3	0.029	5.0D-3	0.028
10	1.3D-3	0.012	1.3D-3	9.9D-3	2.8D-3	0.013
20	5.3D-4	0.024	4.6D-4	6.6D-3	1.0D-4	4.0D-3
30	2.7D-4	1.7D-3	3.7D-4	0.028	1.0D-7	2.6D-5
40	1.8D-4	1.2D-3	1.9D-4	3.4D-3		
50	1.3D-4	0.011	1.4D-4	2.4D-3		

^a ΔE in a.u. from the converged energy value, $|G| = \langle g | g \rangle^{1/2}$ in a.u./Bohr.

^b In 32 cycles the BFGS method has reduced $|g|$ to 2×10^{-6} a.u./Bohr.

monotonic fashion, whereas this is seldom the case for the MS method. Neither update method produces a reliable Hessian matrix when the maximum gradient has been reduced to 10^{-4} a.u./Bohr, a value at which the geometries are usually reliable. If a more detailed knowledge of the second derivatives is required, these derivatives must be evaluated analytically or through numerical differentiation of the first derivatives.

C. A SURVEY OF OPTIMIZATION PROCEDURES FOR STABLE STRUCTURES AND TRANSITION STATES

1. Introduction

Theoretical determination of molecular structure by both empirical and semiempirical methods is becoming a powerful tool for the chemist. Reliable structures for stable molecules can be calculated as well as geometries of

experimentally inaccessible species, such as transition states. Derivatives of the energy with respect to nuclear coordinates play an essential role in efficient optimization algorithms. This section surveys some of these optimization algorithms which are included in the QUIPU quantum chemistry package at the University of Florida². However, these optimization algorithms are also appropriate for any potential energy hypersurface regardless of the Hamiltonian used, providing the correct derivative expressions are available. There is now a large literature on energy derivatives and for recent reviews see references (31-34).

In all optimization methods examined here, the first derivative of the energy is needed. Second derivatives are also required for some of the schemes we discuss. To calculate the exact second derivative, however, is costly and time-consuming. If one is interested in vibrational frequencies, it is important to calculate the second derivative matrix exactly. However, for geometry optimizations, an inexact second derivative obtained by systematic approximations to the coupled perturbed Hartree-Fock equations is reliable enough for successful application of most algorithms (30).

The next section discusses three algorithms for determining stable geometries. The third section presents three methods for transition state optimizations. The final section gives some examples and comparisons of application of the methods.

2. Minimization Techniques

Determining the lowest point on a potential energy hypersurface is straightforward. One simply follows the decrease in energy until a local minimum is found with the gradient vector \mathbf{g} zero. Verifying that the surface is a local minimum is also straightforward. The analytical second derivative matrix can be computed at the appropriate point and tested for positive definiteness. Or, more simply, the geometry of a stationary point can be distorted to give another initial coordinate set for reoptimizing the geometry. This reoptimization should return to the same local minimum. A distortion which lowers the symmetry of the molecule will be the most effective test for a true local minimum. For full optimizations, where all the molecular coordinates are allowed to vary, there is no real advantage in using internal rather than

cartesian coordinates: if the procedure is carried out correctly the same number of optimization steps is required. For convenience, however, mass weighted coordinates are used and the lighter atoms move more than do heavier ones. Thus, the optimization follows a path more in accord with physical intuition.

Three minimization algorithms are described below. Each algorithm consists of two essential parts: (1) selecting a search direction, and (2) determining by a line search a step length to give an acceptable reduction in the energy. An exact line search finds the minimum of energy along the chosen direction; partial line searches are less demanding, and generally accept any reduction of the energy.

A compromise can be reached between exact line searches and accepting any reasonable reduction in energy, and then proceeding to estimate a new search direction. In general, we have found that exact line searches are seldom worth the extra energy calculation to obtain them (35).

a. Newton and Quasi-Newton Methods.

The Newton methods can be derived from the Taylor's series expression

$$g(x + \delta) = g(x) + G(x)\delta \quad (25)$$

where the minimum $g(x+\delta) = 0$ so that a search direction s is obtained as

$$\delta = as = -a(G^{-1}) g(x) \quad (26)$$

where G is either the exact second derivative (Hessian) matrix for the Newton method or some matrix approximating the second derivatives for the Quasi-Newton method. The parameter a is determined by a line search algorithm so that energy exhibits a reasonable reduction in value. Both the Newton and Quasi-Newton methods use the same line search algorithm, the details of which are given elsewhere (35). When the Hessian is positive definite the Newton method often shows quadratic convergence to a local minimum. Unfortunately the Newton method

requires explicit calculation of the second derivative matrix which require computational time comparable to N Hartree Fock Self-Consistent Field (SCF) calculations, where N is the size of the basis set used. Quasi-Newton methods, on the other hand, only depend on gradient information to reach the minimum. They use the gradients calculated at the different search geometries to build an approximate inverse second derivative matrix $H \sim (G^{-1})$. Using the "Quasi-Newton" conditions,

$$Y = g(x + \delta) - g(x) \quad (27a)$$

$$HY = \delta \quad (27b)$$

as a constraint to obtain

$$H(x + \delta) = H(x) + U \quad (27c)$$

The search direction s is then the matrix product

$$s = -H(x + \delta)g \quad (28)$$

Thus the approximate Hessian is updated at each cycle. An advantage to this is that a great deal of time is not spent evaluating an accurate second derivative matrix, which is useful only locally on the surface. Such detailed information is only useful during the course of an optimization about the local quadratic region. We have examined many such update formula (35) and find the most successful given by Broyden-Fletcher-Goldfarb-Shanno (BFGS) (25-28) as

$$\begin{aligned} H_{\text{BFGS}}^{k+1} &= H^k + \frac{(\langle \delta^k | Y^k \rangle + \langle Y^k | H^k | Y^k \rangle) | \delta^k \rangle \langle \delta^k |}{|\langle \delta^k | Y^k \rangle|^2} \\ &\quad - \frac{|\delta^k \rangle \langle Y^k | H^k + H^k | Y^k \rangle \langle \delta^k |}{\langle \delta^k | Y^k \rangle} \end{aligned} \quad (29)$$

We note from Eq. (28) a minimum is obtained, $s=0$ and $g=0$, providing $H(x + \delta)$ is reasonable. The inverse Hessian, H , need not be accurate. An important feature of the BFGS formula is that it retains positive definiteness on update if it is used with the appropriate line search algorithm. This positive definiteness feature implies that

$$\langle s | g \rangle = -\langle g | H | g \rangle < 0 \quad (30)$$

which is the condition for descent in energy. That is, the BFGS formula has the property of always providing a search direction towards the local minimum. This will happen even when the true Hessian is indefinite.

b. Augmented Hessian or Restricted Step Methods.

This algorithm is useful for obtaining minimum even when the exact second derivative is not available. The search direction s is found by a Newton-like expression

$$s = -(G - \lambda I)^{-1} g \quad (31)$$

where $\lambda < \lambda(\text{low})$, the lowest eigenvalue of G , ensures that the matrix $(G - \lambda I)$ is positive definite. This choice of λ forces the descent condition $\langle g | s \rangle < 0$ to be satisfied. The step length $|s|$ is a function of λ . A variety of algorithms, usually based on the extent of the quadratic nature of the potential energy hypersurface at the point of interest, exist for selecting the maximum allowed $|s|$.

In our implementation the step length is found by diagonalizing the "augmented Hessian"

$$\begin{pmatrix} G & \alpha g \\ \alpha g^T & 0 \end{pmatrix} \begin{pmatrix} v \\ \beta \end{pmatrix} = \lambda \begin{pmatrix} v \\ \beta \end{pmatrix} \quad (32a)$$

for the lowest eigenvalue λ and lowest normalized eigenvector $v^2 + \beta^2 = 1$. The form of the augmented Hessian automatically requires $\lambda < \lambda(\text{low})$. By expanding Eq. (32a) two new equations are obtained

$$Gv + \alpha \beta g = \lambda v \quad (32b)$$

$$\alpha \langle g | v \rangle = \lambda \beta \quad (32c)$$

Rearranging (32b) gives the step

$$s = \frac{v}{\alpha \beta} = -(G - \lambda I)^{-1} g \quad (33)$$

where α is a parameter which can be varied to give the required step lengths, β is defined by Eq. (32c) and I is the unit matrix. In the diagonalization one of the following three situations are obtained.

1. $\lambda < 0$ and $\beta = 0$. In this case $v = v(\text{low})$ is the eigenvector of G corresponding to the lowest eigenvalue. $\langle v(\text{low}) | g \rangle$ is zero and $\lambda = \lambda(\text{low})$. A displacement along $v(\text{low})$ will reduce the energy. Alternatively, if a displacement along $v(\text{low})$ is not desired, then $v(\text{low})$ is shifted to a higher eigenvalue by

$$G' = G + \lambda(\text{shift}) |v(\text{low})\rangle \langle v(\text{low})| \quad (34)$$

and the Augmented Hessian reformed.

2. $\lambda < 0$ and $\beta \approx 1$. G is now positive definite. The step will vary from Newton like for small λ to steepest descent for large λ . The step length will usually be inside the restricted region.
3. Intermediate between the two conditions is $\lambda < 0$ and $\beta \neq 0$. G has a negative eigenvalue but s given by Eq. (33) will give a reduction in energy along the negative eigenvector mode.

A great deal of thought has been given to choosing an effective λ for the restricted step algorithm of Eq. (33) (36-38), but we find the simple matrix diagonalization suggested by Eq. (32a) as good as any for finding minima.

c. Norm of Gradient Squared Methods

Here the sum σ of the squares of the gradient is minimized

$$\sigma = \langle g | g \rangle = \sum_i g_i^2 \quad (35)$$

This method can be applied to find any stationary point and will not necessarily find a local minimum with respect to the energy; rather the nearest stationary point is usually uncovered. Proceeding as before

$$D_j = \frac{d\sigma}{dx_j} = 2 \sum_i g_i \frac{dg_i}{dx_j} \quad (36a)$$

$$D = 2Gg \quad (36b)$$

where D requires knowledge of the second derivative matrix G . Second derivatives of σ require third derivatives of the energy. To circumvent this requires a Newton-like selection of a search direction.

$$s = -G^{-1}g \quad (37)$$

where G is explicitly calculated or obtained by the BFGS formula, Eq. (29). In the line search algorithm we require

$$\sigma_{k+1} < \sigma_k \quad (38)$$

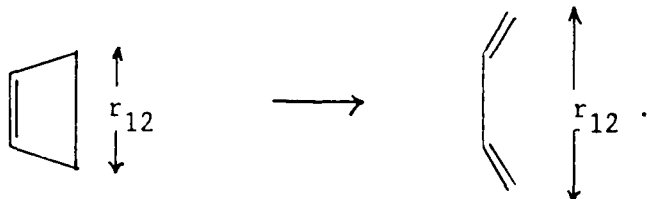
3. Transition State Search Algorithms

The determination of transition space structures is necessarily a more difficult problem relative to local minimum optimization. Here one attempts to find a maximum in the energy along the reaction direction and minima for all remaining directions. For a true transition state structure the second derivative matrix should have one and only one negative eigenvalue. The three algorithms are then documented.

a. Constrained Internal Coordinates

For unconstrained optimization most algorithms can be forced to be invariant to coordinate selection and, as mentioned, there is no advantage of using internal over cartesian coordinates. However, internal coordinates become a valuable tool in constrained optimizations. Internal coordinates allow natural valence bond parameters, such as bond lengths or bond angles, to be constrained as the remaining structural parameters are optimized.

When using internal coordinates for finding a transition state structure one performs a series of minimizations on a molecule with some coordinates constrained. A simple example is the ring opening reaction of cyclobutene to cis-butadiene



One performs several minimization with r_{12} held constant at different distances. The transition state corresponds to the maximum of the energy with respect to r_{12} while the energy is minimized with respect to all the other coordinates. An

advantage of this approach is that no second derivatives are needed to reach the saddle point. The disadvantage is that one needs to be able to identify a coordinate important in the reaction.

b. Augumented Hessian

Several algorithms for walking uphill, based on the Augmented Hessian have been suggested (36-38). We have implemented the procedure of Nguyen and Case (39). The search direction is obtained by a similar expression used for the minimum

$$\mathbf{s} = -(\mathbf{G} - \lambda \mathbf{I})^{-1} \mathbf{g} \quad (39)$$

It is convenient to write the step direction as

$$\mathbf{s} = - \sum_i \frac{|\psi_i\rangle \langle \psi_i| g\rangle}{\lambda_i - \lambda} \quad (40)$$

where λ_i and $|\psi_i\rangle$ are the eigenvalues and eigenvectors of \mathbf{G} , respectively. If we now choose $\lambda_i < \lambda < \lambda_2$ the step will go uphill along $|\psi_i\rangle$ and downhill along the remaining eigenvector $|\psi_i\rangle$ modes.

In general the lowest eigenvector $|\psi_i\rangle$ is not the direction we seek for an uphill walk. If, instead, $|\psi_x\rangle$ overlaps most strongly with the preferred uphill search direction, we then scale λ_x so that

$$\lambda'_x = \lambda_2/4 \quad (41)$$

The search direction is now given by

$$\mathbf{s} = - \frac{|\psi_x\rangle \langle \psi_x| g\rangle}{\lambda'_x - \lambda} - \sum_i \frac{|\psi_i\rangle \langle \psi_i| g\rangle}{\lambda_i - \lambda} \quad (42)$$

with the scale factor $n = 2\sqrt{\lambda_x'/\lambda_2}$. We use

$$\lambda = (\lambda_2 + 1/2 \lambda'_x)/2 \quad (43)$$

to determine \mathbf{s} . The step is further scaled to get a step length appropriate to

the extent of quadratic region. Once the Hessian G develops a negative eigenvalue we use the square of the norm of the gradient to find the stationary point.

c. Norm of the Gradient Squared Methods

Once we are at a point on the potential energy hypersurface where G has a negative eigenvalue we minimize

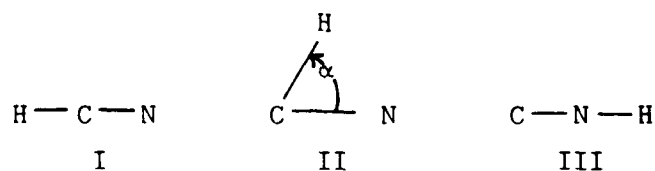
$$\sigma = \langle g | g \rangle , \quad (44)$$

as discussed above. This approach for transition states was originally suggested by McIver and Korminicki (24).

4. Some Examples

We summarize some examples of minimizations in Table 5. Methods which require the calculation of the exact Hessian converge with fewer energy evaluations, but since each second derivative evaluation takes a factor of N times as long as the SCF calculation itself, (a factor of 15 for cis 1,2 -bromofluorocyclopropane) the approximate Hessian methods are faster. Especially effective, even for these small systems, is the "V1 method" (30) that approximates the coupled perturbed Hartree-Fock solution. The Augmented Hessian usually requires a greater number of energy evaluations than does the Newton method. The reason for this is the restricted step nature of the augmented Hessian (Eq. (40)). When searching for a minimum $\lambda(\text{low}) < 0$, all other $\lambda_i > 0$, and the step is damped.

As a first example of a transition state calculation, Table 6 presents a search for the transition state in the reaction.



The initial structure is the optimized linear structure of HCN. The direction of search is given as the bending mode. Nine searches of the Augmented Hessian type are then required to find a single negative eigenvalue of the Hessian.

TABLE 5. A SUMMARY OF SOME OPTIMIZATIONS.

For each type of optimization the number of cycles is given. The number in parenthesis is time (min:sec) on a Vax 11/780, and because of system, are in possible error of 20%. The test calculations are INDO SCF.

System	NH ₃	CH ₃ OH	cis 1,2-Br,F cyclopropane
Initial ^a			
Grad Norm	0.169	0.160	0.143
BFGS, Eq. 5	8	25 (4:45)	29 (10:24)
Minimize g ⁺ g Eq. 12	7	25 (7:12)	
Newton Method ^b			
Approx. Hessian, Eq. 2	6	4 (1:42)	9 (5:46)
Aug. Approx. ^b Hessian, Eq. 8	5	9 (2:28)	17 (10:30)
Newton Method, exact Hessian, Eq. 2	3	7 (4:30)	8 (37:32)
Aug. Hessian, exact Hessian Eq. 8	3	9 (5:28)	17 (84:42)

^aInitially all symmetry is broken. For convergence all gradients have been reduced to below 5*10⁻⁴ a.u./bohr.

^bThe approximate Hessian is formed from the V(1) method.

TABLE 6. HCN TO CNH TRANSITION STATE SEARCH.

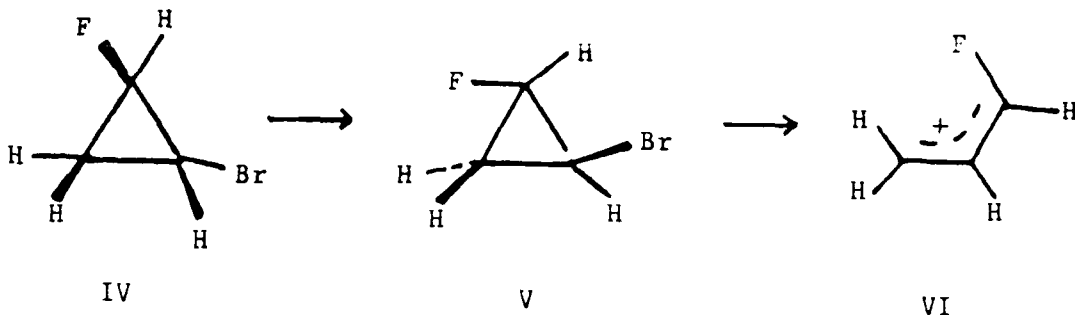
Cycle	Energy (a.u.)	Angle	Grad Norm	Max Grad	Alpha
0	-17.399659	180.	0.000009	0.000007	0.000000
1	-17.399332	172.	0.012114	0.008997	0.000000
2	-17.397598	170.	0.013596	0.010633	0.000000
3	-17.396393	167.	0.016541	0.013954	0.000000
4	-17.393372	162.	0.022758	0.018559	0.000000
5	-17.387683	155.	0.031371	0.026375	0.000000
6	-17.377439	146.	0.041703	0.032579	0.000000
7	-17.360093	134.	0.054164	0.044396	0.000000
8	-17.340161	123.	0.060774	0.043167	0.000000
9	-17.318690	112.	0.061493	0.045832	0.000000
0	-17.318690	112.	0.061493	0.045832	0.000000
1	-17.305166	105	0.057417	0.044127	0.043937
2	-17.293763	98.	0.048153	0.037835	0.136931
3	-17.285888	91.	0.032596	0.025713	0.302938
4	-17.282615	85.	0.010536	0.007121	0.695352
5	-17.282563	83.	0.000301	0.000228	1.000000

TABLE 7. CIS 1,2 BROMOFLUOROCYCLOPROPANE TRANSITION STATE SEARCH.

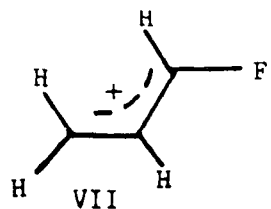
Cycle	Energy (a.u.)	C-Br, C-C	Grad Norm	Max Grad	Alpha
0	-60.921237	1.92,1.49	0.000000	0.000483	0.000000
2	-60.919410	1.94,1.49	0.012906	0.007870	0.000000
4	-60.910574	1.98,1.49	0.030662	0.019198	0.000000
6	-60.895073	2.02,1.49	0.046260	0.028827	0.000000
8	-60.879683	2.06,1.49	0.055757	0.034111	0.000000
10	-60.861925	2.07,1.49	0.063907	0.037261	0.000000
12	-60.841640	2.07,1.50	0.072336	0.039998	0.000000
14	-60.817903	2.08,1.51	0.080903	0.042538	0.000000
16	-60.791225	2.09,1.51	0.088479	0.044238	0.000000
18	-60.768511	2.08,1.52	0.092289	0.045723	0.000000
20	-60.747962	2.09,1.53	0.096211	0.047915	0.000000
21	-60.735117	2.09,1.54	0.096953	0.048456	0.000000
0	-60.735117	2.09,1.54	0.096953	0.048456	0.000000
2	-60.715634	2.11,1.55	0.091909	0.045909	0.044725
4	-60.724647	2.11,1.55	0.076953	0.038289	0.088425
6	-60.738067	2.07,1.55	0.062593	0.030933	0.105320
8	-60.749658	2.04,1.57	0.048845	0.023988	0.127181
10	-60.758475	2.02,1.57	0.036117	0.017943	0.154638
12	-60.764553	2.00,1.58	0.024674	0.012363	0.194934
14	-60.768260	1.99,1.59	0.014560	0.007292	0.269270
16	-60.770030	1.97,1.59	0.005689	0.002728	0.469534
17	-60.770315	1.97,1.59	0.001676	0.000817	0.796780

From this point five searches are made to minimize σ , Eq. (44). This might be compared with a similar search of Baker on the same system that required 10 cycles to obtain the transition state, but starting from $\alpha = 90^\circ$ [40].

Table 7 summarizes the transition state search of cis-1,2-bromofluorocyclopropane opening with loss of Br⁻,



The product is 100% that shown, rather than



A picture of the transition state appears in Figure 1. Starting with the optimized structure of IV, cis 1,2-B,F cyclopropane, 21 Augmented Hessian iterations are required to find the negative eigenvalue of the Hessian, then 17 cycles are required to find the stationary point. This search is of the SCF type: thus the calculated transition state might not be that actually found as separation into ionic products would require a quantum chemical treatment including electron correlation. In addition, separation into ionic products might also require consideration of solvent effects (41).

D. STRUCTURE AND PROPERTIES OF $C_3H_3^+$ CATIONS

1. Introduction

Two possible mechanisms have been proposed for the formation of soot in fuel rich flames. One mechanism invokes radical reactions, the other ion/molecule reactions involving small ions. The latter mechanism has been advanced by the observation that $C_3H_3^+$ is the most intense ion observed in sooting flames (7,10) and motivates this theoretical study along with

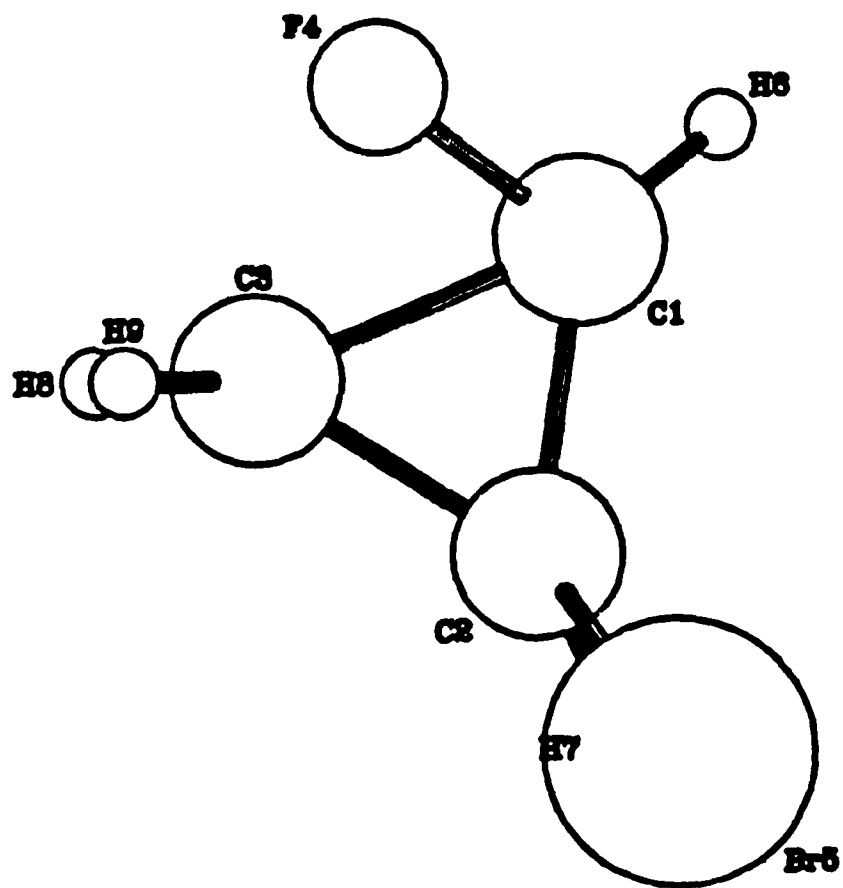


Figure 1. The Calculated Transition State for the Opening of Cis 1,2-Bromo-fluorocyclopropane, see text.

experimental studies of ion/molecule reactions involving small hydrocarbon ions using Fourier Transform Ion Cyclotron Resonance techniques (Eq. 4?). A good characterization of possible $C_3H_3^+$ isomers would be helpful identifying their presence in sooting flames. The presence of such species are experimentally determined through mass spectroscopic techniques and the techniques presently being used cannot distinguish isomeric structures unambiguously.

Various mass spectrometric studies suggest that $C_3H_3^+$ possesses reactive and nonreactive components. The most stable form of $C_3H_3^+$, the cyclopropenylum cation I, Figure 2, is relatively unreactive toward acetylene and polyacetylenes as well as toward other small hydrocarbons (42,43). The propargylium cation II, is considerably more reactive toward C_2H_2 , and leads to the formation of $C_5H_3^+$ and $C_5H_5^+$ ions, both with reactive and unreactive components. The propargylium cation II is believed to lie some 25 kcal/mol (44) higher in energy than the cyclopropenylum cation I, but this species, as well as others potentially important, might be formed under the reaction conditions observed in sooting flames. We thus embark in this study to uncover possibly reactive species of $C_3H_3^+$.

Carbocations such as $C_3H_3^+$ have been of interest for some time. Cyclopropenylum ions represent the first members of the $2 + 4n$ aromatic series and, as such, have been the object of much theoretical discussion. A rather complete study of the relative stability of many $C_3H_3^+$ structures has been reported by Radom, Hariharan, Pople and Schleyer (45). Although the earlier calculations are of somewhat lesser accuracy than those we report here, in general we agree with their ordering of stabilities and their structures, with one exception as discussed later.

2. Methods.

The initial structures of this study were obtained through INDO calculations (46). These geometries were then refined using the STO-3G, then 3-21G and finally 6-31G* basis sets advocated by Pople (Eq. 47). The use of this larger basis set has been prompted by our observation that stable minima at the 3-21G level can become "unstable" transition states at a higher level of calculation. Such a case will occur here. A Broyden-Fletcher-Goldfarb-Shanno quasi-Newton update procedure was used to obtain all structures (30, 48) with no

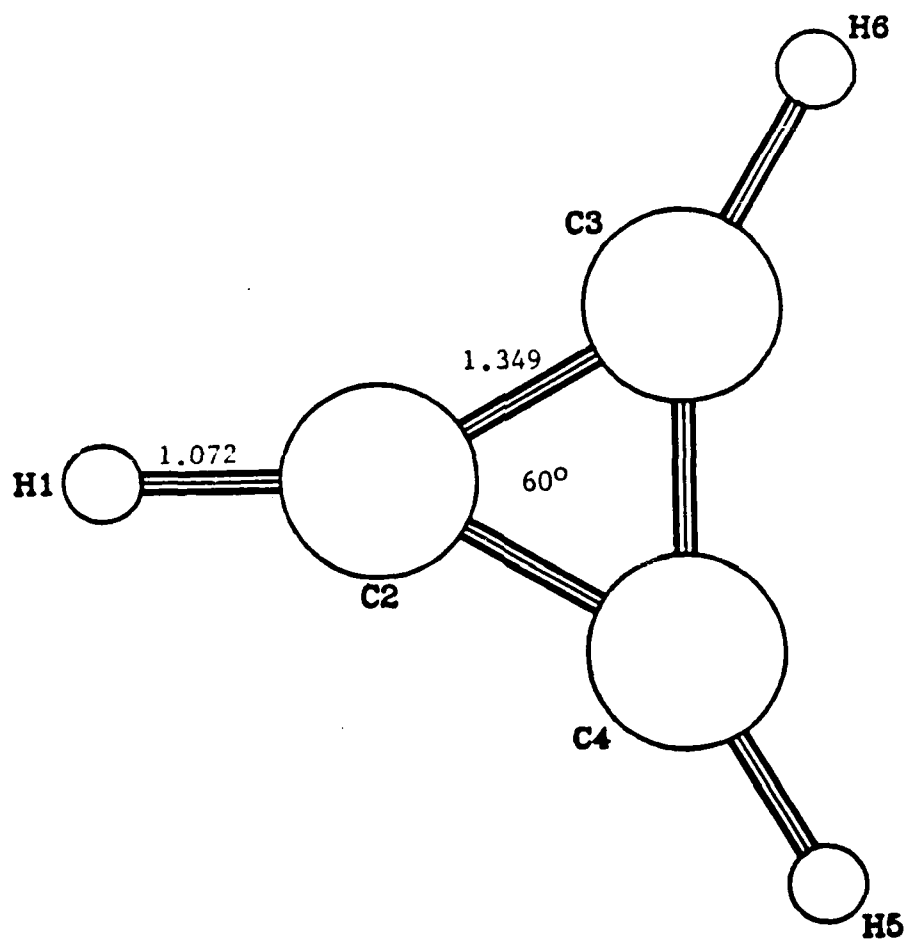


Figure 2. Optimized Structure (6-31G*) of Cyclopropenyl cation (I).

constrained degrees of freedom. The ab initio calculations were performed with the Gaussian 82 program³ suitably modified with this search algorithm. All calculations begin with structures of no symmetry; when symmetry was obtained it was as a result of the geometry search. The geometries believed most accurate are those obtained from the 6-31G* calculation, although all the calculated structures are reported for comparisons. Vibrational frequencies were calculated using both the 3-21G geometries and wavefunctions and the 6-31G* geometries and wavefunctions (49), and they are unscaled. When comparing with experiment multiplication by a factor of 0.85 has been found to greatly improve predictions. At optimized 6-31G* structures single point 6-31G** SCF calculations were performed and then corrected through fourth order in Møller-Plesset Rayleigh-Schrodinger perturbation theory but leaving the core "electrons" uncorrelated (50). Our best calculations on the relative energy of these structures are thus characterized by MP4-6-31G**//6-31G*.

The electronic spectra of these optimized structures were estimated using the INDO-CI spectroscopic method (51, 52).

3. Results

The relative energies obtain for five structures are summarized in Table 8. Calculated geometries are summarized in Figures 2 - 6 and Tables 9 - 13. As expected, all calculations predict the cyclopropenylum ion (I) lowest in energy followed by the propargylium cation (II). The best estimate of the difference in energy between those two structures is 28.9 kcal/mol, in reasonable agreement with the value of 34.4 kcal/mol calculated by Radom et. al. (45). Correction for zero point vibrational energy reduces this value to 27.7 kcal/mol, to be compared with an experimental estimate of 25±4 kcal/mol (44). Structure IV, the prop-2-en-1-yl-3-ylidine cation is calculated next higher in energy, some 72.4 kcal/mol higher than the cyclopropenylum ion, a value reduced to 70.9 kcal/mol corrected through inclusion of 0.85 times the zero-point vibrational energy.

Structure III, the 1-propynyl cation, possesses C_{3v} symmetry and a pair of degenerate pi-like orbitals sharing two electrons. Such a situation gives rise to a triplet and three singlets. The lowest energy singlet is calculated using complex orbitals and is estimated to lie some 101 kcal/mol higher in energy than the cyclopropenylum cation reference.

TABLE 8. RELATIVE STABILITIES OF $C_3H_3^+$ ISOMERS (A.U.)^a.

	I Cyclic $(CH)_3$	II $H_2-C-C-CH$	III $H_3-C-C-C$	IV $H_2C-CH-C$	V Cyclic H_2CCCH	
	S ^a	(T) ^a	S ^a	(T) ^a		
STO-3G	<u>-113.6203</u> ^b	0.0564	0.2900 [0.1831] ^c	(0.1136)	0.1110 [0.1680]	0.2049
3-21G	<u>-114.3296</u> ^b	0.0201	0.2819 [0.1705] ^c	(0.1117)	0.0820	0.1991
6-31G*	<u>-115.0070</u> ^b	0.0559	[0.1928] ^c	(0.1413)	0.1104	0.2090 ^g
6-31G** ^h	<u>-115.0133</u> ^b	0.0564	0.3160 [0.1935] ^c		0.1111	0.2236
+MP2	<u>-115.3694</u> ^b	0.0526	0.3253 [0.1873] ^c		0.1283	0.2659
+MP4	<u>-115.4081</u> ^b	0.0460	0.2949 [0.16] ^{c,d}		0.1153	0.2261
Radom et. al. ^e		0.0548	[0.1753] ^c		0.1109	0.2039
Exp. ^f			0.040±0.01			

a) 1 a.u. = 627.5 kcal/mole. S = Singlet, (T) = Triplet

b) Calculated total energies.

c) Complex calculation.

d) Estimated.

e) Reference 45.

f) Reference 44.

g) 6-31G*//3-21G

h) 6-31G**//6-31G*

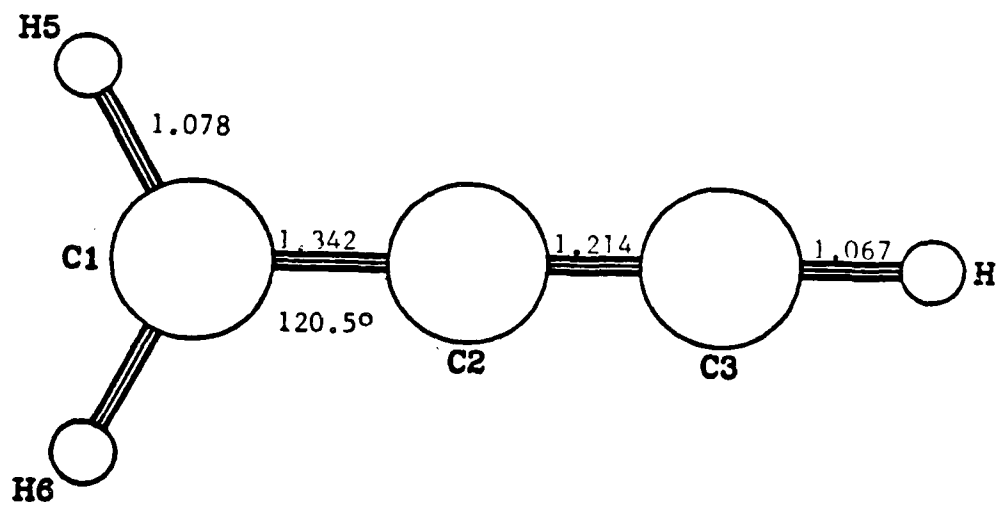


Figure 3. Optimized Structure (6-31G*) of Propargyl cation (II).

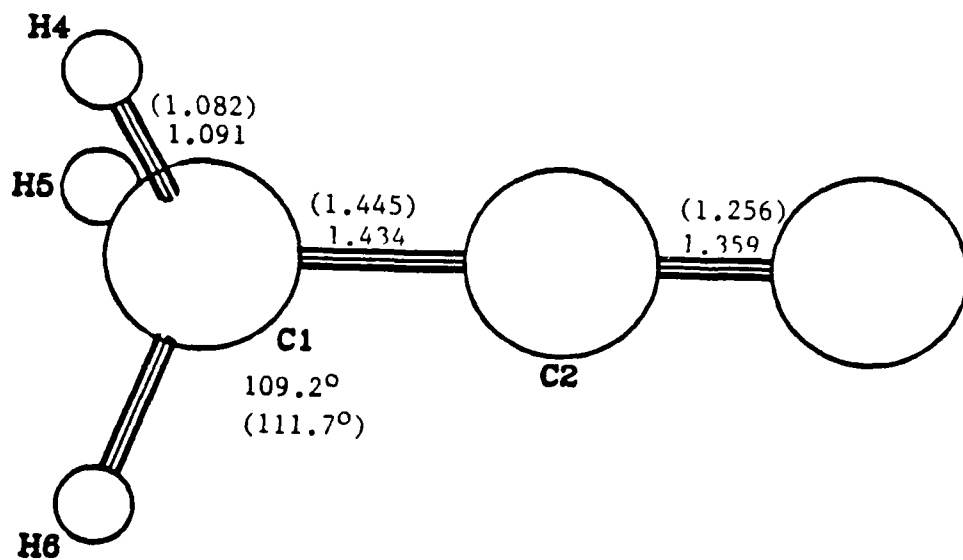


Figure 4. Optimized Structure (6-31G*) of 1-Propynyl Cation (III). The numbers in parenthesis are for the triplet.

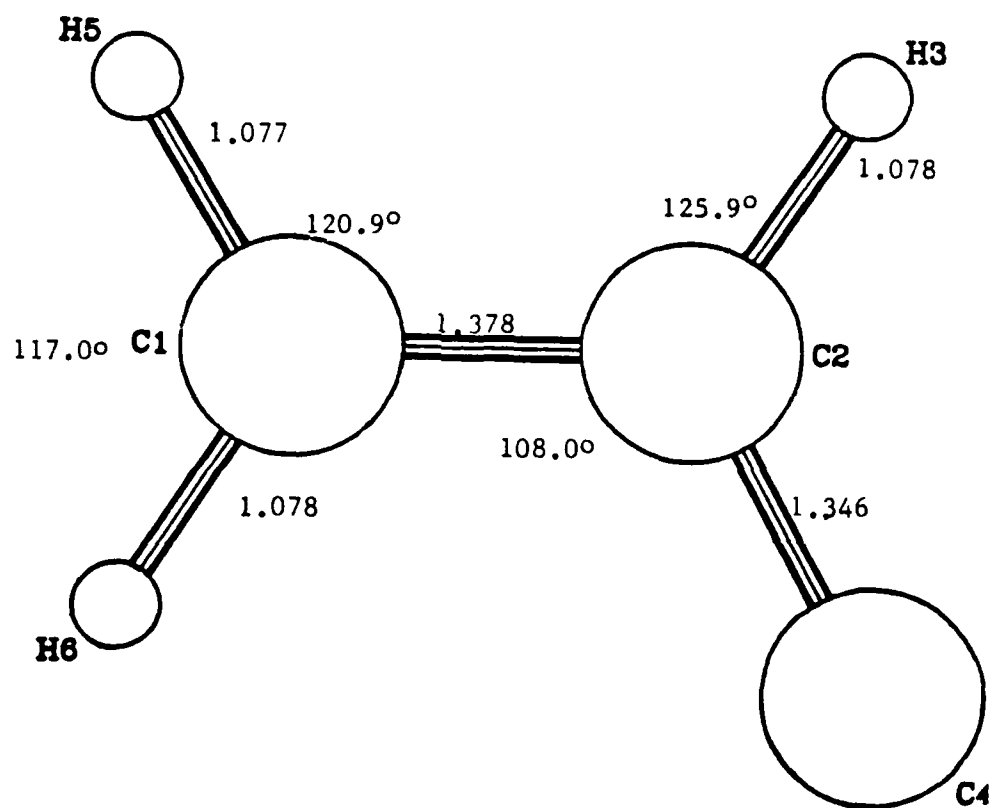


Figure 5. Optimized Structure (6-31G*) of Prop-2-en-yl-3-ylidene Cation (IV).

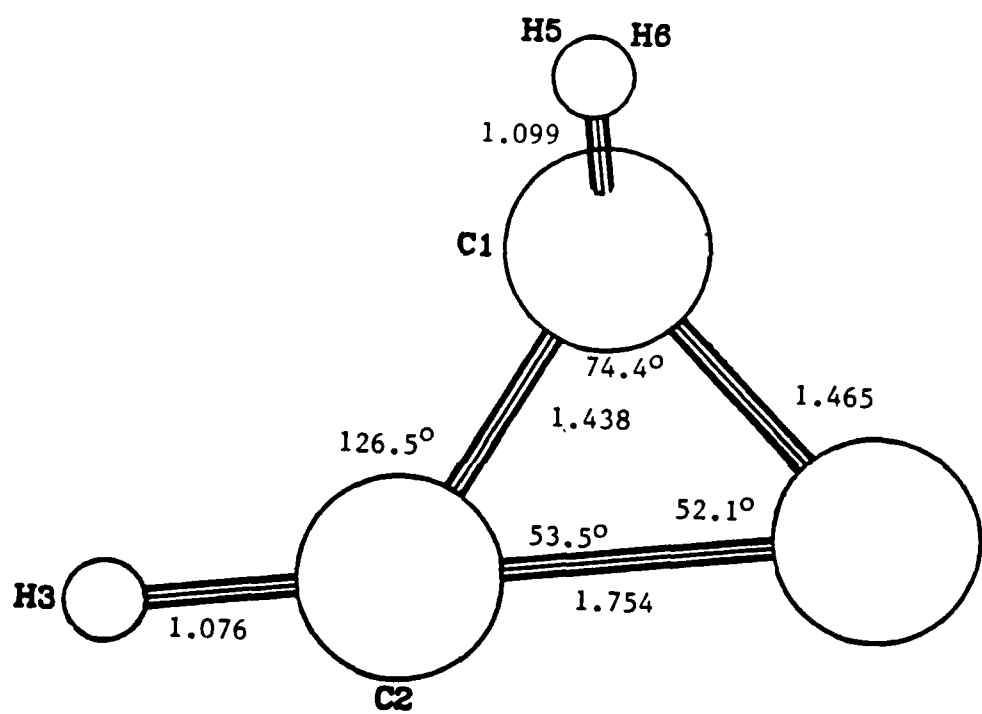


Figure 6. Optimized Structure (3-21G) of Cycloprop-1-yl-2-ylidene Cation (V). This structure opens to that of Figure 5 with the 6-31G* basis.

TABLE 9. THE CALCULATED GEOMETRIES (\AA) OF THE CYCLOPROPENYLUM ION, I,
FIGURE 2.

COORDINATE	INDO	STO-3G	3-21G	6-31G*
CH	1.087	1.095	1.062	1.072
CC	1.386	1.377	1.361	1.349
CCC	60°	60°	60°	60°

TABLE 10. THE CALCULATED GEOMETRIES OF THE PROPARGYLUM ION II, FIGURE 3.

COORDINATE	INDO	STO-3G	3-21G	6-31G*
C1-C2	1.407	1.360	1.334	1.342
C2-C3	1.341	1.214	1.213	1.214
C3-H4	1.079	1.091	1.061	1.067
C1-H5	1.091	1.109	1.078	1.078
H5-C1-C2	123.0°	121.1°	120.5°	120.5°

TABLE 11. THE CALCULATED GEOMETRIES OF THE 1-PROPYNYL CATION, III, FIGURE 4.

COORDINATE	INDO ^a	Singlet		Triplet ^c		
		3-21G ^b	6-31G ^b	INDO ^d	3-21G	6-31G*
C1-C2	1.382	1.418	1.434	1.430	1.435	1.445
C2-C3	1.242	1.357	1.359	1.272	1.267	1.257
C1-H	1.110	1.095	1.091	1.11	1.082	1.082
H-C1-C2	110.2°	110.2°	109.2	108.9°	112.3	111.7

a) Two determinant ROHF optimization.

b) Complex orbital optimization.

c) UHF calculations.

d) A slight break in symmetry.

TABLE 12. THE CALCULATED GEOMETRIES OF THE PROP-2-EN-1-YL-3-YLIDINE CATION, IV,
FIGURE 5.

COORDINATE	STO-3G	3-21G	6-31G*
C1-C2	1.377	1.372	1.378
C2-C3	1.396	1.347	1.346
H5-C1	1.102	1.074	1.077
H6-C1	1.102	1.076	1.078
H3-C2	1.090	1.081	1.078
H5-C1-H6	116.9°	117.3°	117.0°
H5-C1-C2	121.2°	120.3°	120.9°
C1-C2-H3	123.6°	122.9°	125.9°
C1-C2-C4	115.8°	118.0°	108.0°

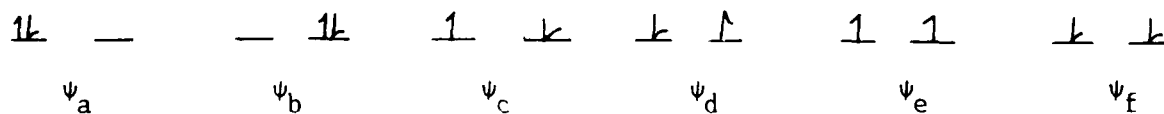
TABLE 13. THE CALCULATED GEOMETRIES OF THE CYCLOPRO-1-YL 2-YLIDINE CATION V,
FIGURE 6.

COORDINATE	INDO	STO-3G	3-21G	6-31G*	STO-3G ^a
C1-C2	NOT	1.478	1.438	NOT	1.456
C2-C3	S	1.700	1.754	S	1.641
C1-C3	T	1.507	1.465	T	1.530
H3-C2	A	1.112	1.076	A	1.104
H5-C1	B	1.102	1.098	B	1.109
C1-C2-C3	L	56.1°	53.5°	L	58.8°
C2-C3-C1	E	54.5°	52.1°	E	54.6°
C3-C1-C2		69.4°	74.4°		66.6°
H3-C2-C1		123.9	126.5°		145.1

a) From reference 45.

The optimized triplet structure lies at considerably lower energy than the corresponding singlets. This structure is predicted to lie 89 kcal/mol above the cyclopropenyl cation reference, but higher in energy than either of the singlet structures II and IV.

Comparisons between states of different multiplicities such as we have made here for structure III are notoriously difficult for all but the most exacting ab initio theories, as these calculations tend to over-stabilize triplet state energies relative to singlets. Considering the partially filled degenerate orbitals of III,



the use of complex orbitals approximates the $\frac{1}{\sqrt{2}} (\psi_a - \psi_b)$ component of the 1E (the other component is $\frac{1}{\sqrt{2}} (\psi_c - \psi_d)$). The 3A_2 state is estimated by a UHF calculation on ψ_e (the other components are ψ_f and $\frac{1}{\sqrt{2}} (\psi_c + \psi_d)$).

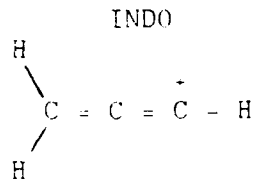
Our calculated energy differences between these two states is likely too large. The INDO/S-CI method, however, has been found quite reliable in estimating these differences at fixed geometries. These calculations, performed at the optimized triplet geometry, suggest that the 3A_2 state lies only 11 kcal/mol lower than the 1E state, and that the 1A_1 state ($1/\sqrt{2}(\psi_a + \psi_b)$) lies 11 kcal/mol higher in energy than the 1E . The difference between the ab initio $^1E - ^3A_2$ energy of 32 kcal/mol with that of 11 kcal/mol estimated by the INDO/S calculations corresponds closely to the observation that ab initio calculations of this type tend to artificially favor triplets by about 20 kcal/mol.

The cyclic structure V, the cycloprop-1-yl-2-ylidine cation, is estimated to lie 142.9 kcal/mol above the reference compound I at the 3-21G level. At the 6-31G* level, structure V is not stable and opens to become structure IV. This finding is in contrast to previous studies (45). With the inclusion of polarization functions the cyclic form V opens to IV, but the angle that has opened, C1C2C4 of Figure 5, has decreased with this better basis from 118° (3-21G) to 108° (6-31G*), Table 12.

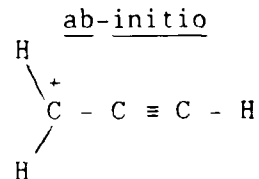
Structure V has two pi-like electrons (a"). A near lying state with four pi-like electrons also is unstable, leading back to the propargylium cation, II. Other structures have been examined by Radom et al. (45) but those are all predicted to be less stable than these we report here. Although these latter calculations are reported at the Hartree-Fock level, Table 8 shows that the use of a slightly better basis set and the inclusion of a fourth order perturbation theory does not affect the differences in energies by more than about 10%. Note, however, that differences calculated at second order deviate more from the fourth order results than do the Hartree-Fock differences themselves. The inclusion of polarization functions in the 6-31G** calculations preferentially stabilizes the cyclopropenyl cation I, and destabilizes structure V.

Table 9, Figure 2, summarize the calculated geometry of cyclopropenylum cation. As usual, the better basis set, 6-31G* yields shorter bond length than does the minimum basis set STO-3G. The INDO results are in good accord.

Table 10 and Figure 3, compare the calculations for the propargylium cation. The INDO and ab initio results suggest different bonding schemes for this ion.

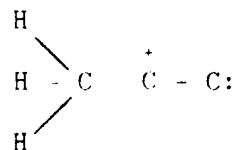


vs.

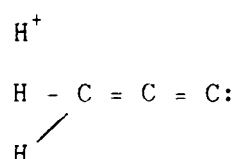


respectively.

Table 11 and Figure 4, summarize the calculated structure of the 1-propynyl cation. The singlet structure is best described as



with the C - C single bond shortened by hyperconjugation,



The triplet, however, is best described as

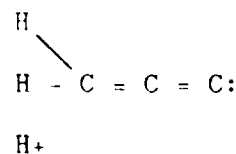
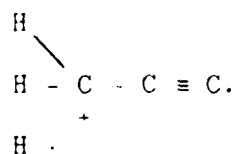
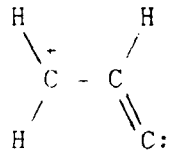


Table 12, Figure 5, gives the calculated geometries of the prop-2-en-1-yl-3 ylidine cation IV. There is a considerable shortening of the C2 - C4 bond when employing the better basis set, implying a more important role to



than

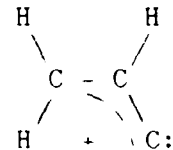


Table 13, Figure 6, presents a summary of our findings for the cyclopro-1-ylidene cation, V. The structure of the figure is that obtained with the 3-21G basis set. As mentioned, this structure opens to the prop-2-en-1-yl-3 ylidine ion IV with the better basis.

Experimental estimates for the heat of formation of the cyclopropenylion range from 256 - 258 kcal/mol with an estimated error of ± 3 kcal/mol (44, 53). Table 8 can then be used to estimate the heats of formation of other tautomers of this series.

The vibrational frequencies we obtain for these lowest lying conformers of $C_3H_3^+$ are reported in Table 14. They are unscaled and we again remark that multiplication of these frequencies by a factor of about 0.85 often gives better results when compared with experiment. Of interest is the observation that lower frequency modes are most affected by the better basis, and are generally decreased. The cyclopropenylion I has no low lying frequencies, distinguishing it from the other less stable structures of this study. We note the very low frequency of structure V at the 3-21G level leading to ring opening at the 6-31G* level.

The calculated UV-visible spectra of six species are presented in Table 15. The 3-21G optimized geometries were assumed for INDO/S-CI calculations (51, 52). This method has been found accurate for a great many hydrocarbons, and especially so for positively charged species where diffuse states are not important. For comparisons results of calculations by Tokada and Ohno for the cyclopropenylion I (54) and by Eyler, Oddershede, Sabin, Diercksen, and Gruner for propargylion II Eq. (55) are included. The former calculations

TABLE 14. CALCULATED VIBRATIONAL FREQUENCIES USING 3-21G A)OPTIMIZED STRUCTURES AND WAVEFUNCTIONS AND B)6-31G* OPTIMIZED STRUCTURES AND WAVEFUNCTIONS, IN CM⁻¹.

	I				II			
mode	(a)	(b)	I(IR) ^f	I(R) ^f	(a)	b)	I(IR)	I(R)
a2"	907.9	842.5	83	00	b1	351.7	280.3	45 00
e'	1041.8	1029.2	27	6	b2	396.4	364.2	25 03
---	----	--	--	--	b2	842.0	741.6	74 01
e"	1136.2	1099.6	00	00	b1	1089.1	1023.9	02 01
---	----	--	--	--	b2	1182.9	1131.5	01 00
a2'	1209.2	1164.0	00	00	a1	1222.8	1216.6	77 57
e'	1373.6	1418.3	74	04	b1	1281.5	1265.1	06 00
---	----	--	--	--	a1	1613.0	1611.1	03 02
a1'	1702.3	1795.2	00	53	a1	2216.5	2194.9	816 28
e'	3466.0	3467.5	86	28	a1	3275.2	3331.1	16 101
---	----	--	--	--	b2	3380.2	3443.3	45 58
a1'	3519.1	3518.5	00	91	a1	3535.8	3569.5	75 47
E ₀ ^e (au)	0.0487	0.0486			0.0464	0.0460		

	III Singlet				III Triplet			
Mode	(a)	(b,d)	I(IR)	I(R)	Mode	(a)	I(IR)	I(R)
e	519.1	306.2	5	0	e	480.9	41	791
---	----	--	--	-	---	---	---	---
a1	820.4	885.7	49	0	a1	839.9	74	03
e	1266.4	973.8	36	0	e	1171.1	10	2096
---	----	--	--	-	---	---	---	---
a1	1560.0	1499.2	24	0	a1	1542.9	76	103
e	1616.9	1484.9	---	0	e	1549.1	106	773
---	----	49	0	---	---	---	---	---
a1	2427.4	1814.7	5	0	a1	1765.3	17	1414
a1	3201.9	3137.1	125	0	a1	3110.2	171	166
e	3296.4	3223.9	55	2	e	3187.5	38	07
---	----	--	--	-	---	---	---	---
E ₀ ^e (au)	0.0488	0.0440						

TABLE 14. CALCULATED VIBRATIONAL FREQUENCIES USING 3-21G A)OPTIMIZED STRUCTURES AND WAVEFUNCTIONS AND B)6-31G* OPTIMIZED STRUCTURES AND WAVEFUNCTIONS, IN CM⁻¹ (CONCLUDED).

Mode	IV				V	
	a)	b)	I(IR)	I(R)	Mode	a)
a'	337.0	254.6	09	07	a"	157.2
a"	521.9	463.7	11	02	a'	417.5
a"	1024.4	996.1	65	00	a	630.9
a'	1091.3	1013.4	09	02	a'	935.1
a'	1256.0	1251.4	13	11	a"	1003.7
a"	1298.0	1265.1	10	01	a'	1051.3
a'	1358.4	1383.3	94	29	a'	1194.2
a'	1649.3	1648.4	254	15	a'	1311.2
a'	1699.3	1685.7	264	04	a'	1333.0
a'	3280.8	3333.2	21	52	a'	3087.6
a'	3303.3	3372.8	67	63	a"	3114.2
a'	3409.6	3444.9	40	40	a'	3342.5
E ₀ ^e (au)	0.0461	0.0458				0.0400

a) 3-21G basis

b) 6-31G* basis

c) Not a stable structure, see text

d) Numerical force constants

e) Zero point vibrational energy in Hartrees.

f) The IR and Raman intensities in km/mol and (Angstroms)⁴/amu, respectively.

TABLE 15. CALCULATED ELECTRONIC SPECTRA OF $C_3H_3^+$. (1000 CM $^{-1}$).

This Work		- I -		This Work		- II -		Ref. 55	
$^1A''_1$	56.1		$^1A''_1$	69.0		1A_2	17.9		18.8
$^1E''$	60.6		$^1E''$	71.0		1A_1	41.0 (0.092)		42.2 (0.154)
	60.6			71.0					
$^1E'$	64.4 (0.166) ^a		$^1A''_2$	71.0		1A_2	49.4		60.1
	64.4 (0.166)		$^1E'$	84.7		1A_2	52.4		66.2 (0.000)
$^1A''_2$	62.2 (0.003)			84.7		1B_1	59.6 (0.003)		73.0 (0.009)
						1A_1	59.8 (0.807)		73.8 (0.787)
						3A_2	14.8	---	
- III -		- III -		- IV -		- V -			
Singlet (1E)		Triplet (3A_2)		This Work		This Work			
1A_2	3.8	3E	14.4 (0.004)	$^1A''$	31.7 (0.019)	$^1A''$	24.7 (0.000)		
			14.4 (0.004)	$^1A'$	35.6 (0.001)	$^1A''$	33.9 (0.024)		
1A_1	18.4			$^1A''$	35.6 (0.001)	$^1A''$	43.8 (0.030)		
1E	19.6 (0.008)	3E	23.0 (0.000)	$^1A'$	44.7 (0.461)	$^1A''$	49.9 (0.003)		
	19.6 (0.008)		23.0 (0.000)						
1E	46.0 (0.000)	3A_1	23.3	$^1A''$	56.1 (0.021)	$^1A'$	57.3 (0.114)		
	46.0 (0.000)			$^1A'$	65.4 (0.000)	$^1A'$	67.9 (0.180)		
		3E	39.5 (0.004)	$^3A'$	66.8 (0.097)	$^3A''$	17.4	---	
			39.5 (0.004)						
	49.0 (0.000)								
	58.9 (1.620)	3A_2	45.3 (0.405)	$^3A'$	20.3	---			
3A_2	-3.8	---	1E	3.8	---				
				3.8					

(a) The numbers in parentheses are oscillator strengths.

(b) Estimated from Figure 6 of reference 54.

are an ab initio SCF-CI calculations, but employ a rather small basis set for this purpose. Our results differ considerably from those of Takada and Ohno. The results reported by Eyler et al. on the propargylium cation II are from good basis set polarization-propagator methodology (56). The lower two excitation energies they obtain are in remarkable agreement with the INDO/S-CI results. Other states they calculate are 10,000 - 15,000 cm^{-1} higher in energy than those we obtain, but the ordering and estimated oscillator strengths are again in good accord.

Of some interest in the formation of soot is the interconversion of propargylium cation to cyclopropenylium cation. The former can form an encounter complex with acetylene, and disproportionate back to either the cyclic or linear C_3H_3^+ . The cyclic isomer does not appear to react with acetylene, based on evidence obtained from deuterium exchange reactions (4). There is no evidence that cyclopropenylium cation tautomerizes to propargylium cation in the absence of an encounter complex with a neutral molecule. In keeping with this we have not been able to find a transition state geometry linking the two structures, and from constrained optimization calculations estimate a transition energy of at least 60 kcal/mol.

4. Discussion

We have examined several stable structures of C_3H_3^+ and report on the five most stable that we have uncovered. The cyclic form, the cyclopropenylium cation, is lowest in energy, followed by the linear propargylium ion, $[\text{H}_2\text{CCCH}]^+$, calculated to lie some 27.7 kcal/mol higher in energy, in reasonable agreement with an experimental estimate of 25 ± 4 kcal/mol. Other structures reported are calculated at least 25 kcal/mol higher in energy than the propargylium ion. All of the structures we report, however, have reasonably high vibrational frequencies, suggesting all but Structure V are resistant to interconversion. Structure V, cycloprop-1-yl-2-ylidene cation $[\text{H}_2\text{CCCH}]^+$, we predict is not stable, either with two or four pi-type electrons. Under the conditions in which we are interested, sooting flames, some, or even all, structures might be observed. In addition, the lowest energy conformer might not be the most abundant, or the most reactive with C_2H_2 or C_4H_2 to form higher molecular-mass precursors of soot. Indeed, as mentioned earlier, the most stable cyclic form is relatively unreactive with C_2H_2 and C_4H_2 .

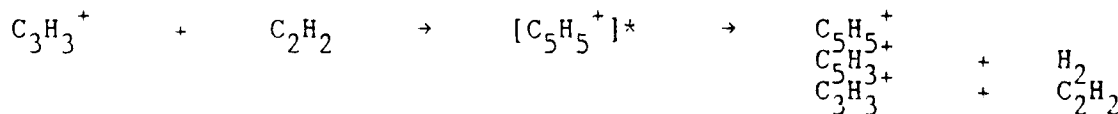
In attempts to locate various species present in flames, or in models of these flames simulated in ion cyclotron resonance experiments (42), we have calculated IR frequencies and electronic transition energies. Especially of interest are those species with low lying allowed electronic transitions below about 40,000 cm⁻¹. Such states might be excited through modern laser techniques and observed through laser induced fluorescence, or through excitation of those ions using afterglow techniques. Above 40,000 cm⁻¹ interference from other species, especially aromatics, might be expected.

E. REACTIONS OF ACETYLENE WITH ISOMERIC FORMS OF THE C₃H₃⁺ IONS.

1. Introduction

The reactions of C₃H₃⁺ with small neutral hydrocarbons such as acetylene and diacetylene are postulated as an initial step in soot formation, followed by sequential condensation and condensation-elimination reactions, forming successively large ions, and eventually yielding soot particles (7,10,14b). Studies of these reactions using Fourier Transform Ion Cyclotron Resonance (FT-ICR) techniques seem to indicate that C₃H₃⁺ does form encounter complexes with acetylene, but under the conditions of the experiment no stable compounds are formed (42). In addition, there are apparently two forms of C₃H₃⁺ present in these experiments, only one of which is reactive. Reactions with diacetylene, however, do lead to the formation of species such as C₉H₅⁺, C₅H₃⁺, C₇H₃⁺ and C₁₁H₅⁺⁵.

With an eye to this mechanism of soot formation, we have previously examined the structures of possible C₃H₃⁺ isomers, and have characterized these species according to their relative energies, and their vibrational and electronic spectra for possible identification in sooting flames (6). The reaction between C₃H₃⁺ and C₂H₂ should yield then, C₅H₅⁺, or C₅H₃⁺, or could yield starting materials back, with perhaps isomerization of the C₃H₃⁺ ion⁷.



The most stable structure of C₅H₅⁺⁹, also presented is a preliminary study for possible reactions of acetylene with the two lowest energy isomers of C₃H₃⁺,

cyclopropenyl cation, Figure 7, and propargylium cation, Figure 8. Many reactions might occur between a neutral molecule and a positive ion, and this is to be the case. Here, however, only the propargylium ion reacts without barrier. In these studies, only one of these reactions leads to a thermodynamically stable product, relative to dissociation back into acetylene and cyclopropenyl cation. Each of the reaction products uncovered are then characterized according to their vibrational spectra to insure they represent stable molecules, and for possible identifications in experiments with sooting flames and in FT-ICR experiments on systems designed to model sooting flames.

2. Theoretical Methods

Possible reactions using were examined, the INDO method (46) searching the potential energy surface with a Broyden-Fletcher-Goldfarb-Shanno quasi-Newton update procedure (30,35). The uncovered structures are then refined using the Gaussian 86³ ab-initio program, first with the STO 3G basis sets, then 3-21G split valence basis sets, and then with 6-31G* split valence plus polarization basis sets (47). Vibrational frequencies are obtained using the 3-21G basis at the geometry obtained for this basis. The correlation energy is estimated utilizing a 6-31G** basis at the 6-31G* geometry and second order Moller-Plesset Rayleigh-Schrodinger perturbation theory (MP2/6-31G**//6-31G*).

3. Results and Discussion

Previous calculations show that the cyclic tautomer lies some 27.7 kcal/mol lower in energy than the propargylium cation⁶, in reasonable agreement with the experimental estimate of 25 kcal/mol (44). All other calculated structures lie at least 20 kcal/mol higher in energy than the propargyl form. We find that the cyclic tautomer forms an encounter complex C₅H₅⁺ of no specific structure as shown from the final geometries given in Figure 9-11. These structures are obtained from initial geometries of no particular symmetry other than the plane of Figures 10 and these initial geometries are all rather similar to the final structures obtained, but, of course with C₂H₂ to C₃H₃⁺ distance greater. At the MP2/6-31G** level of theory these complexes are stabilized by about 6 kcal/mol. No attempt has been made to correct this energy for basis set superposition, as it was not our intention to study these weak complexes. No further reaction occurs without sizeable barrier.

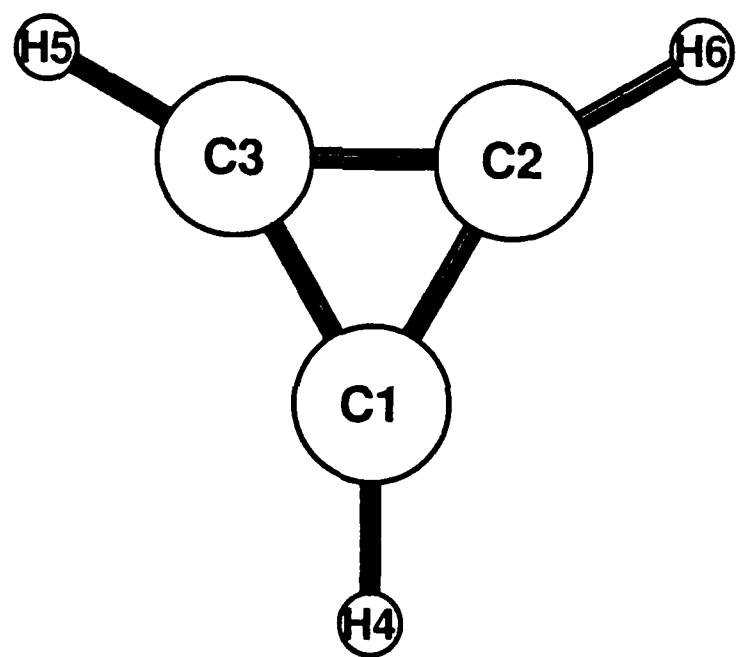


Figure 7. The Cyclopropenylium Cation.

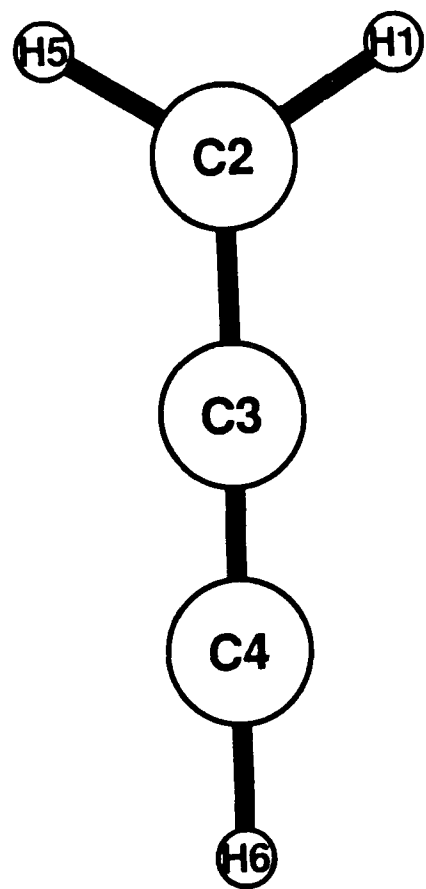


Figure 8. The Propargylium Cation. The calculated geometries are given in Section II.D.

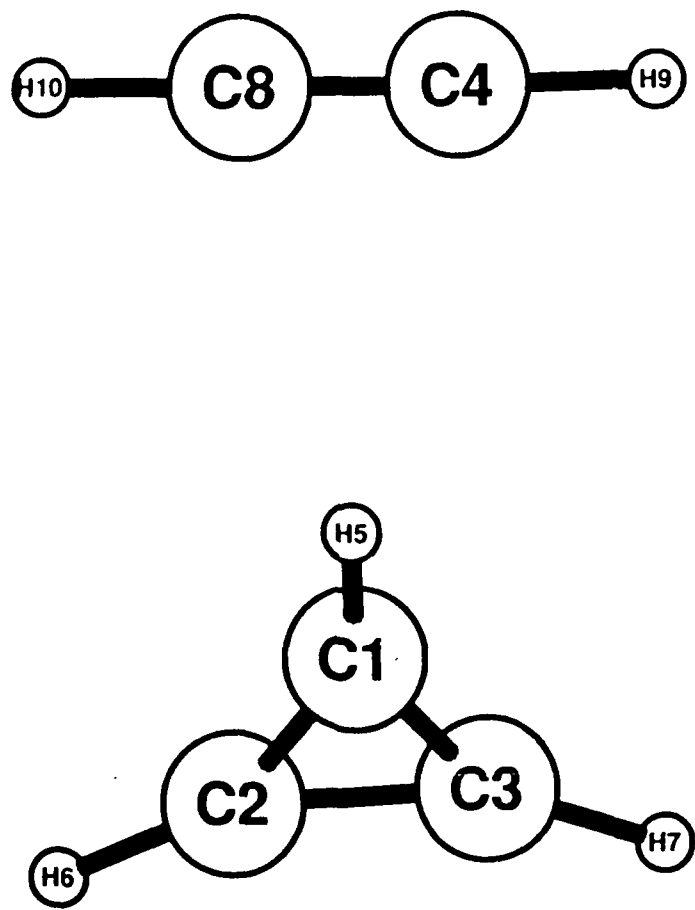


Figure 9. An Encounter Complex Formed in the Association of C_2H_2 with the Cyclic Form of C_3H_3^+ . The resulting structure reflects the initial geometry used for these calculations.

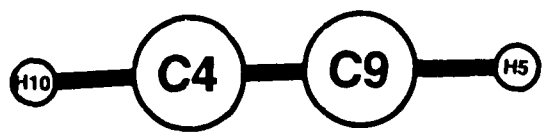
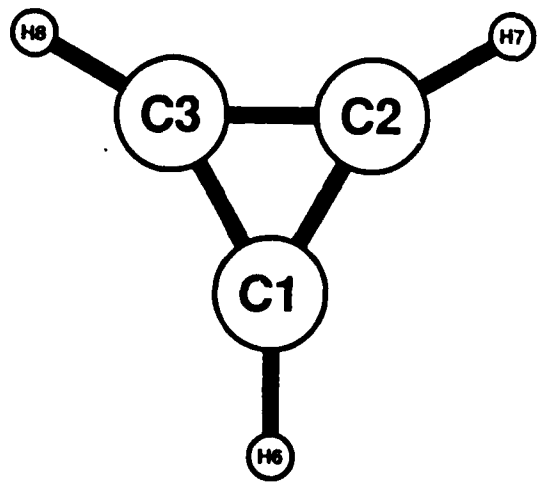


Figure 10. An Encounter Complex formed in the Association of C_2H_2 with the Cyclic Form of $C_3H_3^+$.

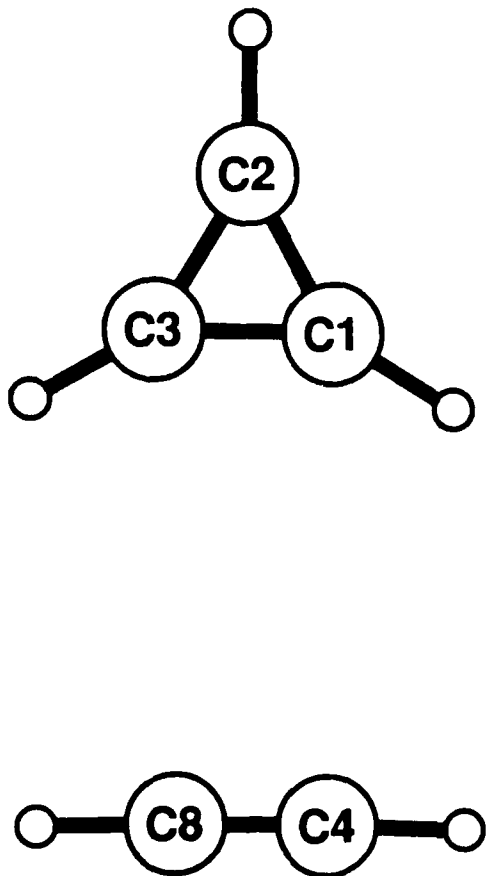


Figure 11. An Encounter Complex formed in the Association of C_2H_2 with the Cyclic Form of C_3H_3^+ .

Five different approaches of C_2H_2 to the propargyl cation were examined, two in-plane and three out-of-plane, as shown in Figures 12 and 13a. Again there was no symmetry in the initial geometries. The two resonance structures of this isomer suggest attack of the electron-rich acetylene to the end carbon:



and this is what we find. The final structures are reported in order in Figure 14 and 13d. Their energies are reported in Table 16, and the calculated frequencies are shown in Table 17.

The energy calculated for the cyclopropenyl cation and acetylene at the MP2/6-31G**/6-31G* level of theory is -115.3694 Hartrees and -77.0795 Hartrees, respectively. Correcting these values by scaling the calculated zero point vibrational energy by 0.9 yields estimated internal energies of -115.3256 kcal/mol and -76.0502 kcal/mol, respectively⁸. Using these values suggests that only systems of lesser total energy than -191.3758 kcal/mol will be thermodynamically stable relative to dissociation back into acetylene and cyclic C_3H_3^+ , if we ignore entropy effects. Only the structure in Figure 14c fulfills this stability requirement. Estimating the entropy from the Sackur-Tetrode equation (and assuming a microcanonical ensemble) (57) and recalling the loss of one mole of gas, we can estimate the free energy of this reaction as

$$\Delta G = E(\text{calc}) + 0.9E(\text{vib}) - 191.3758 + 0.03T$$

where the $E(\text{calc})$ is at the MP2/6-31G** level of theory, and T is the temperature in Kelvin.

With the initial geometry in Figure 13a, and with the acetylene slightly skewed and directly over the central atom of the propargyl cation, we followed the reaction using the optimization scheme generated by the Broyden-Fletcher-Goldfarb-Shanno method (30). Initially the acetylene drifts to the most positive end carbon atom, then attaches to this atom to form a three membered ring. Figure 13b shows a point along this path, and 13c and 13d are two different views of the product formed. This species is not stable relative to disproportionation into the cyclic isomer and acetylene, as mentioned previously.

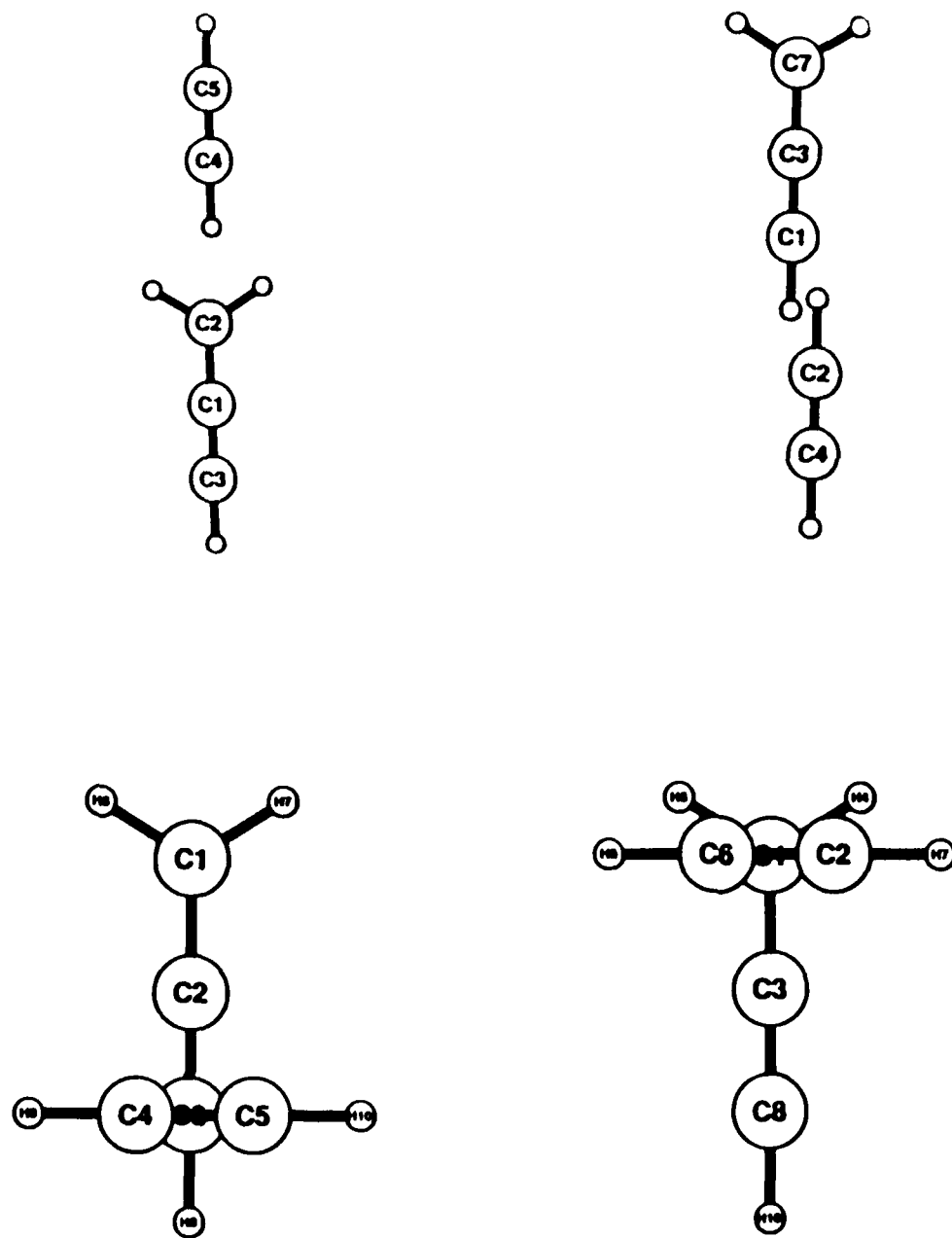


Figure 12. Four Starting Geometries for the Reaction of Propargyl cation with Acetylene. Note that none of these initial geometries has any initial symmetry.

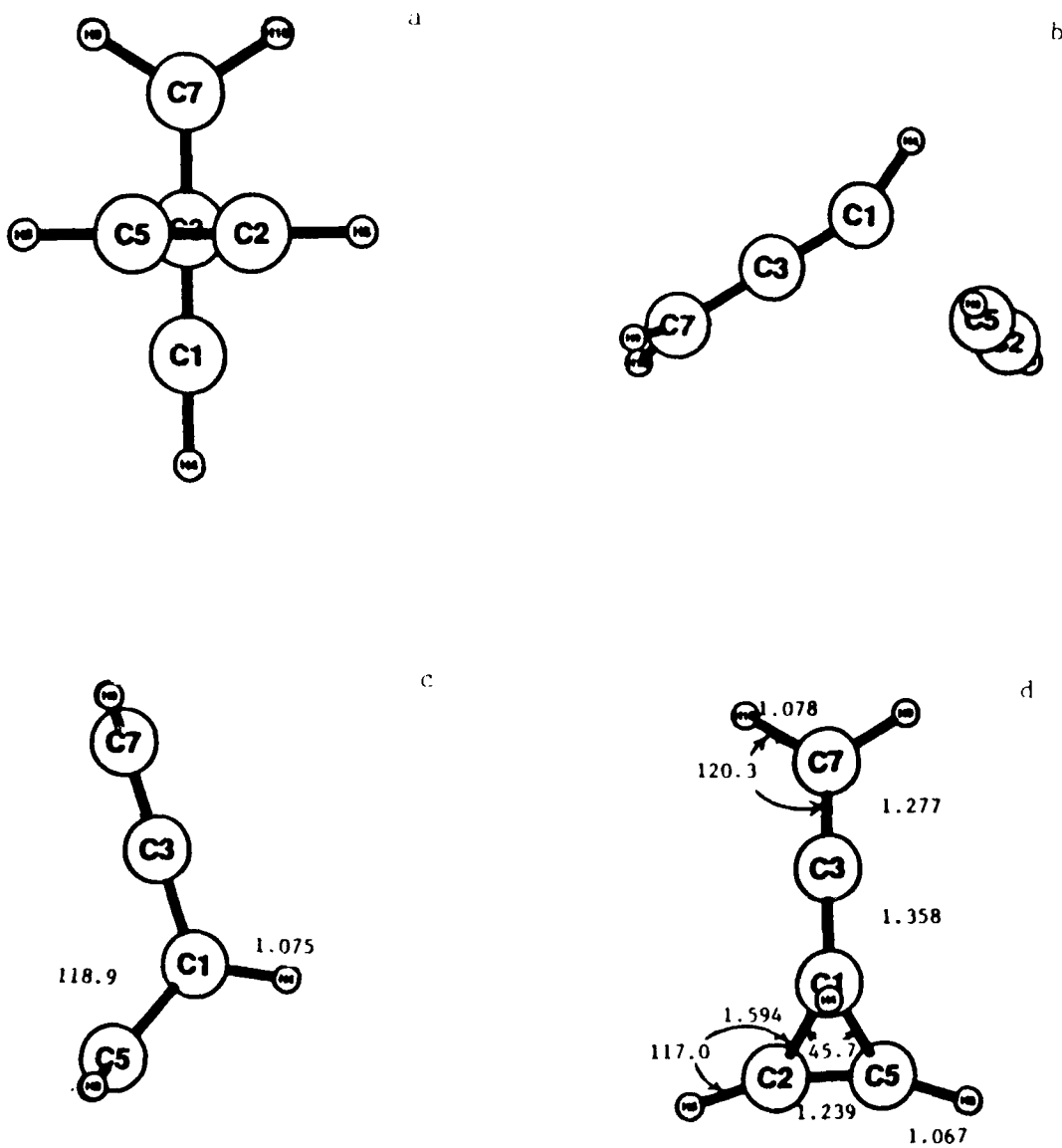


Figure 13. A study of one of the reactions between Acetylene and the Propargylium Cation. a) the starting geometry, b) an intermediate structure, c) and d) two views of the final product of this particular encounter.

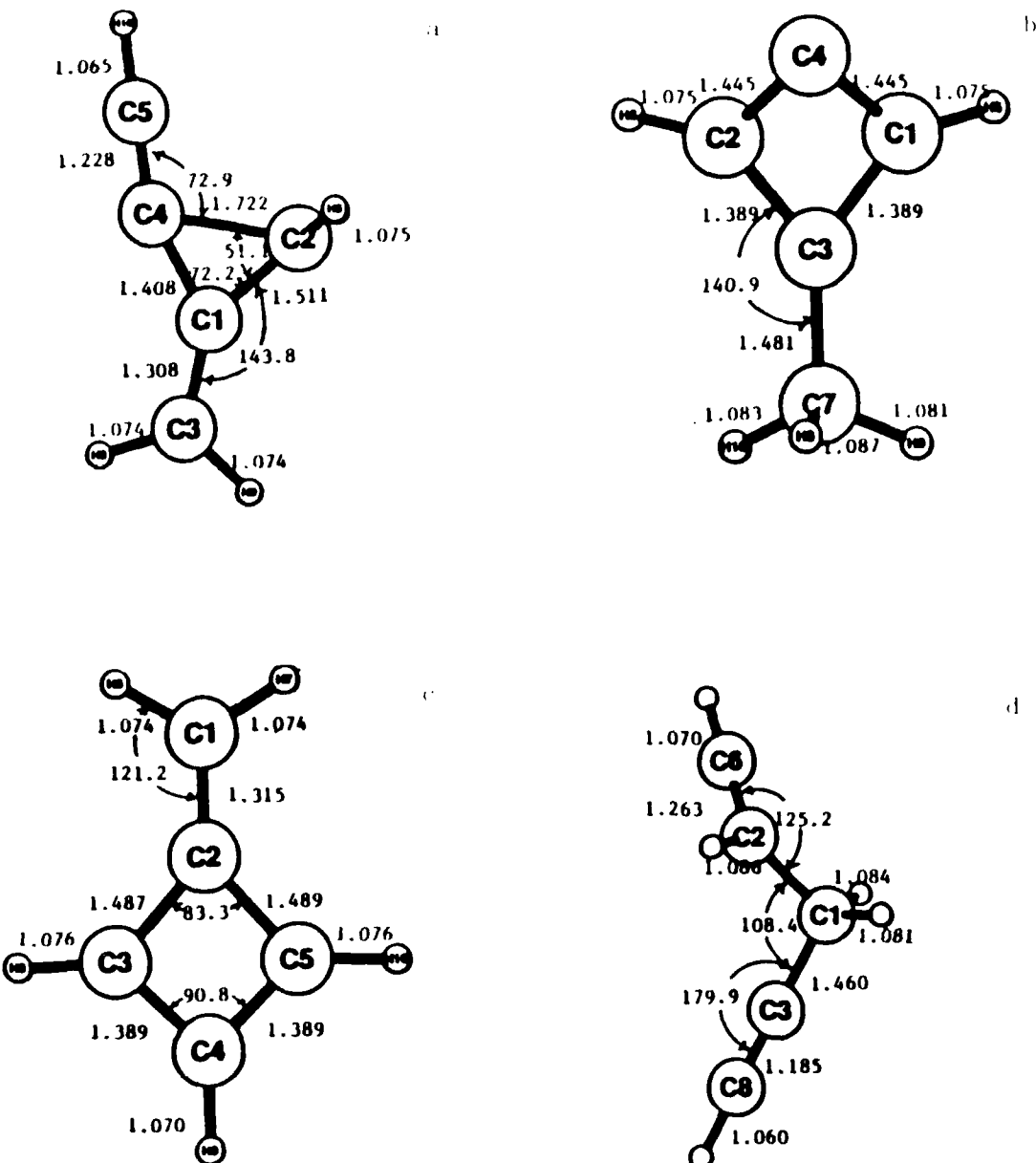


Figure 14. The Final Structure that Result from the Four Initial Conditions as Shown in Figure 12. Only the structure of Figure 14c is stable relative to the cyclopropenyl cation and acetylene, see text.

TABLE 16. THE CALCULATED ENERGIES OF THE REACTION PRODUCTS $C_5H_5^-$. ENERGIES ARE IN HARTREES.
GEOMETRIES ARE OPTIMIZED WITH THE $6-31G^*$ BASIS SETS UNLESS OTHERWISE STATED.

Theory	Fig.	g^b	10^b	11	14_a	14_b	14_c	14_d	13d
$6-31G^*$		-191.8276	-191.8280	-191.8298	-191.8310	-191.8342	-191.8828	-191.8852	-191.8856
$6-31G^*$		-191.8379	-191.8387	-191.8356	-191.8403	-191.8379	-191.8924	-191.8137	-191.8145
2MP_2		-192.4559	-192.4584	-192.4521	-192.4844	-192.4588	-192.5124	-192.4322	-192.4387
$E_0(\text{vib})$				0.0828	0.0822	0.0848	0.0819	0.0805	
$E_0(\text{est})^a$				-192.4099	-192.3848	-192.361	-192.2580	-192.1529	

a. $E(^2MP_2-6-31G^*/6-31G^*) + 0.9 \times E_0(\text{vib})$

b. These are very flat potentials. 2_a are $2b$ and STO 3G geometries. 2_c is a $6-31G^*$ geometry. In the latter case the $6-31G^*$ optimization starting from the STO 3G geometry lowered the energy by 0.0043 Hartrees, a correction that might be added to the energies of 2_a and 2_b .

TABLE 17. CALCULATED VIBRATIONAL FREQUENCIES OF THE REACTION PRODUCTS
USING 3-21G OPTIMIZED STRUCTURES AND WAVEFUNCTIONS (cm^{-1}).

Structure Fig. 14a	Structure Fig. 14b	Structure Fig. 14c	Structure Fig. 14d	Structure Fig. 13d
169.4	73.2	150.7	104.5	135.0
291.2	293.5	358.9	237.8	231.3
305.7	364.8	425.1	270.7	335.9
467.6	519.9	774.2	419.3	517.1
475.5	665.3	793.2	542.0	532.5
765.5	699.8	815.9	747.6	560.7
818.2	860.1	954.1	759.6	733.0
834.2	1006.4	1021.6	888.0	869.9
908.3	1010.5	1070.6	959.3	922.4
986.7	1151.1	1104.9	977.6	985.9
1023.7	1165.2	1190.2	996.6	1043.1
1148.3	1204.3	1204.8	1047.3	1089.2
1206.6	1243.7	1224.4	1125.0	1115.4
1243.3	1322.0	1257.8	1240.3	1125.3
1256.3	1390.5	1306.0	1367.9	1159.7
1579.0	1566.0	1425.0	1457.5	1427.1
1616.0	1619.8	1540.5	1616.3	1534.3
1914.8	1624.1	1610.3	1836.0	1947.1
2249.6	1651.6	1911.6	2415.6	2106.3
3297.6	3187.9	3331.9	3243.7	3285.0
3345.7	3261.8	3408.0	3271.6	3368.4
3425.1	3309.4	3410.0	3309.3	3409.3
3440.3	3440.0	3419.1	3482.6	3500.9
3579.6	3448.2	3495.4	3638.6	3586.2

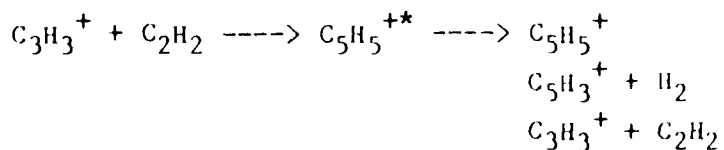
Experimentally, propargyl iodide cation can be dissociated into the propargylium cation and iodine atom in FT ICR experiments. Upon collision with acetylene and deuterioacetylene, a complex is formed with a long enough lifetime to scramble the deuterium. This reaction has been kinetically modelled with some detail⁷ and it is apparent that in the absence of three body collisions, such $C_3H_3^+$ complexes are short lived, yielding two forms of $C_3H_3^+$ one that can further react to again form stable associations, again scrambling deuterium, and one that is unreactive. These calculations suggest that the cyclic tautomer is the stable species. The encounter complex is formed, however, with considerable excess internal energy, thus explaining the lack of any $C_5H_5^+$ stable structures in the FT ICR experiments. These same experiments carried out with diacetylene do lead to stable structures within the lifetime of the measurement of formula $C_7H_7^+$, $C_7H_5^+$, $C_7H_3^+$, $C_9H_5^+$ and $C_{11}H_6^+$. Even so, models of this reaction also require collisional deactivation of the appropriate species to carry away the excess internal energies before the complexes can fractionate.

F. STRUCTURES AND PROPERTIES OF $C_5H_5^+$

1. Introduction

The reaction of $C_3H_3^+$ with small neutral hydrocarbons such as acetylene and diacetylene is postulated in the mechanism for soot formation. This is followed by sequential condensation and condensation-elimination reactions, forming successively larger ions, and eventually yielding soot particles.

Previous examinations of the structures of possible $C_3H_3^+$ isomers had characterized these species according to their relative energies, and their vibrational and electronic spectra for possible identification in sooting flames⁶. The reaction between $C_3H_3^+$ and C_2H_2 should yield $C_5H_5^+$, $C_5H_3^+$, or cyclic $C_3H_3^+$ ^{7,9}.



This work examined the most stable structures of $C_5H_5^+$. Each of the most stable structures were then characterized according to their uv/visible spectra and their vibrational spectra for possible identification in experiments with sooting flames and in coupled laser-FT-ICR experiments on systems designed to model sooting flames.

2. Theoretical Methods

Possible isomeric structures of $C_5H_5^+$ were examined using the INDO method (46,51) searching the potential energy surface with a Broyden-Fletcher-Goldfarb-Shanno quasi-Newton update procedure (30,35). The uncovered structures were then refined using the Gaussian 86³ and GAMESS (58) ab initio programs, first with the STO-3G basis sets, then 3-21G split valence basis sets, and then with 6-31G* split valence plus polarization basis sets (47). Vibrational frequencies were obtained using the 3-21G basis at the geometry obtained for this basis. The correlation energy was estimated utilizing a 6-31G** basis at the 6-31G* geometry and second order Moller-Plesset Rayleigh-Schrodinger perturbation theory (MP2-6-31G**//6-31G*). The uv/visible spectra was calculated using the INDO/S spectroscopic method (51,52) at the optimized 6-31G* geometries. The oscillator strengths of the transitions were estimated using the dipole length operator and only one-center terms, as described elsewhere (51).

3. Results

Twenty-one possible structures, uncovered from the INDO calculations and from suggestions reported in the literature, were initially examined. The nine most stable structures are reported in Table 18, and their optimized geometries calculated at the 6-31G* level are reported in Figures 15 to 23. The best estimates of relative energies in this table were obtained from the MP2-6-32G**//6-31G* calculations. It is difficult to compare the open shell structures of the cyclic species IV, V, and VI, with the closed shell species, and this problem is not removed through the addition of second order perturbation theory corrections. These species appear to be biased by about 0.03 Hartrees, or about 19 kcal/mol. This correction has been included in estimates in the Table 18, and is consistent with results from the INDO

TABLE 18. THE ENERGIES OF DIFFERENT ISOMERS OF $C_5H_5^+$, IN HARTREES. SEE FIGURES FOR THE CORRESPONDING STRUCTURES.

Method	I	II	III	IV	V (Triplet)
STO-3G	-189.5968	-189.5614	-189.5724	-189.6333	-189.6011
3-21G	-190.8140	-190.7364	-190.7866	-190.8433	-189.8160
6-31G*					
1 Det.	-191.9183	-191.8652	-191.8828	-191.9334	-191.9024
GVB					-191.9340
6-31G**//					
6-31G*	-191.9278	-191.8757	-191.8924	-191.9426	-191.9117
+MP2	-192.5468	-192.5263	-192.5124	-192.5511	-192.5322
estimated rel. energy (kcal/mol)	0.00	12.9	21.6	16.4	9.2

Method	VI	VII	VIII	IX
STO-3G	-189.6006	-189.5542	-189.5542	-189.5600
3-21G	-190.8160 ^a	-190.8093	-190.8984	-190.8019
6-31G*				
1 Det.	-191.9021 ^a	-191.8801	-191.8828	-191.8744
GVB	-191.9309			
6-31G**//				
6-31G*	-191.9105	-191.8891	-191.8919	-191.8844
+MP2	-192.5326	-192.5134	-192.5181	-192.5049
estimated rel. energy (kcal/mol)	9.2	21.0	18.0	26.3

^a This structure is a transition state leading to a distortion of the structure given in Figure 20, which possesses an energy about 0.0002 Hartrees lower than the structure shown.

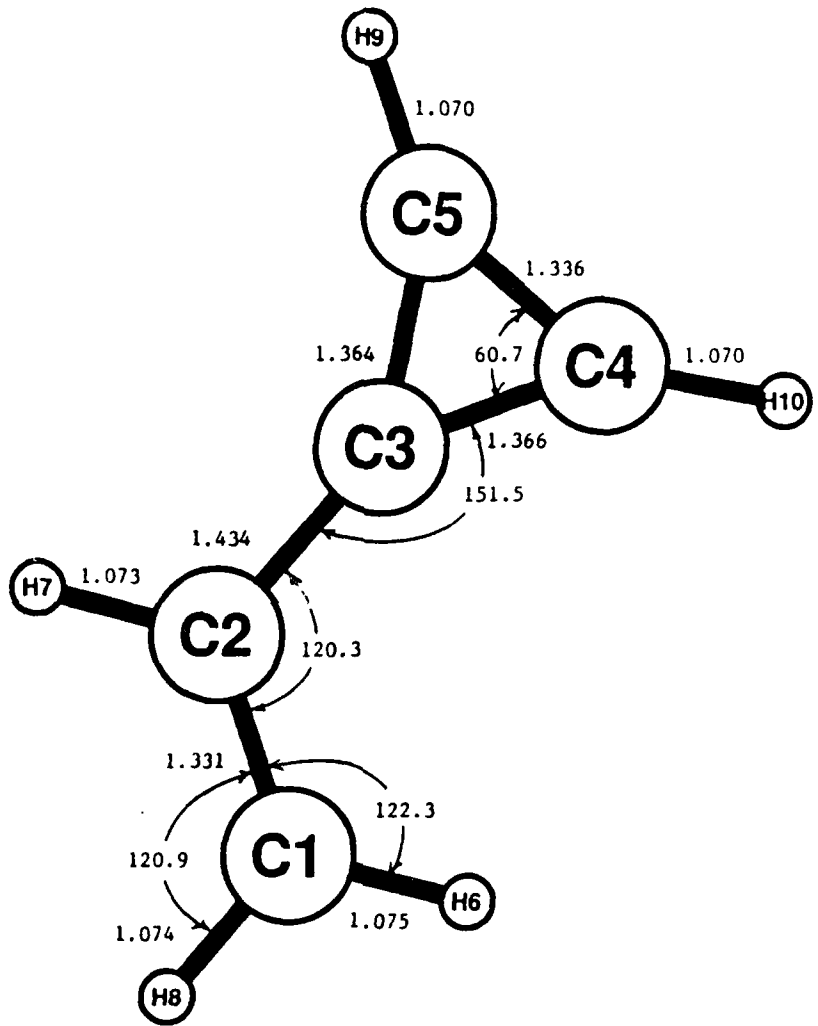


Figure 15. Structure 1.

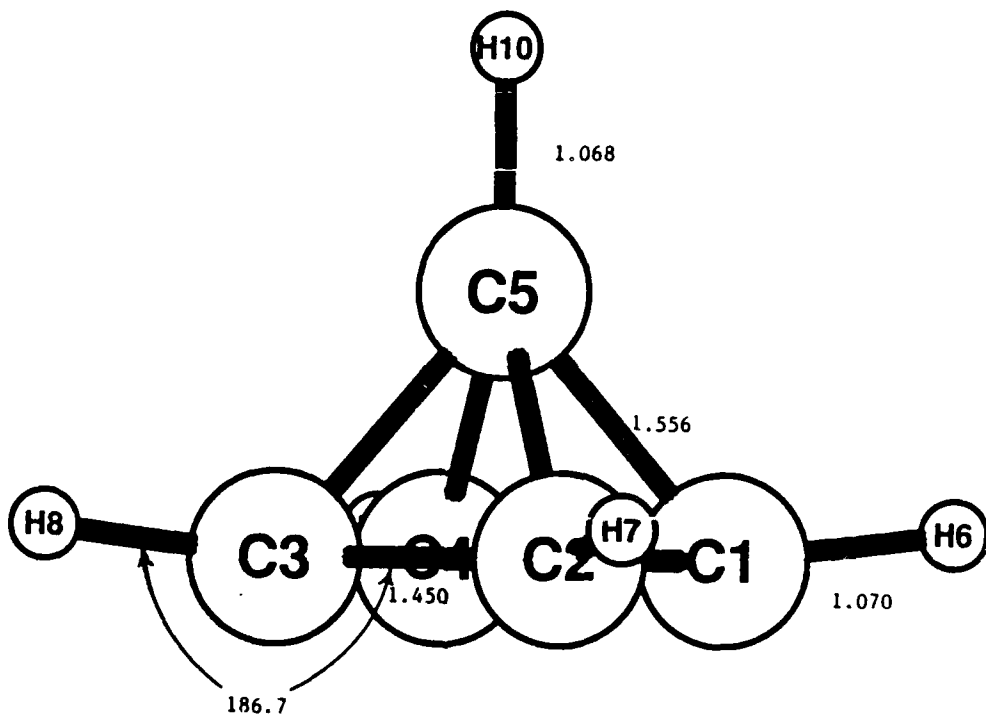


Figure 16. Structure II.

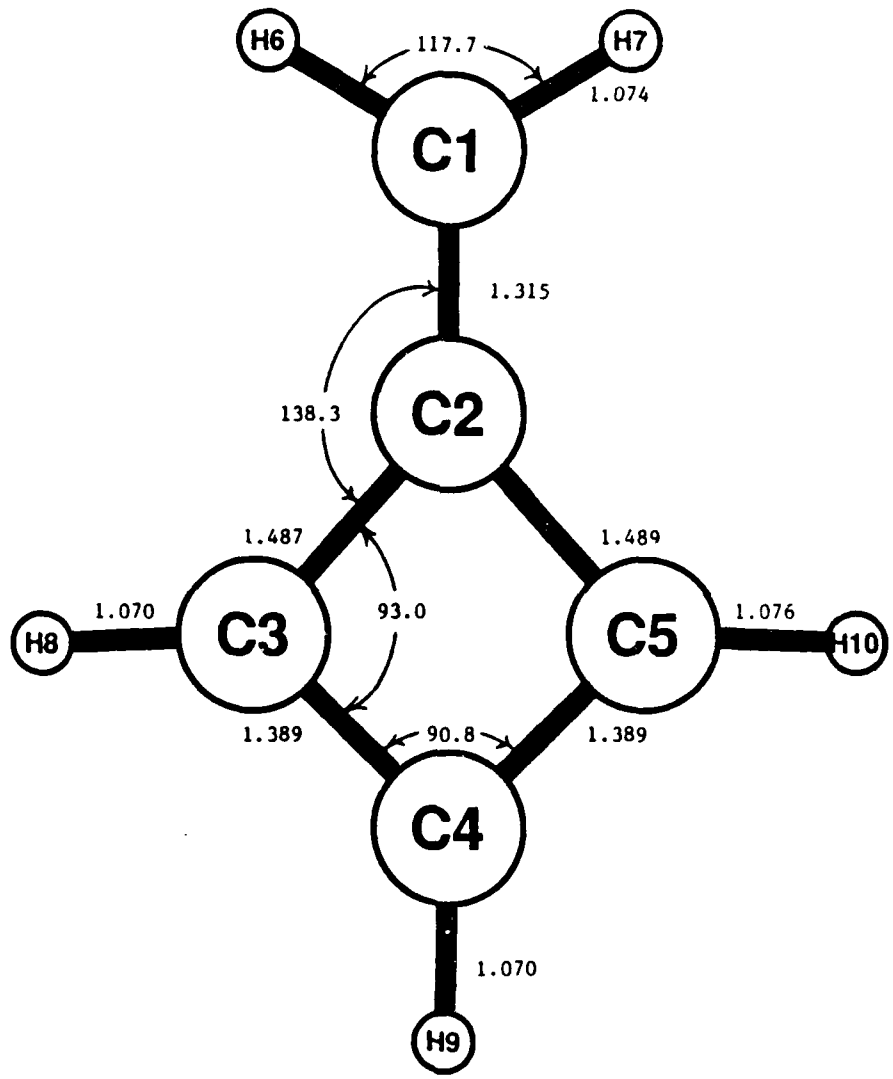


Figure 17. Structure III.

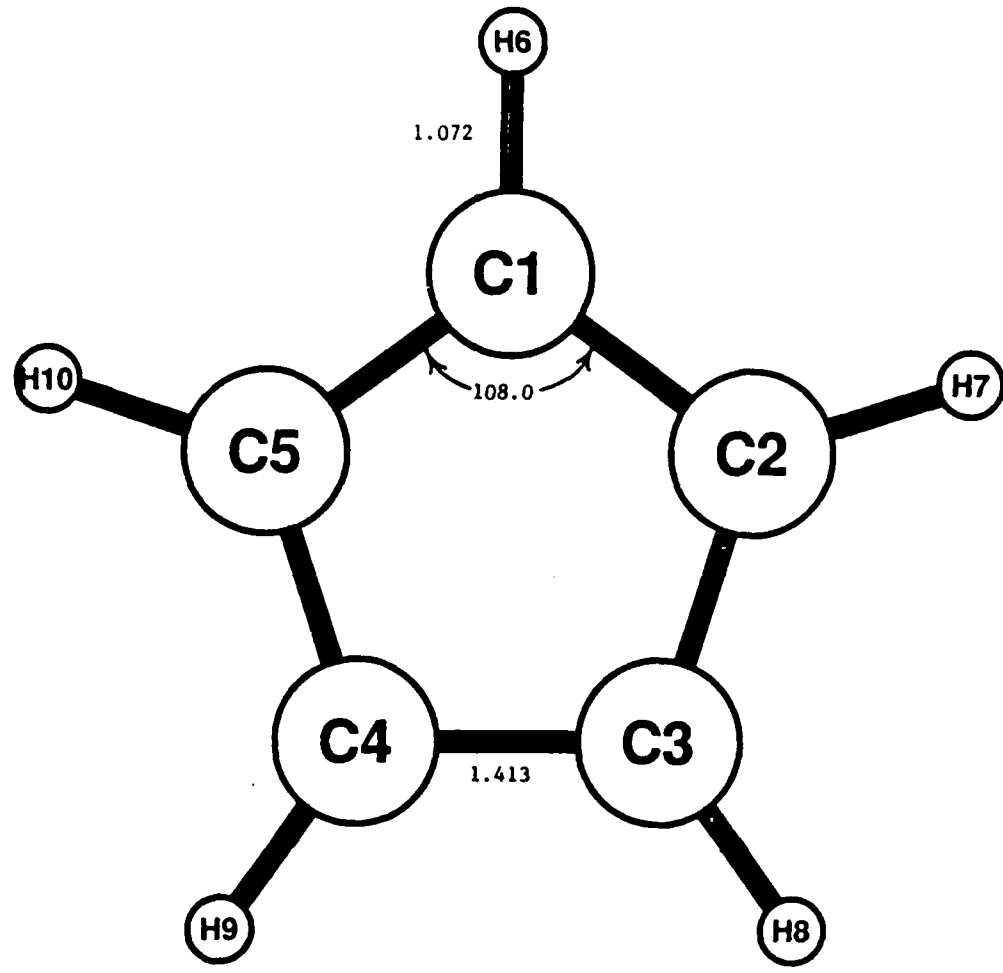


Figure 18. Structure IV.

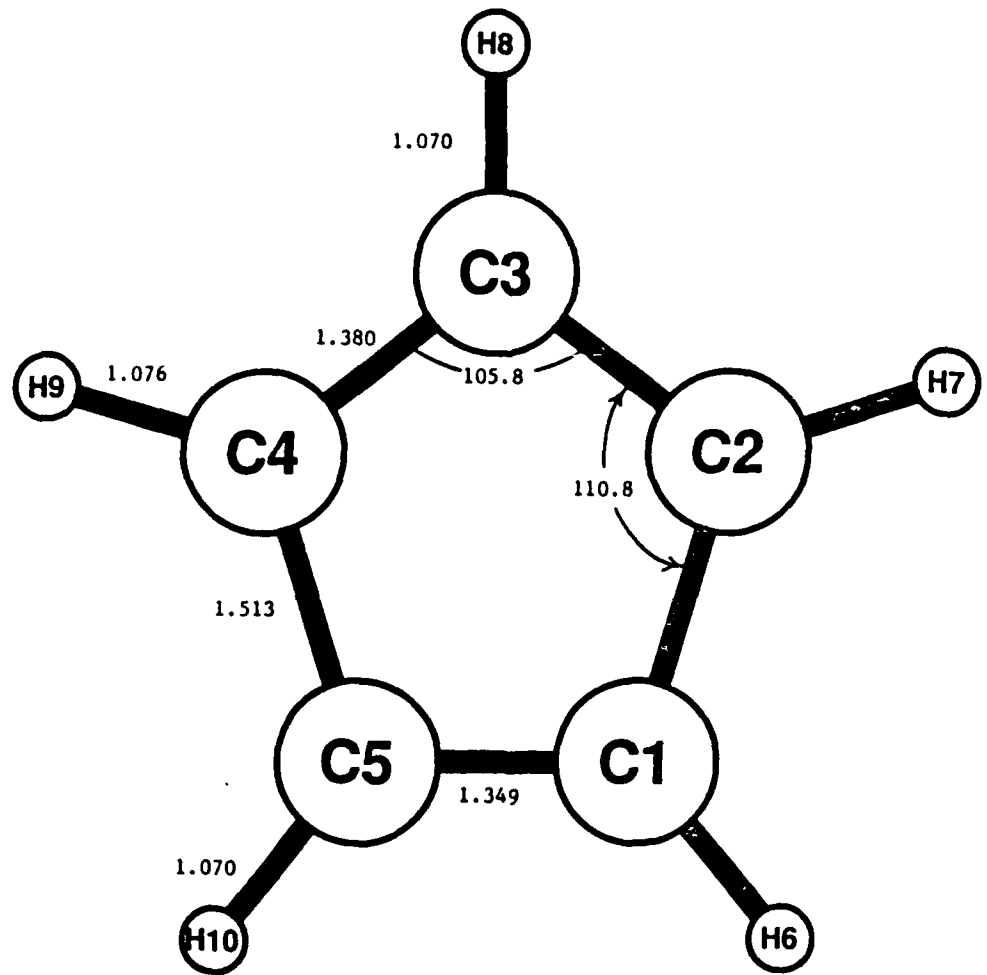


Figure 19. Structure V.

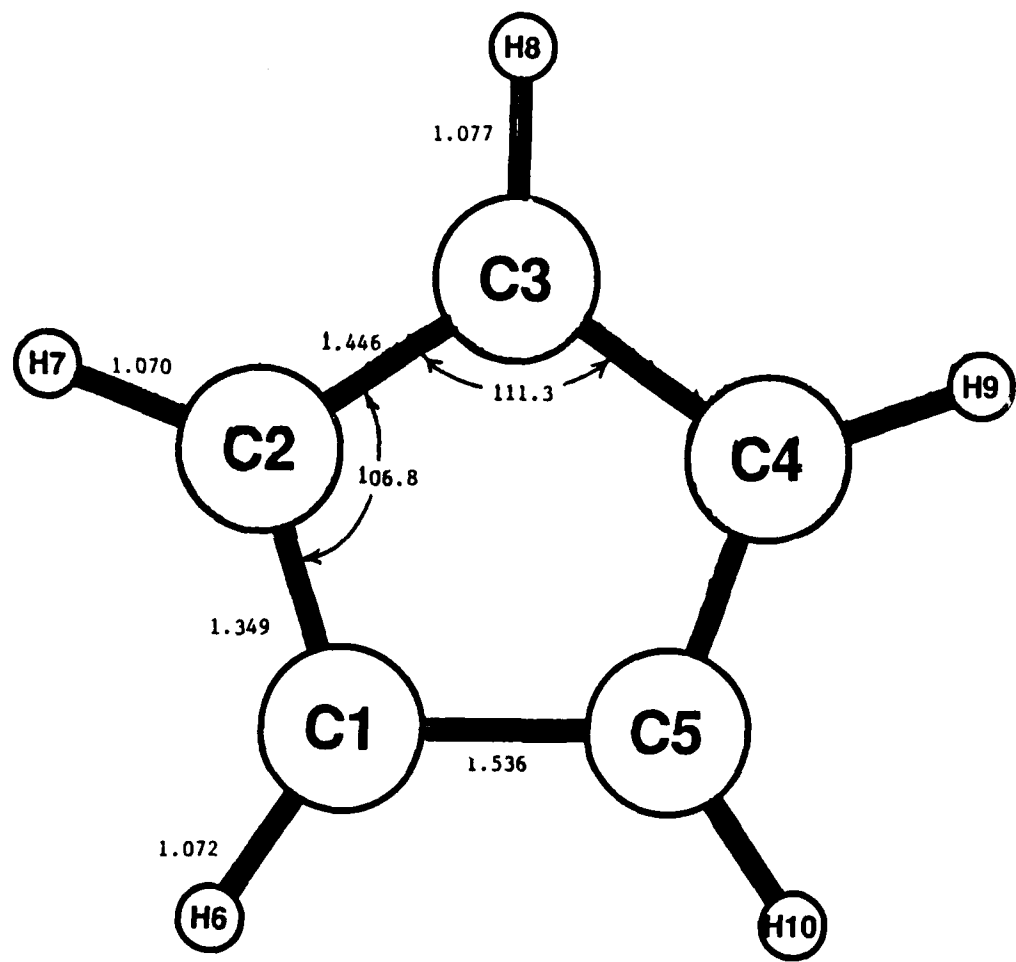


Figure 20. Structure VI.

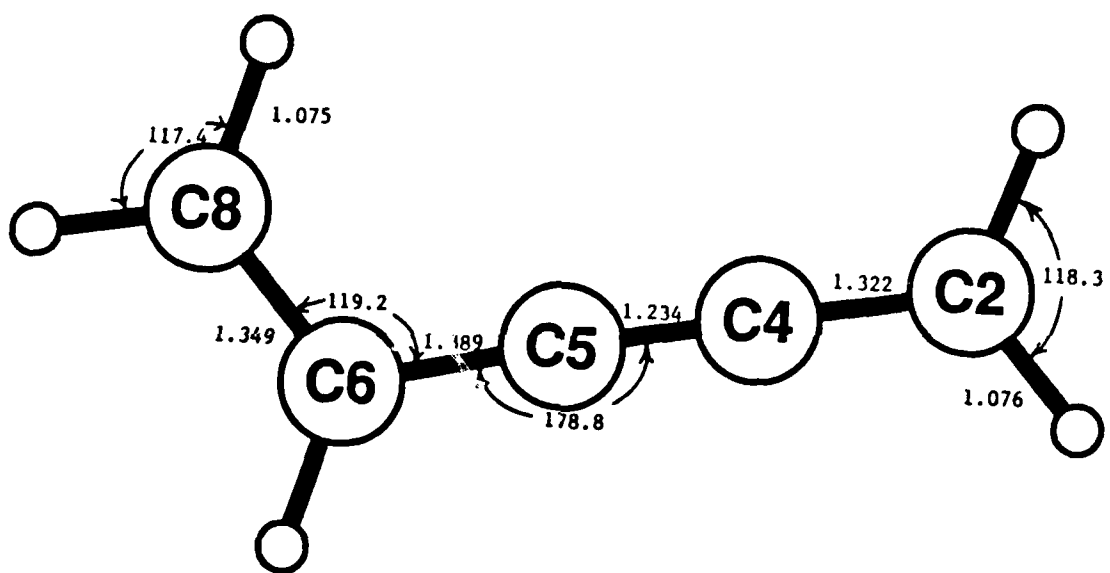


Figure 21. Structure VII.

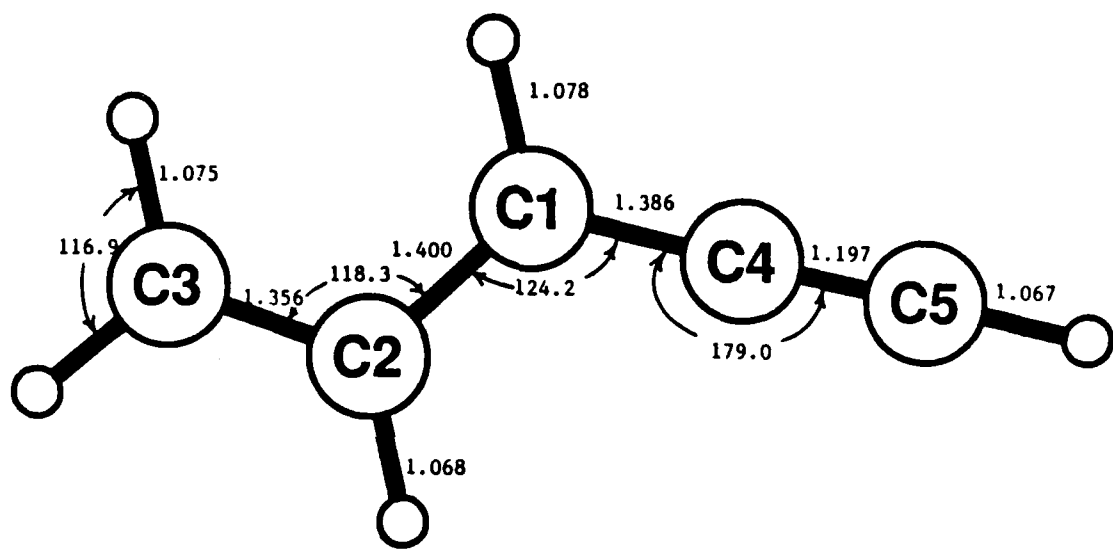


Figure 22. Structure VIII.

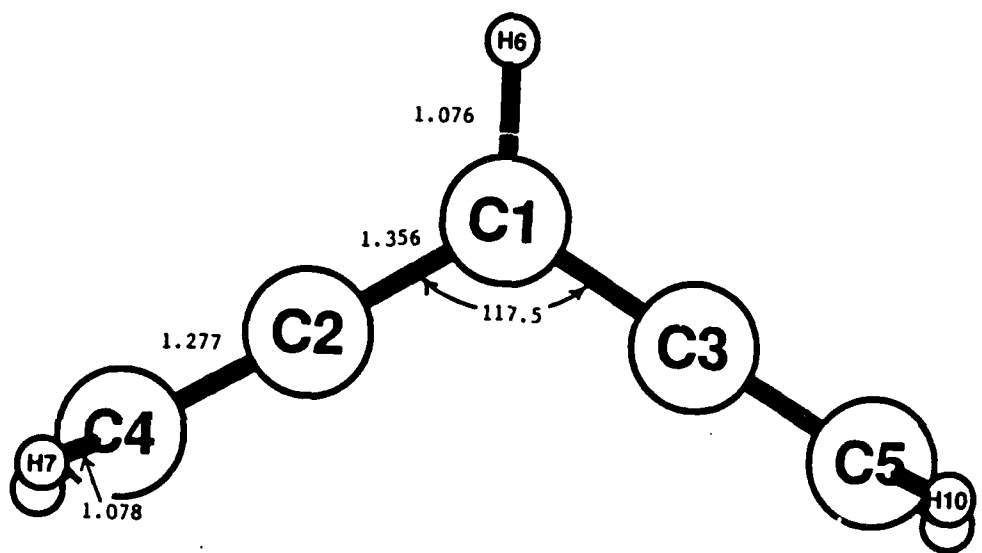
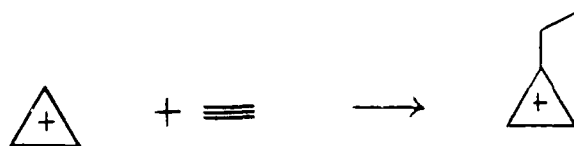


Figure 23. Structure IX.

spectroscopic values as described later.

Heats of formation of all of these species can be obtained from consideration of the following reaction:



	C ₃ H ₃ ⁺	HCCH	C ₅ H ₅ ⁺	ΔR
experiment(kcal/mol)	256±2	54.19	--	--
E(scf) (3-21G,a.u.)	-114.3296	-76.3960	-190.8140	-0.0884
E(scf) (6-31G*,a.u.)	-115.0070	-76.8178	-191.9183	-0.0935
E(scf+MP2)(6-31**//6-31G*)	-115.3694	-77.0795	-192.5468	-0.0979
0.9*E(vib)(3-21G,a.u.)	0.04382	0.02930	0.08131	0.0082
E(scf)+0.9*E(vib)(6-31**MP2)	-115.3256	-76.0502	-191.4655	-0.0897
S (cal/mol-K)	54.4	47.1	69.7	-31.8

The calculated ΔE of the reaction is -0.0897 Hartrees, or -56.3 kcal/mol. From this and the experimental heats of formation of the cyclopropenyl cation and acetylene, we estimate ΔE of formation of the vinyl-cyclopropenyl cation, structure I, to be 256.7 ± 5 kcal/mol.

Estimates for the other structures of this study can then be made utilizing the energy differences in Table 18. We remark that contributions from the zero point vibrational energy appear to make some difference in the energy of the reaction, reducing it by 5 kcal/mol. Assuming ideal gas relations, ΔH, the enthalpy of formation, can be estimated from

$$\Delta H = \Delta E - 1.98 \times 10^{-3} T \text{ (kcal/mol)} \quad (45a)$$

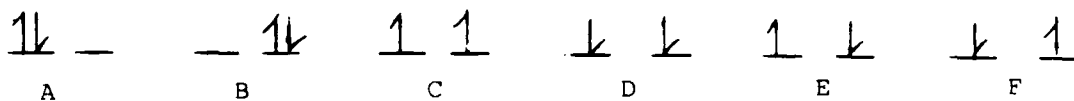
and the Gibb's Free energy of formation from

$$\begin{aligned}\Delta G &= \Delta E - 1.98 \times 10^{-3} T - 3.18 \times 10^{-2} T \\ &= \Delta E - 0.0338 T\end{aligned}\quad (45b)$$

The entropy of each species is estimated using the Sackur-Tetrode Equation (57), the calculated vibrational frequencies, and moments of inertia.

The vibrational frequencies calculated for these low lying species are reported in Table 19, and they are unscaled. Multiplication by a factor of 0.9 usually gives quite satisfactory agreement with observed vibrational frequencies. The calculated electronic spectra are reported in Table 20.

The calculation of the 5 membered cyclic forms, structures IV, V, and VI requires further comment. For the cyclic D_{5h} geometry, as with the triplet structure V, the highest occupied orbitals are degenerate, pi like and of E_{1g} symmetry. This then leads to six possible states,



The triplet state, of $^3A_{2g}$ type, has components made from $O(C)$, $O(D)$, and $(O(E) + O(F))$, where $O(A)$ is the wavefunction corresponding to diagram A above. The 1E_g state has components $(O(E) - O(F))$ and $(O(A) + O(B))$, and is subject to a first order Jahn-Teller distortion. The $^1A_{1g}$ state lies considerably higher in energy. The triplet state has perfect D_{5h} symmetry as indicated in Figure 18. Structures V and VI as reported in Figures 19 and 20 can be understood as arising chiefly from $O(A)$ and $O(B)$, and these structures are estimated from a two determinant generalized valence bond calculation.

4. Discussion

The 9 most stable $C_5H_5^+$ structures that we have examined are given in Table 18. These systems have been examined previously (59-63), and we note that a bent cyclic form of $C_5H_5^+$ is not stable relative to the planar forms, in contrast to the suggestions of Dewar and Haddon on the basis of MINDO/3

TABLE 19. CALCULATED VIBRATIONAL FREQUENCIES USING 3-21G OPTIMIZED STRUCTURES AND WAVEFUNCTIONS (cm^{-1}).

I	II	III	IV	V	VI	VII	VIII	IX
167.1	247.4	150.7	505.3	255.6	-273.9	167.8	154.1	155.9
251.6	--	358.9	--	360.2	389.9	198.4	195.4	274.7
412.1	553.9	425.1	794.4	469.0	445.9	365.4	401.7	380.9
579.5	858.6	774.2	940.9	807.2	811.5	395.3	453.5	389.7
768.1	994.4	793.2	--	895.4	825.8	554.1	622.0	574.0
804.0	--	815.9	977.4	900.1	931.9	633.0	644.1	591.5
994.1	1002.4	954.1	--	933.7	833.1	898.0	672.2	
1089.6	1003.5	1021.6	1006.1	1007.7	1005.3	846.5	1036.6	1015.8
1120.2	--	1070.6	--	1107.3	1070.6	1104.1	1038.8	1050.4
1129.8	1059.5	1104.9	1092.6	1129.8	1127.9	1181.3	1106.8	1075.5
1131.9	1152.9	1190.2	--	1158.6	1159.0	1212.8	1138.9	1106.8
1235.7	1155.3	1204.8	1290.8	1176.2	1178.2	1238.1	1211.1	1112.5
1245.9	--	1224.4	1297.7	1179.4	1213.5	1267.6	1271.0	1115.6
1335.9	1246.9	1257.8	--	1267.2	1268.6	1430.5	1359.2	1173.1
1466.4	1259.6	1306.0	1549.5	1355.0	1356.3	1469.9	1434.1	1490.6
1479.9	1295.4	1425.0	--	1429.4	1439.1	1582.0	1500.6	1522.0
1589.6	1316.7	1540.5	1566.7	1500.2	1475.0	1660.2	1642.6	1539.3
1777.3	1445.6	1610.3	1580.6	1581.4	1691.1	1721.8	1726.2	2041.0
1807.6	--	1911.6	--	1800.0	1715.9	2309.5	2308.8	2112.9
3331.7	3480.7	3331.9	3474.2	3404.1	3389.2	3298.6	3316.9	3274.4
3394.8	3489.1	3408.0	--	3404.7	3430.7	3332.6	3324.4	3279.1
3425.5	--	3410.0	3480.8	3447.6	3435.9	3380.7	3400.3	3345.3
3474.3	3509.2	3419.1	--	3465.7	3465.9	3395.9	3425.7	3360.6
3512.8	3585.9	3495.4	3688.8	3474.0	3472.2	3431.6	3594.0	3360.9

TABLE 20. CALCULATED ELECTRONIC SPECTRA, USING INDO-CI SPECTROSCOPIC METHOD FOR 6-31G* OPTIMIZED GEOMETRIES (1000 cm⁻¹). THE NUMBERS IN PARENTHESES ARE OSCILLATOR STRENGTHS.

I	II	III	IV	V	VI	VII	VIII	IX
Singlets	Singlets	Singlets	Triplets	Singlets	Singlets	Singlets	Singlets	Singlets
43.1 (0.582)	61.7 (0.177)	18.5 (0.924)	28.6 (0.000)	9.9 (0.003)	8.5 (0.004)	15.7 (0.000)	22.6 (0.000)	23.0 (0.000)
50.3 (0.080)	61.7 (0.177)	38.4 (0.006)	28.6 (0.000)	39.0 (0.005)	39.6 (0.004)	34.6 (0.762)	33.1 (0.662)	27.9 (0.000)
50.4 42.3	71.1	44.3	43.7	48.0	46.4	42.9	44.6	s3
(0.001)	(0.005)	(0.667)	(0.001)	(0.005)	(0.000)	(0.000)	(0.000)	(1.002)
55.4 (0.003)	71.1 (0.005)	48.8 (0.004)	33.7 (0.001)	49.1 (0.240)	48.9 (0.244)	46.4 (0.001)	46.6 (0.363)	48.6 (0.001)
57.2 (0.001)	49.6 (0.000)	49.0 (0.510)	50.6 (0.000)	50.3 (0.000)	50.3 (0.000)	46.5 (0.476)	47.8 (0.000)	53.6 (0.009)
58.3 (0.000)	59.6 (0.000)	49.0 (0.510)	50.8 (0.000)	50.5 (0.000)	54.0 (0.000)	54.0 (0.0010)	53.3 (0.002)	53.7 (0.361)
		49.7 (0.004)	51.6 (0.000)	51.6 (0.000)	54.1 (0.002)			
Triplets	Triplets	Triplets	Singlets	Triplets	Triplets	Triplets	Triplets	Triplets
20.8 36.4	50.2 50.2	12.6 16.2	2.3 2.3	1.1 22.6	0.0 21.5	13.4 15.1	16.7 20.2	20.3 22.1
42.4 47.3	65.1 65.1	34.2 35.9	18.5 48.7	30.7 36.6	30.2 37.3	25.4 27.3	29.9 32.1	23.4 25.0
49.8 53.1	42.1	48.7 50.2	40.6 45.4	39.0 44.5	40.9 42.1	40.9 42.1	39.0 41.3	26.3 39.9
55.9			53.4 53.8		43.8			39.9

calculations (62). Similarly, much speculation has focused on the stability of the pyramidal form of $C_5H_5^+$, structure II, postulated to lie lowest on the surface by Stohrer and Hoffmann some time ago (59). Although this is most certainly a stable structure, as indicated by the reported force field of Table 19, it is far from our most stable singlet structure I, estimated to lie 12.9 kcal/mol lower in energy. This is a value similar to that reported by Kohler and Lischka (63), but an estimate of theirs using the CEPA method predicts the square based pyramid lower than the cyclic form by 24 kcal/mol. Although the differential correlation energy does seem to favor structure II more than structure IV, this is only by about 19 kcal/mol. Although we do not believe that structure II is lowest in energy, it is a well defined structure, and judging from our calculated force constants, stable to tautomerization. Experimentally this form has been reported to exist in solution (64,65).

SECTION III

EXPERIMENTAL STUDIES

A. INTRODUCTION

A Nicolet FTMS-1000 Fourier transform ion cyclotron resonance (FTICR) mass spectrometer with a superconducting magnet of fixed magnetic field (3.0 tesla) was used for the work reported here. Basic principles of the technique and its applications in ion/molecule reaction studies have been reviewed in several recent articles (66-68). Reaction pathways were delineated using the ejection capabilities (69) of FTICR which make it possible to eject one ion from a complicated reaction mixture to determine its contribution to the mass spectrum of all the other ions.

For studies of ion spectroscopy, a Quantel Nd:YAG-pumped dye laser system was used. Photodissociation of ions trapped in the FTICR analyzer cell was followed as a function of laser wavelength. Light from the laser was brought through sapphire windows into the mass spectrometer vacuum chamber, and entered and exited the analyzer cell through Cu mesh-covered holes in the cell plates.

B. EXPERIMENTAL METHODS

Reaction rate coefficients were determined by monitoring the intensity of the $C_xH_y^+$ ions as a function of time (typically at least 2 seconds) after ejection of all other ions from the analyzer cell. Neutral gas pressures were measured with an ionization gauge. Ionization gauge readings were then corrected by constructing calibration curves of ionization gauge versus capacitance manometer (MKS-Baratron) readings in the 1×10^{-6} to 1×10^{-4} torr range. A correction factor was required because the ionization gauge and capacitance manometer were located at different points on the vacuum system, somewhat removed from the FTICR analyzer cell. This was obtained by determining the rate coefficient of a well-studied reaction ($C_2H_4^+ + C_2H_4 \rightarrow$ products, $k_{\text{average}} = (1.0 \pm 0.3) \times 10^{-9} \text{ cm}^3/\text{s}$)¹⁰ (70-74), where the ionization gauge pressure readings were corrected using the capacitance manometer. This

experimentally determined rate coefficient was then compared with the average of published values (70,74) and the ratio of the published value to the measured, which was 3.3 ± 1.1^{11} was used as a correction factor. This factor was used in calculating the absolute rate coefficients given in this report. All calculations of rate coefficients and 95 percent confidence limits were performed using a menu-driven FORTRAN computer program.

Reactive and non-reactive $C_3H_3^+$ ions were produced by charge transfer reactions of various precursors with Xe^+ , formed with an electron beam pulse of 5 ms duration at an ionizing electron energy of about 15 eV. Propargyl iodide was used as a precursor for $C_3H_3^+$ in studies of the reaction of this ion with acetylene, deuterated acetylene, and diacetylene. A number of different precursors (propargyl iodide, propargyl bromide, propargyl chloride, propyne and allene) were used to investigate the reaction mechanisms leading to $C_5H_5^+$ ion formation. In some studies $C_3H_3^+$ ions were produced directly from the above-mentioned precursors by electron impact to compare the effect of ionization technique on the ratio of reactive to unreactive isomers.

Propargyl iodide was prepared from propargyl chloride by a halogen exchange reaction (75). The details of purification are given elsewhere (76). Propargyl chloride, propargyl bromide, allene, propyne and acetylene were obtained commercially and their purity was checked by obtaining wide mass range spectra. In the case of acetylene, some production of protonated acetone was observed at long delay times indicating the presence of a small amount of acetone as an impurity. Propargyl bromide was distilled before use in order to remove toluene which was present as a stabilizing agent. Deuterated acetylene was prepared from D_2O and CaC_2 . Diacetylene was prepared by the method of dehydrochlorination of 1,4-dichloro-3-butyne in aqueous potassium hydroxide/dioxane solution (77).

$C_5H_3^+$ ions were produced from 50 eV electron ionization of 2,4-hexadiyne and by the reaction of $C_3H_3^+$ with diacetylene. $C_3H_3^+$ ions used to produce $C_5H_3^+$ were formed by Xe^+ charge transfer reactions with propargyl iodide at an ionizing energy of 15 eV. After 30 ms reaction time with C_4H_2 , all the other ions except $C_5H_3^+$ were ejected from the cell to follow the reactions of this ion with diacetylene as a function of time. $C_5H_5^+$ ions were produced by

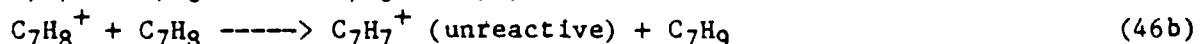
charge transfer reactions of various precursors (dicyclopentadiene, cyclopentadiene, norbornadiene, 1-penten-3-yne, cycloheptatriene) with different charge transfer agents (Xe^+ , N_2^+ , Ar^+) formed with an electron beam pulse of 5 ms duration at ionizing energies of 13, 16.5, and 20 eV, respectively.

Cyclopentadiene was prepared by cracking dicyclopentadiene (78) and was kept in dry ice when not used to prevent the dimerization process. All the other compounds used were obtained commercially and their purity was checked by obtaining wide mass range spectra. All the samples were used after multiple freeze-pump-thaw cycles.

All C_5H_3^+ and C_5H_5^+ reactions were followed at a cell temperature of 363 K. C_5H_3^+ and C_5H_5^+ ions used in rate constant determination studies were all produced by charge transfer chemical ionization using the lowest possible ionization energy in order to minimize the internal energy imparted to the ions. Also, since the total pressure in the reaction cell was almost 1×10^{-5} torr and the charge transfer time was 100 ms, substantial collisional relaxation of the ions took place before kinetic data were collected.

C_7H_7^+ ions were produced from toluene, cycloheptatriene and norbornadiene by dissociative charge transfer. Percentages of reactive/unreactive isomers were determined when the three neutrals above reacted with different charge transfer agents (C_4H_2^+ , Xe^+ , Kr^+ and Ar^+) formed with an electron beam pulse of 5ms duration at ionizing energies of 11.5, 13, 15, and 20eV, respectively. To do this, all ions except C_7H_7^+ were ejected from the cell and enough reaction time (typically 3s) at the pressures used (typically 10^{-6} - 10^{-5} torr) was allowed so that the reactive structures could be lost via ion/molecule reactions, thus leaving an unreactive population.

As reported earlier (79,80), with cycloheptatriene unreactive C_7H_7^+ is formed as a function of reaction time due ion/molecule Reactions (46a) and (46b). The above approach thus required some adjustments in the experimental sequence to obtain accurate percentages of C_7H_7^+ populations.



At long reaction times $C_7H_8^+$ was ejected continuously during the reaction time in order to avoid Reaction 46b.

C. REACTIONS OF $C_3H_3^+$ WITH ACETYLENE AND DIACETYLENE

1. Introduction

As discussed in Section II, of the many possible $C_3H_3^+$ isomers, two are most important in assessing the role of $C_3H_3^+$ in ion/molecule reaction mechanisms. The first is the cyclopropenylum ion, recognized as the most stable isomer, and the second is the linear propargylium ion.

The importance of different precursors in affecting the reactivity of $C_3H_3^+$ ions was reported in a thermochemical study by Holmes and Lossing (81). In an ICR study of $C_3H_3^+$ reactions, Ausloos and Lias (82) showed that significant fractions of the linear isomer can be produced by charge transfer reactions of small ions (Ar^+ , Xe^+ , CO^+ , Ne^+ , etc.) with propargyl chloride and bromide. Later it was reported (76) that even higher proportions of the propargylium isomer can be obtained with propargyl iodide either by electron impact or charge exchange using Xe^+ .

A study by Smyth et al. (43) demonstrated that the cyclopropenylum ion was relatively unreactive toward simple hydrocarbon fuels whereas the linear, propargylium ion was quite reactive. In particular, the reaction of propargylium ions with acetylene was reported to produce $C_5H_3^+$ and $C_5H_5^+$ ions with an overall $C_3H_3^+$ disappearance rate coefficient of $1 \times 10^{-9} \text{ cm}^3/\text{s}$. Since this sequence of reactions is critical in the initial stages of the postulated ion/molecule mechanism of soot formation, it was studied as a part of the work carried out under this contract. Results substantially different from those reported earlier were found and the study was expanded to investigate possible production of $C_5H_5^+$ ions from ionic sources other than $C_3H_3^+$. Reactions of propargylium ions with C_2D_2 were also studied in order to delineate further a proposed mechanism for the $C_3H_3^+$ /acetylene reaction.

Diacetylene is another important flame neutral which has been postulated to react with $C_3H_3^+$ ions in an ion/molecule soot formation mechanism (14a).

Reaction pathways and the rate coefficient for the reaction of propargylium ions with diacetylene near room temperature were thus also investigated. In this Section, results for the reactions of $C_3H_3^+$ ions with acetylene, deuterated acetylene, and diacetylene are reported and discussed in relation to previous work involving $C_3H_3^+$ Reactions (43,76,82) and the proposed (14a,b) ionic route to soot formation.

2. Results

a. $C_3H_3^+$ reactions with acetylene.

Despite an earlier report (43) that linear $C_3H_3^+$ is quite reactive with acetylene, only very low intensities of $C_5H_3^+$ and $C_5H_5^+$ produced via this reaction could be found in this work. Experimental conditions of the earlier study were duplicated as closely as possible, and then varied substantially with respect to relative pressures of neutrals (C_2H_2/C_3H_3I ratio = 1 to 8) and overall system pressure (from 5×10^{-7} to 3×10^{-5} torr). $C_3H_3^+$ ions were formed from propargyl chloride, bromide, and iodide by both charge transfer using Xe^+ and electron impact. In order to determine other possible sources of $C_5H_5^+$ observed under the earlier reaction conditions, binary mixtures of acetylene and each one of the $C_3H_3^+$ precursors reported (43,76,82) earlier were used. Intensities of $C_5H_5^+$ and $C_5H_3^+$ were first measured after a 125 ms reaction time. Then the parent ion, $C_2H_2^+$, and $C_3H_3^+$ were each ejected separately during the 125 ms reaction period to assess their contribution to $C_5H_5^+$ and $C_5H_3^+$ formation.

For each different neutral precursor, the sources and amounts of $C_5H_5^+$ ions produced were found to be different. Propyne and allene were similar in producing large amounts of $C_5H_5^+$ and no $C_5H_3^+$ ion. However, the $C_3H_3^+ + C_2H_2$ reaction was not responsible for $C_5H_5^+$ formation. The main reactions leading to $C_5H_5^+$ were



and



in both cases. On the other hand, when propargyl iodide, propargyl bromide and propargyl chloride were used as precursors, relatively smaller amounts of C_5H_5^+ ions were observed, but C_5H_3^+ ions were also formed. In the propargyl chloride case



and



were the major reactions leading to C_5H_5^+ formation. For propargyl bromide the



reaction was the only source of C_5H_5^+ ions observed. Any contribution to C_5H_5^+ formation from linear C_3H_3^+ was less than the experimental uncertainty. Finally, very little (almost negligible) amounts of C_5H_5^+ ions were observed when propargyl iodide was used as a precursor. The reactions



and



were the major contributors in this case. An upper limit for the rate constant for Reaction (53) was estimated as $5 \times 10^{-12} \text{ cm}^3/\text{s}$ by assuming that the very small C_5H_5^+ signal observed resulted from this reaction, and using the expression $[\text{C}_3\text{H}_3^+](t) = [\text{C}_3\text{H}_3^+]_0 - [\text{C}_5\text{H}_5^+](t) = [\text{C}_3\text{H}_3^+]_0 e^{-nkt}$, where n is the C_2H_2 number density. Overall results for the production of C_5H_5^+ and C_5H_3^+ ions with different neutrals which have been reported (43,76,82) as precursors of C_3H_3^+ are summarized in Table 21.

TABLE 21. PRODUCTION OF $C_5H_5^+$ AND $C_5H_3^+$ IONS IN MIXTURES OF VARIOUS NEUTRALS AND ACETYLENE.

Neutral	Ionic sources ^b of $C_5H_5^+$ after Xe^+ charge transfer ionization of a mixture of the neutral and acetylene	Ratio of $C_5H_5^+$ prod. relative to that in allene case ^c	Ionic sources ^b of $C_5H_3^+$	Intensity of $C_5H_5^+$ vs. $C_5H_3^+$	Percent reactive $C_3H_3^+$ ions
Allene	$C_2H_2^+(40\%)$ $C_3H_4^+(60\%)$	1.0	-	-	<5
Propyne	$C_2H_2^+(40\%)$ $C_3H_4^+(60\%)$	0.75	-	-	30
Propargyl chloride	$C_2H_2^+(40-50\%)$ $C_3H_3Cl^+(50-60\%)$	0.25	$C_3H_3Cl^+(20\%)$ $C_3H_3^+(20\%)$ $C_2H_2^+(60\%)$	3.0	15
Propargyl bromide	$C_3H_3Br^+(90-100\%)$	0.08	$C_2H_2^+(70\%)$ $[C_3H_3^+ +$ $C_3H_3Br^+](30\%)$	2.0	85
Propargyl iodide	$C_2H_2^+(40\%)$ $C_3H_3^+(60\%)$	<0.02	$C_2H_2^+(50\%)$ $C_3H_3^+(50\%)$	1.7	90

^a All ions were produced by chemical ionization charge transfer from Xe^+ .

^b Percentages show the relative contributions to $C_5H_5^+$ and $C_5H_3^+$ production as determined by double resonance experiments and have an estimated uncertainty of $\pm 10\%$.

^c Neutral reactants all had the same pressure (7×10^{-7} torr) as measured by the ionization gauge. Xenon and acetylene pressures were 5.6×10^{-6} and 1.8×10^{-6} torr, respectively.

Because propargyl iodide produced the highest reactive/unreactive ratio of $C_3H_3^+$ ions both in earlier (76,81) and the present work (see Table 22), it was

TABLE 22. PERCENTAGES^a OF REACTIVE $C_3H_3^+$ FOUND FROM VARIOUS PRECURSORS BY VARIOUS IONIZATION TECHNIQUES (MONITORED BY OBSERVING REACTION WITH THE PRECURSOR NEUTRAL).

Ionizing technique	Precursor		
	Propargyl iodide	Propargyl bromide	Propargyl chloride
Electron impact (15 eV)	90%	40%	10%
Chemical ionization charge transfer with Xe^+	90%	85%	15%

^a Estimated error is $\pm 5\%$.

used as a precursor for $C_3H_3^+$ ions in these reaction kinetics studies. Since the precursor neutral molecule was always present in the FTICR analyzer cell, it was a competitor with the reactant neutral of interest in ion/ molecule reactions involving $C_3H_3^+$. To determine the rate coefficient of reactions of $C_3H_3^+$ with the neutral reactant, it was necessary to monitor the reactions of this ion with C_3H_3I and subtract the rate coefficient for this reaction from the total rate coefficient observed in the presence of both the precursor neutral and the reactant of interest. Reactions of $C_3H_3^+$ with propargyl iodide were monitored as a function of time following charge transfer chemical ionization of C_3H_3I by Xe^+ and ejection of all ions but $C_3H_3^+$ from the analyzer cell. Results obtained were identical to $C_3H_3^+$ reaction channels with propargyl iodide which have been reported elsewhere (76).

b. Isomerization of linear $C_3H_3^+$.

In addition to the absence of any significant $C_5H_3^+$ and $C_5H_5^+$ formed by reaction of linear $C_3H_3^+$ with C_2H_2 , it was also observed that C_2H_2

led to the isomerization of linear $C_3H_3^+$ ions to their cyclic form, thus rendering them unreactive toward their parent neutral (C_3H_3I) as well as toward C_2H_2 . This isomerization was followed as a function of C_2H_2 pressure and a direct pressure dependence was found, as shown in Figure 24.

c. $C_3H_3^+$ reactions with C_2D_2 .

To achieve a better understanding of the isomerization of linear $C_3H_3^+$, C_2D_2 instead of C_2H_2 was used as the neutral reactant. The following isotope exchange reactions were observed.



Using FTICR ejection capabilities, it was found that reactions (55) and (56) contribute equally to the production of $C_3HD_2^+$ while reaction (58) produces more of $C_3D_3^+$ (80 percent) than reaction (57) (20 percent).

Ion intensity versus time curves for the $C_3H_3^+/C_2D_2$ reaction are shown in Figure 25. The overall rate coefficient for the disappearance of $C_3H_3^+$ was calculated by subtracting the observed rate coefficient for the reaction with propargyl iodide from the total observed rate coefficient in the presence of C_2D_2 . This observed rate coefficient was then converted to the true rate coefficient using the corrected pressure of C_2D_2 . A value of $(4.5 \pm 1.9) \times 10^{-10} \text{ cm}^3/\text{s}$ was found at a cell temperature of 373 K for the disappearance of $C_3H_3^+$ (reactions (54) and (55)). In Figure 26, ion intensity versus time curves of $C_3H_3^+$ are compared for reactions with and without C_2D_2 .

d. $C_3H_3^+$ reactions with diacetylene

After ejection of all ions except $C_3H_3^+$ following charge transfer chemical ionization by Xe^+ of a mixture of diacetylene and propargyl iodide, the ion/molecule reactions as a function of time were monitored. Consecutive

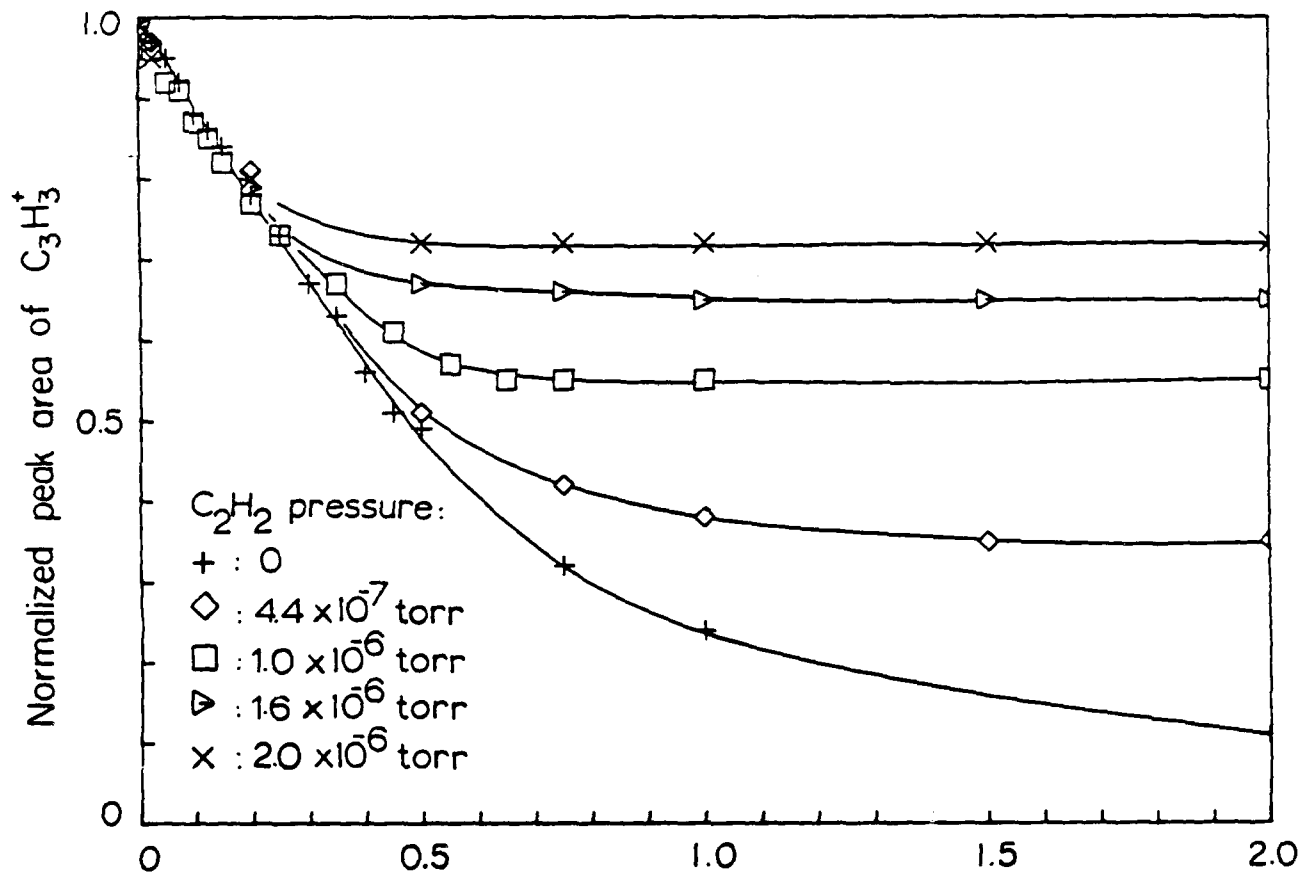


Figure 24. Isomerization of Linear C_3H_3^+ Ions at Different Pressures of C_2H_2 . C_3H_3^+ ions were produced by charge transfer reactions with Xe^+ . $p_{\text{C}_3\text{H}_3\text{I}} = 1.1 \times 10^{-7}$ torr; p_{Xe} was adjusted to maintain a constant total pressure of 2.6×10^{-6} torr as measured on the ionization gauge. (All pressures are capacitance-manometer corrected.)

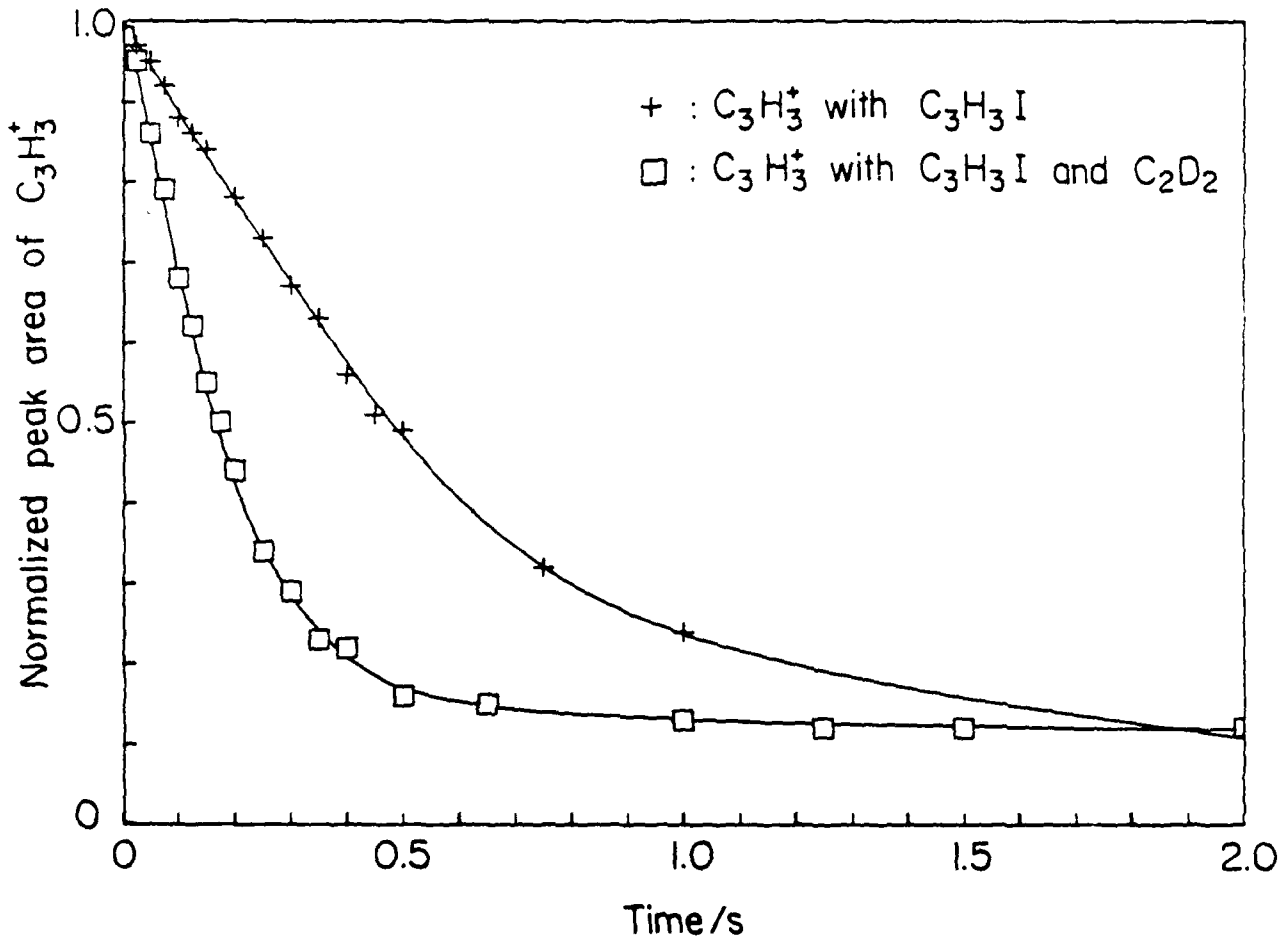


Figure 25. Isotope Exchange Reactions of C_3H_3^+ with C_2D_2 . Disappearance of C_3H_3^+ ion includes reactions with propargyl iodide. Note that the sum of all isotopic forms of C_3H_3^+ remaining at the end of the reaction with C_2D_2 approximately equals the total unreactive C_3H_3^+ when C_2H_2 is used as a neutral reactant at the same pressure (see Figure 24). $p_{\text{C}_3\text{H}_3\text{I}} = 1.1 \times 10^{-7}$ torr; $p_{\text{C}_2\text{D}_2} = 1.2 \times 10^{-6}$ torr; $p_{\text{Xe}} = 6.2 \times 10^{-6}$ torr.

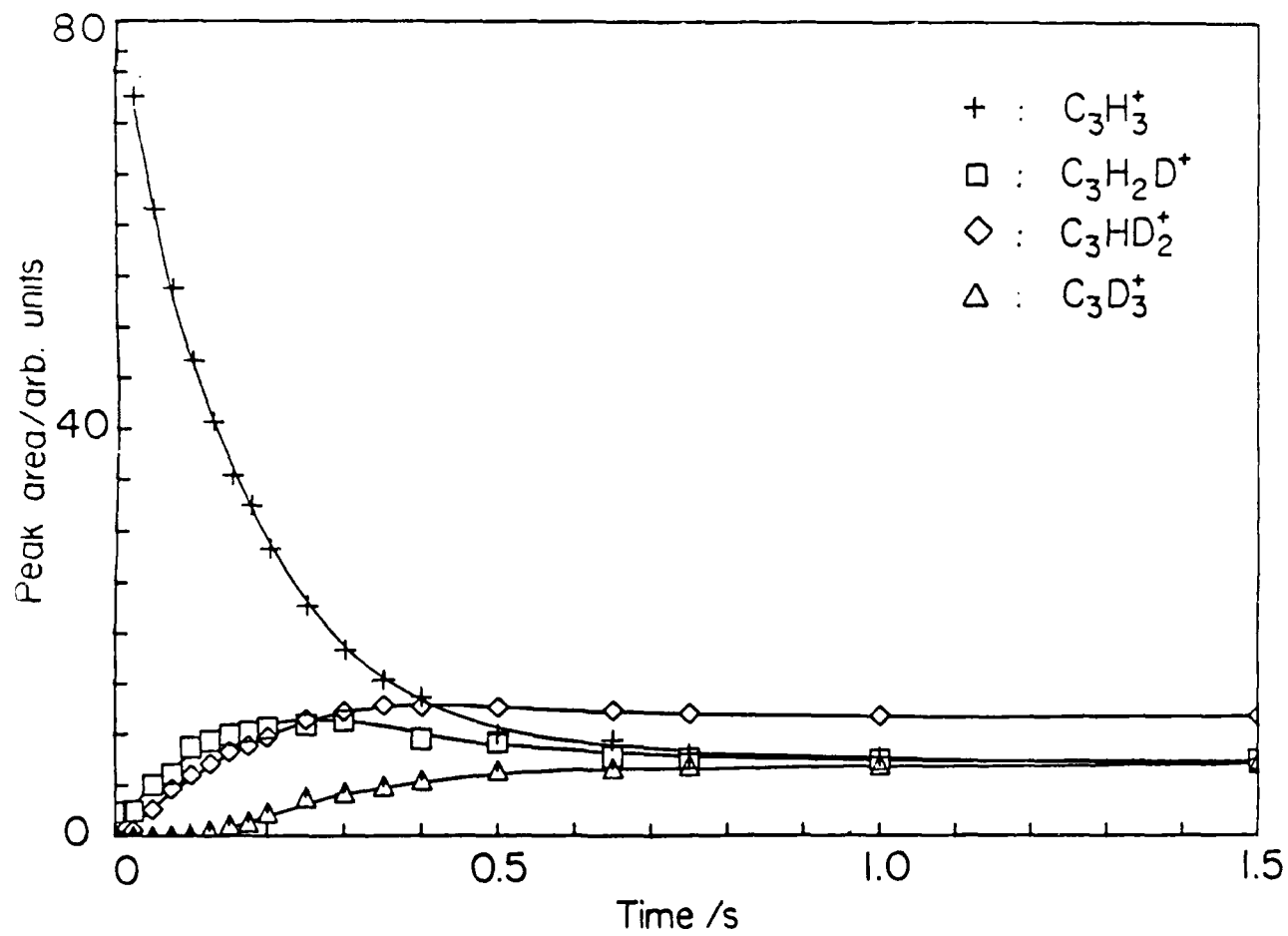
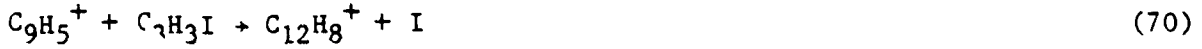


Figure 26. C_3H_3^+ Ion Decay Curves for Reaction with $\text{C}_3\text{H}_3\text{I}$ and C_2D_2 .
(Pressures are the same as given for Figure 25.)

C_2 and C_4H_2 addition reactions were observed:



Some of these product ions were seen to react further with propargyl iodide by displacement of atomic iodine:



Ion intensity versus time curves for the $C_3H_3^+/C_4H_2$ reaction are shown in Figure 27. The rate coefficient for the disappearance of $C_3H_3^+$ (Reactions (59) and (60), Figure 28) was calculated as described earlier, and a value of $k = (1.4 \pm 0.7) \times 10^{-9} \text{ cm}^3/\text{s}$ was found.

Propargyl iodide, bromide, and chloride were all used as precursors of $C_3H_3^+$ in studying its reactions with diacetylene. For each precursor, both electron impact and charge transfer chemical ionization techniques were used. The percentages of reactive isomer in the reaction with diacetylene are shown in Table 23. When these percentages of reactive isomer were compared to those in the absence of C_4H_2 (see Table 22), it was clear that some isomerization of the reactive linear $C_3H_3^+$ ion, as well as Reactions (59) and (60), had taken place (see also Figure 5). This isomerization was followed as a function of C_4H_2 pressure and a direct pressure dependence was found, as can be seen in Table 24.

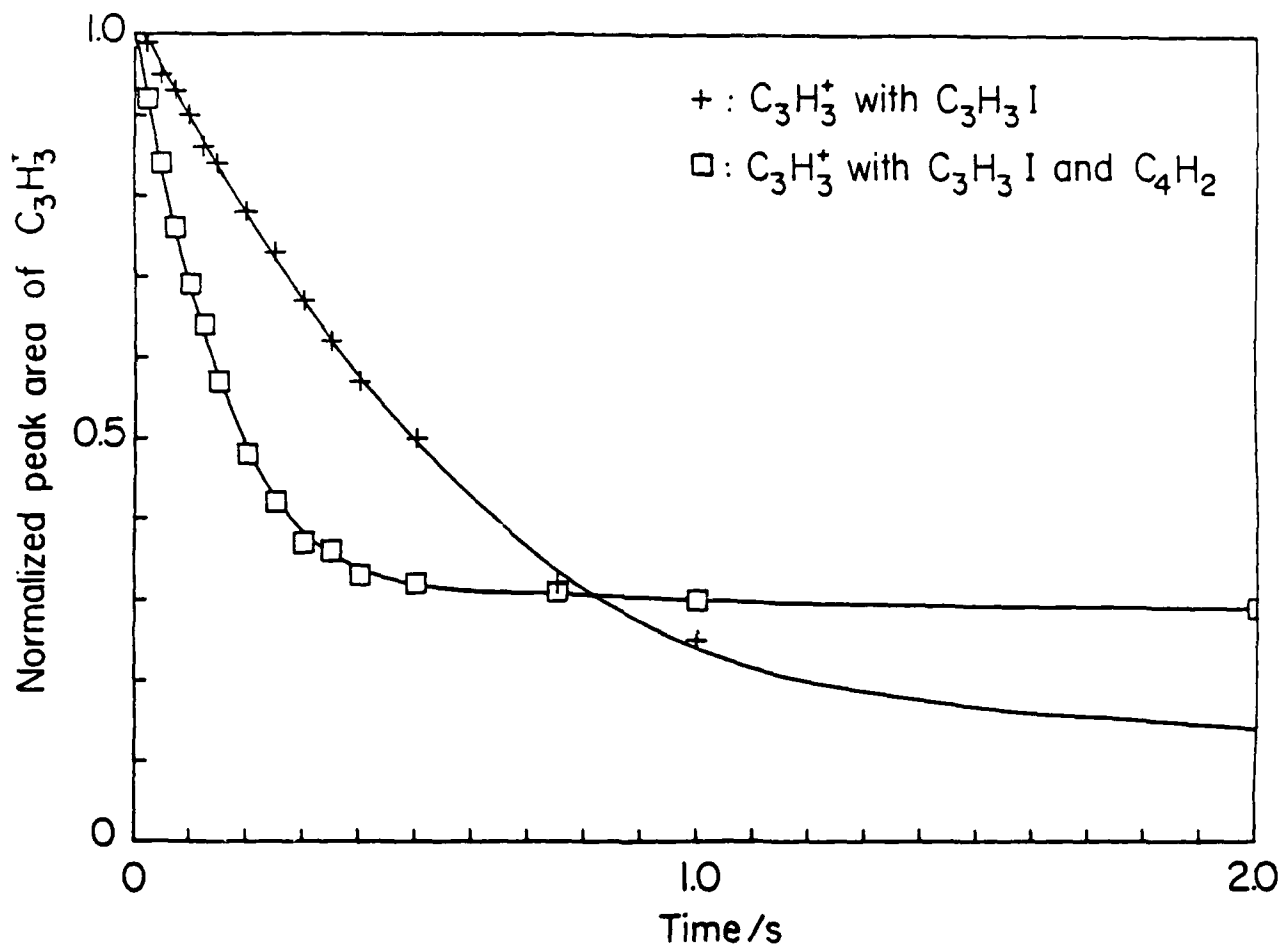


Figure 27. Reactions of C_3H_3^+ with C_4H_2 . Disappearance of C_3H_3^+ and product ions include reactions with propargyl iodide. $p_{\text{C}_3\text{H}_3\text{I}} = 1.1 \times 10^{-7}$ torr; $p_{\text{C}_4\text{H}_2} = 4.8 \times 10^{-7}$ torr; $p_{\text{Xe}} = 6.2 \times 10^{-6}$ torr. (All pressures are capacitance-manometer corrected.)

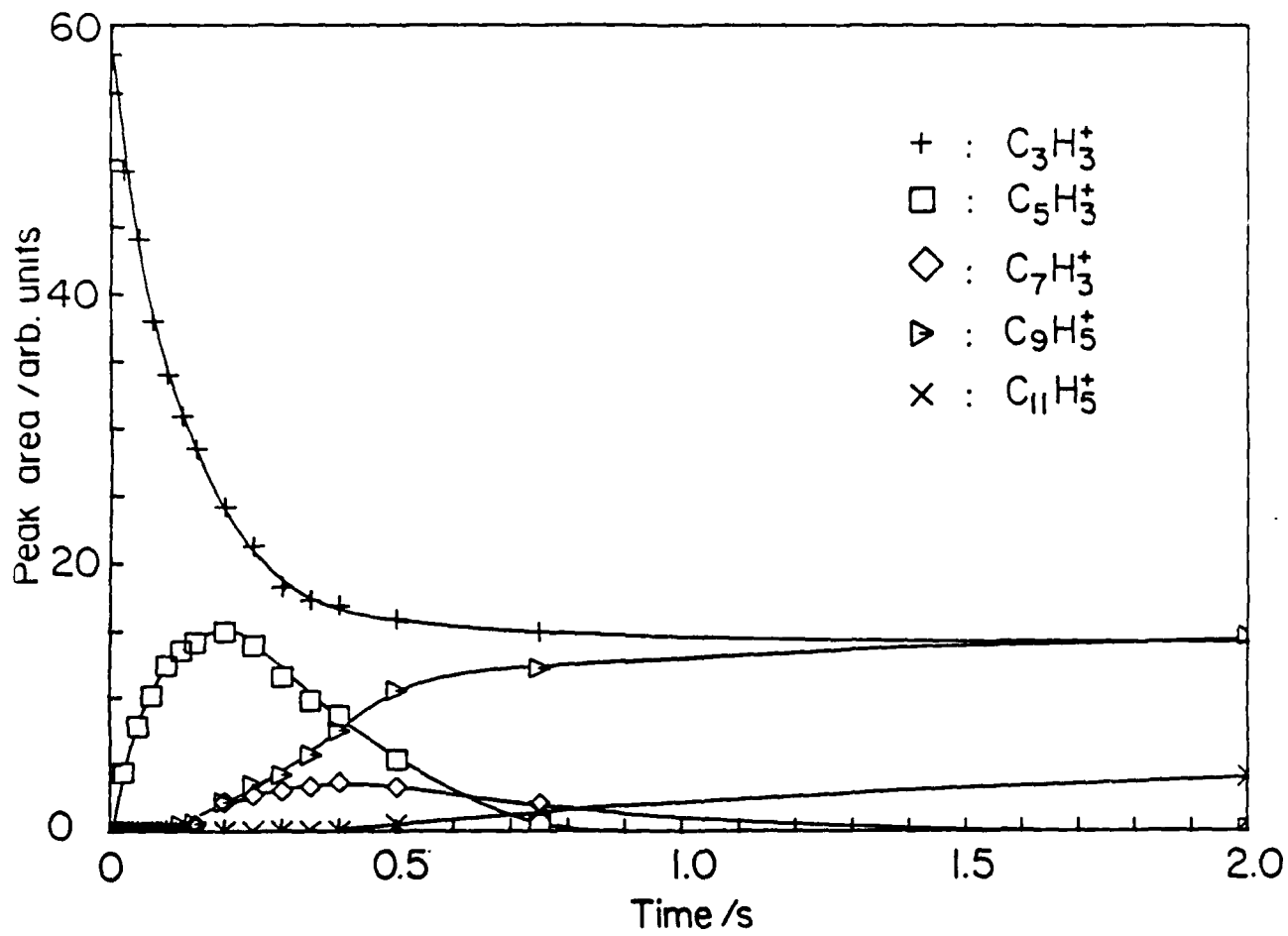


Figure 28. C_3H_3^+ Decay Curves for the Reactions with $\text{C}_3\text{H}_3\text{I}$ and C_4H_2 .
(Pressures are the same as given for Figure 27.)

TABLE 23. PERCENTAGES^a OF REACTIVE $C_3H_3^+$ OBSERVED IN THE REACTION WITH C_4H_2 .^b

Ionization technique	Precursor		
	Propargyl iodide	Propargyl bromide	Propargyl chloride
Electron impact (15 ev)	75%	30%	5%
Charge transfer by Xe^+	75%	65%	5%

^a Estimated error is $\pm 5\%$.

^b $P_{C_4H_2} = 4.8 \times 10^{-7}$ torr.

TABLE 24. CHANGES IN $C_3H_3^+$ REACTIVITY^a AT DIFFERENT PRESSURES OF DIACETYLENE.

Pressure of $C_4H_2/10^{-7}$ torr	% of unreactive $C_3H_3^+$
0.8	16
1.6	17
4.8	25
7.2	32
8.0	35
9.6	40

^a $1-C_3H_3^+$ ions were produced from propargyl iodide by chemical ionization charge transfer with Xe^+ . ($P_{C_3H_3I} = 1.1 \times 10^{-7}$ torr; P_{Xe} was adjusted to maintain a constant total pressure of 2.6×10^{-6} torr as read on the ionization gauge).

^b All pressures are capacitance-manometer corrected.

3. Discussion

Although the results of this work are not in agreement with the earlier report (43) of $C_3H_3^+$ /C₂H₂ reactivity, the discrepancy is probably due to limitations of the older pulsed ICR (43) instrumentation for studying ion/molecule reaction pathways in complicated systems when compared to newer FTICR capabilities. Facile ejection of all ions, except the one whose ion/molecule reactions are being investigated, offers a very clean monitoring opportunity for product-parent relationships even in complicated consecutive and competitive reaction systems. Various alternative pathways for the production of $C_5H_3^+$ and $C_5H_5^+$ which have been described above probably contributed significantly to the intensities of these ions seen in the earlier work. Additional support for the low reactivity of $C_3H_3^+$ with C₂H₂ is found in a recent report (83) in which the rate coefficient for this reaction is reported to be less than $0.01 \times 10^{-9} \text{ cm}^3/\text{s}$, although the isomeric form of $C_3H_3^+$ is not given. It is also possible that the highest pressures used in this work did not reach those of the earlier study (43). Higher pressures might lead to third-body stabilization of $C_5H_5^+$ collision complexes.

The most likely mechanism of the observed isomerization of $C_3H_3^+$ ions by collisions with acetylene is a "reactive" rather than a "nonreactive" one. That is, it results from an intimate encounter of the ion and neutral in the $C_5H_5^+$ collision complex. This hypothesis is confirmed by the fact that deuterated forms of $C_3H_3^+$ were produced when C₂D₂ was the neutral reactant (see Figure 26). In most cases the $C_5H_5^+$ collision complex dissociates to give the cyclic, unreactive $C_3H_3^+$ isomer, instead of the linear form. The possibility of non-reactive collisional isomerization of linear $C_3H_3^+$ to the cyclic isomer has been ruled out because experiments at elevated pressures of xenon (to ca. $1 \times 10^{-5} \text{ torr}$) showed no interconversion. Similar interconversion of $C_4H_4^+$ ions from a linear to cyclic form has also been reported (84) in the reaction with C₂H₂ and has also been shown to take place via complex formation by using isotopically labeled C₂H₂. To confirm the hypothesis that higher energy, reactive, (linear) $C_3H_3^+$ ions interconvert to more stable, unreactive ones, cyclic $C_3H_3^+$ ions were also reacted with C₂D₂ and no isotope exchange reactions were observed.

Plots of $C_3H_3^+$ ion intensity versus time for reaction with C_4H_2 (Figure 28) indicate a 10-12 percent increase in the intensity of the unreactive isomer relative to the reaction when only the parent precursor is present. Isomerization of reactive $C_3H_3^+$ was also seen when different precursors were used (compare Tables 22 and 23). A similar mechanism involving complex formation may be responsible for this isomerization as well, although it was not investigated in any detail.

The extensive ion/molecule condensation reaction sequences (Reactions (59-65)) observed when $C_3H_3^+$ reacts with C_4H_2 suggest that this aspect of the proposed (14a,b) ionic path to soot formation is quite credible. The rate coefficient determined in this work for $C_3H_3^+$ disappearance ($1.4 \pm 0.7 \times 10^{-9} \text{ cm}^3/\text{s}$) is in good agreement with that determined earlier (43) ($1.0 \pm 0.5 \times 10^{-9} \text{ cm}^3/\text{s}$). Some of the product ions formed (e.g. $C_5H_3^+$ and $C_7H_5^+$) have been seen to be abundant in both nonsooting and sooting flames (10). On the other hand, the observation of $C_3H_3^+$ isomerization and not condensation with acetylene suggests that the proposed sequential acetylene addition reactions with $C_3H_3^+$ in the ionic soot formation mechanism be reconsidered. Other channels such as direct reaction of neutral aromatics with $C_3H_3^+$ (9,76) may be as important in the formation of small polycyclic ions.

These experiments and those reported earlier (43) were carried out at relatively low pressures ($< 5 \times 10^{-5} \text{ torr}$). It is quite possible that third body collisions in atmospheric pressure flames can stabilize a fraction of the $C_5H_5^+$ reaction complexes before the "reactive" deactivation observed in this work can take place. However, direct bimolecular reaction of linear $C_3H_3^+$ with acetylene to form $C_5H_3^+$ and $C_5H_5^+$ does not appear to occur readily.

D. REACTIONS OF $C_5H_5^+$ AND $C_5H_3^+$ IONS WITH ACETYLENE AND DIACETYLENE

1. Introduction

As noted in Section IIIC., study of the reactions of $C_3H_3^+$ with acetylene and diacetylene did not reveal facile formation of $C_5H_5^+$ or $C_5H_3^+$ by reaction of this ion with acetylene, although $C_3H_3^+$ did react readily with diacetylene, yielding $C_5H_3^+$ and $C_7H_5^+$. All three of the postulated products of

$C_3H_3^+$ reactions with acetylene and diacetylene ($C_5H_5^+$, $C_5H_3^+$, $C_7H_5^+$) have been identified by mass spectrometry (9,10) in flames, but it remains to be determined which, if any, of them may be important in soot formation mechanisms. Thus, as a part of this project, investigations were extended to include study of the reactions of $C_5H_3^+$ and $C_5H_5^+$ ions with certain flame neutrals.

Two previous experimental studies on the structures of $C_5H_3^+$ involved determination of the heats of formation of the $C_5H_3^+$ ion from different precursors (85,86). The results of these studies suggested the presence of two different linear structures for $C_5H_3^+$, each produced from a different precursor (85).

Many possible structures exist for the $C_5H_5^+$ ion, and despite a number of theoretical and experimental studies involving it, few definitive results exist regarding the specific relative energies of various isomeric forms (87,88). Experimental studies concentrated on determining the appearance potential and heats of formation of $C_5H_5^+$ ions from different sources by mass spectrometric methods (89-95). These resulted in heat of formation values ranging from 239 to 309 kcal/mole, depending on the source and technique of $C_5H_5^+$ production. Early ICR experiments in these laboratories were carried out to identify structures of $C_5H_5^+$ according to their reactivity with different neutrals (87,88,96). Several precursors were used in the formation of $C_5H_5^+$ ions and the results of the reactivity studies indicated the possibility of four different isomers of $C_5H_5^+$ (88). Acetylene reacted quite slowly with the $C_5H_5^+$ ions (87,88) while diacetylene and aromatics with side chains reacted at an appreciable rate (87). As a result, it has been suggested that soot nucleation may proceed by adding a few large molecules rather than through addition of many smaller ones (76,87). No definitive assignment of $C_5H_5^+$ isomeric structure was possible in the earlier studies (87,88). Proton-transfer reactions involving one relatively unreactive $C_5H_5^+$ isomer gave (87) a proton affinity of 227.9 ± 0.3 kcal/mol for the C_5H_4 neutral which remained after proton transfer. When combined with estimates of the heats of formation of possible C_5H_4 species, the results were consistent with (but did not conclusively prove) a vinyl cyclopropenylum form for the $C_5H_5^+$ isomer.

A number of theoretical studies have examined $C_5H_5^+$ structures⁸ (59-

62,97). Schleyer and co-workers located two minimum energy forms on the $C_5H_5^+$ potential surface, the more stable one corresponding to planar cyclopentadienyl, the other one to a square-based pyramid structure (60,61). Similar results were reported by Stohrer and Hoffman (59), although they proposed the pyramidal structure as the more stable form compared to the planar cyclopentadienyl. Calculations carried out under this contract are reported in Section IIF.

In this work, the kinetics and reaction mechanisms of $C_5H_3^+$ and $C_5H_5^+$ ions produced from different precursors were studied with acetylene and diacetylene in order to identify different structures and to obtain rate coefficients. Also, the energetics of $C_5H_5^+$ formation from two different precursors were studied to investigate the different pathways of $C_5H_5^+$ formation which could lead to different structures as identified by different reactivity.

2. Results

a. Reactions of $C_5H_3^+$.

A very low number of $C_5H_3^+$ ions were produced from 2,4-hexadiyne at electron energies above 30 ev. Reactivity of these ions was monitored at an electron energy of 50 ev although the ion intensity was still very low. Even though almost all of the $C_5H_3^+$ ions produced reacted with the 2,4-hexadiyne precursor, no reaction was observed with either C_2H_2 or C_4H_2 . Reactions of $C_5H_3^+$ with 2,4-hexadiyne were:



$C_5H_3^+$ ions produced as products of the reaction of $C_3H_3^+ + C_4H_2$ were 100 percent reactive with both propargyl iodide and diacetylene (the neutrals present in the reaction medium). $C_5H_3^+$ reactions with C_4H_2 were:



Some of the product ions were observed to react further with propargyl iodide by displacing atomic iodine:



$C_5H_3^+$ reactions with propargyl iodide were:



The $C_8H_6^+$ ion reacted further with C_4H_2 :



Ion intensity versus time curves for the $C_5H_3^+/(C_4H_2 + C_3H_3I)$ system are shown in Figure 29. The decay of $C_5H_3^+$ ions seen in Figure 29 involved reaction with both C_4H_2 and propargyl iodide.

The procedure for rate coefficient determination used in previous studies of $C_3H_3^+$ and $C_5H_5^+$ ion/molecule Reactions (42) required subtraction of the observed rate constant for the reaction of the ion with the precursor neutral from the observed rate constant for the sum of the reactions with precursor and reactant neutrals. In this case, however, the reactant neutral (C_4H_2) had to be included in the reaction mixture in order to produce the ion of interest ($C_5H_3^+$), and thus the subtraction procedure could not be used. An alternative method for rate constant determination was thus required. If all other ions are ejected from the FTICR cell, the decay of $C_5H_3^+$ as a function of time is given by $[C_5H_3^+] = [C_5H_3^+]_0 e^{-(n_p k_p + n_d k_d)t}$, where $n_p k_p$ and $n_d k_d$ refer to the products of the number densities and ion/molecule rate coefficients for

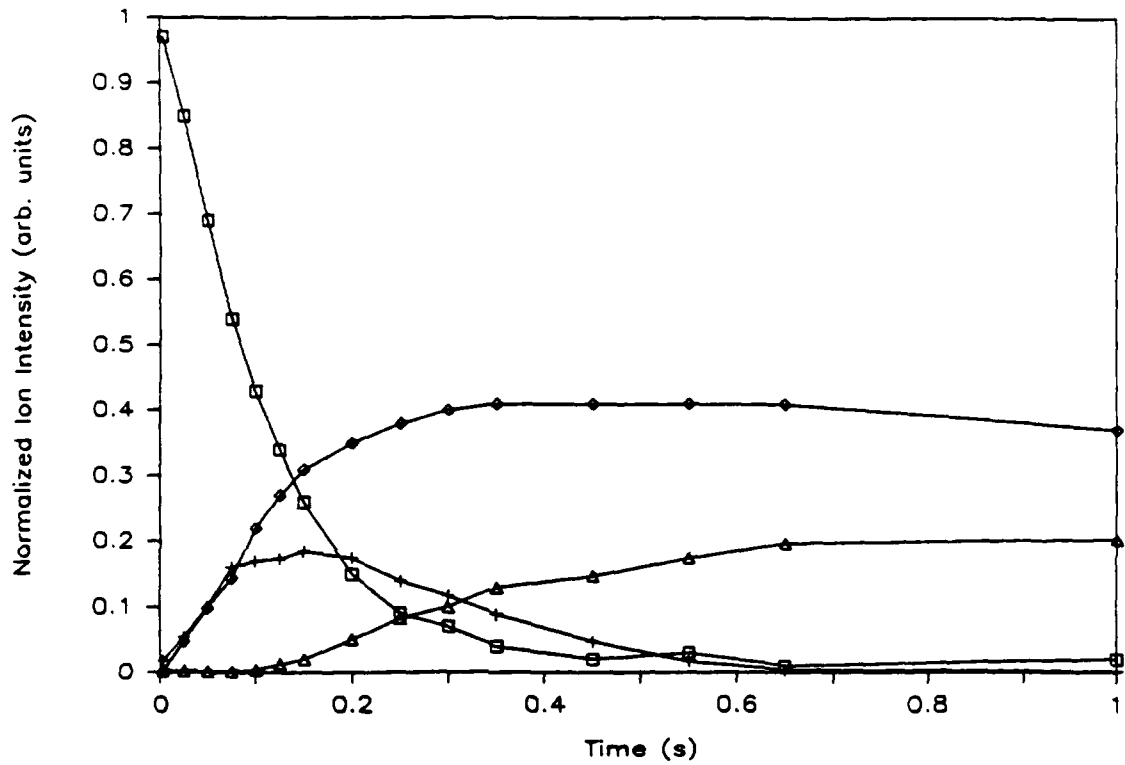


Figure 29. Reactions of C_5H_3^+ with C_4H_2 . C_5H_3^+ (□), $\text{C}_7\text{H}_3^+(+)$, C_9H_5^+ (◊) and $\text{C}_{11}\text{H}_5^+$ (Δ). Disappearance of C_5H_3^+ and product ions includes reactions with propargyl iodide. C_5H_3^+ ions were produced from the reaction of C_3H_3^+ with diacetylene within 30 ms reaction time. C_3H_3^+ ions were produced from propargyl iodide by charge transfer reactions with Xe. $P_{\text{C}_3\text{H}_3\text{I}} = 1.9 \times 10^{-7}$ torr, $P_{\text{C}_4\text{H}_2} = 1.3 \times 10^{-6}$ torr, $P_{\text{Xe}} = 5.4 \times 10^{-6}$ torr.

propargyl iodide and diacetylene, respectively. The quantity $n_d k_d + n_p k_p$ can thus be determined from the slope of a semilog plot of $C_5H_3^+$ decay as a function of time. At short reaction times, the following expressions hold true:
 $dD/dt = n_d k_d [C_5H_3^+]_o e^{-(n_p k_p + n_d k_d)t}$ and $dP/dt = n_p k_p [C_5H_3^+]_o e^{-(n_p k_p + n_d k_d)t}$
where D and P refer to product ions of the reaction with diacetylene ($C_7H_3^+$ and $C_9H_5^+$) and with propargyl iodide ($C_8H_6^+$), respectively. Thus, the ratio $n_d k_d / n_p k_p$ was calculated from the ratio of slopes of product formation as a function of time. Next $n_d k_d$ was obtained using the calculated sum and ratio of the two rate constants. Finally the absolute rate constant was determined following the usual procedure (42). It was found that $C_5H_3^+$ ions reacted with C_4H_2 with a rate constant of $(5.6 \pm 1.7) \times 10^{-10} \text{ cm}^3/\text{s}$.

b. Formation of $C_5H_5^+$.

$C_5H_5^+$ ions produced from different precursors exhibited behavior indicative of both reactive and unreactive populations toward the precursors and the reactant neutrals. Figures 30 and 31 show $C_5H_5^+$ normalized ion intensity versus time curves for two (1,3,5-cycloheptatriene and 1-penten-3-yne) of the five precursors used for reactions with precursor neutral, diacetylene and acetylene. Following an exponential decay indicative of pseudo-first order kinetics, a substantial fraction of unreactive ions remains at long reaction times. Table 25 shows the method of preparation of $C_5H_5^+$ ions from different precursors and the percent of unreactive ions remaining at long reaction times.

Two (norbornadiene and cycloheptatriene) of the five precursors mentioned above produced $C_7H_8^+$ parent ions which could lead to two different channels of $C_5H_5^+$ ion formation. Thus, $C_5H_5^+$ ion formation pathways have been studied somewhat in more detail for these two precursors. When different charge transfer gases were used for ionization of norbornadiene, different percentages of reactive $C_5H_5^+$ were observed, as noted in Table 25. Also the abundances of $C_7H_7^+$, $C_5H_6^+$ and $C_5H_5^+$ ions were measured following charge transfer ionization. Different behavior was observed for compounds with ionization potentials in the range of 14 to 16 eV. Table 26 shows this effect for two reagent gases (Kr^+ and N_2^+) which have ionization energies of 14.0 and 15.7 eV respectively.

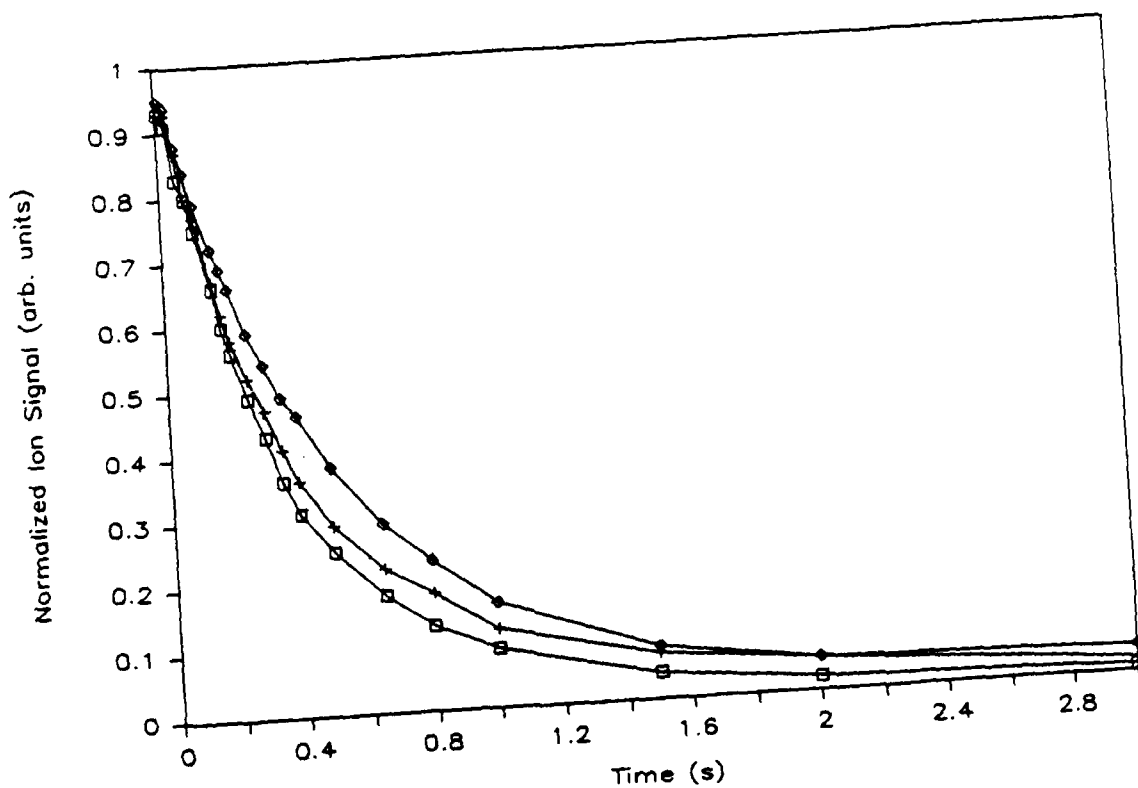


Figure 30. $C_5H_5^+$ Ion Decay Curves for Reactions with Cycloheptatriene (□), Cycloheptatriene and Acetylene(+), and Cycloheptatriene and Diacetylene(◊). $C_5H_5^+$ ions were produced from cycloheptatriene by charge transfer reactions with Ar^+ . $P_{C_7H_8^+} = 1.3 \times 10^{-7}$ torr, $P_{C_2H_2^+} = 1.1 \times 10^{-6}$ torr, $P_{C_4H_2} = 6.6 \times 10^{-7}$ torr, $P_{Ar} = 10.4 \times 10^{-6}$ torr.

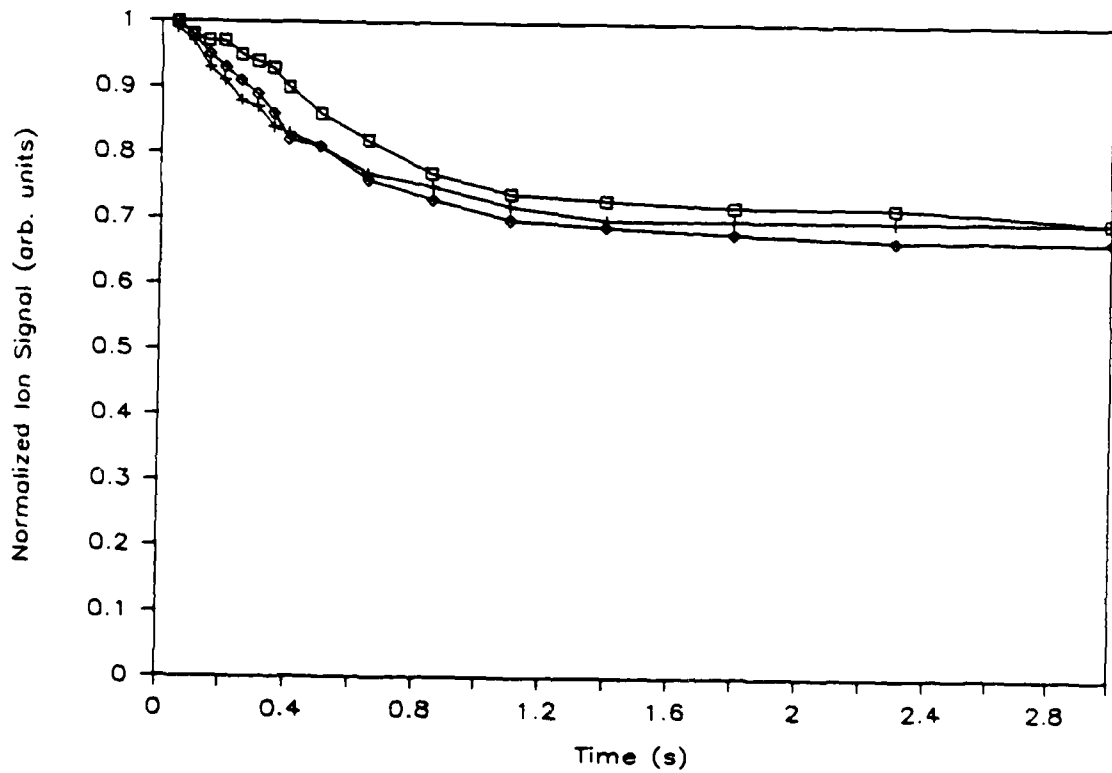


Figure 31. C_5H_5^+ Ion Decay Curves for Reactions with 1-Penten-3-yne(\square), 1-Penten-3-yne and Acetylene(+), and 1-Penten-3-yne and Diacetylene(\diamond). C_5H_5^+ ions were produced from 1-penten-3-yne by charge transfer reactions with Xe^+ . $P_{\text{C}_5\text{H}_6^+} = 4.2 \times 10^{-7}$ torr, $P_{\text{C}_2\text{H}_2} = 1.4 \times 10^{-6}$ torr, $P_{\text{C}_4\text{H}_2} = 8.4 \times 10^{-7}$ torr, $P_{\text{Xe}} = 5.4 \times 10^{-6}$ torr.

TABLE 25. PERCENTAGES^a OF UNREACTIVE $C_5H_5^+$ FOUND FROM VARIOUS PRECURSORS BY CHARGE TRANSFER CHEMICAL IONIZATION MONITORED BY OBSERVING REACTION WITH THE PRECURSOR NEUTRAL.

Precursor neutral	Ionizing technique	Percent unreactive $C_5H_5^+$
dicyclopentadiene	N_2^+ /Ar ⁺ charge transfer	20
cyclopentadiene	Xe ⁺ charge transfer	17
1-penten-3-yne	Xe ⁺ charge transfer	65-70
cycloheptatriene	Ar ⁺ charge transfer	0-5
norbornadiene	N_2^+ /Ar ⁺ charge transfer	18-20
	Kr ⁺ charge transfer	5-10

^a Estimated error is $\pm 5\%$.

TABLE 26. CHANGES IN ION ABUNDANCES AT TWO DIFFERENT IONIZATION ENERGIES FOR NORBORNADIENE.

Ionizing energy/eV (ionizing technique)	Abundances as a fraction of total ion signal			
	$C_7H_8^+$	$C_7H_7^+$	$C_5H_6^+$	$C_5H_5^+$
14.0 (Kr ⁺ charge transfer)	0.07	0.45	0.32	0.16
15.7 (N ₂ ⁺ charge transfer)	0.09	0.28	0.16	0.47

To further investigate this behavior, the relative ion abundances versus electron energy for cycloheptatriene and norbornadiene were obtained (see Figures 32-35). Electron impact ionization was used for this study, therefore, the energy scale in Figures 32-35 should be considered as approximate with at least ± 1 eV uncertainty.

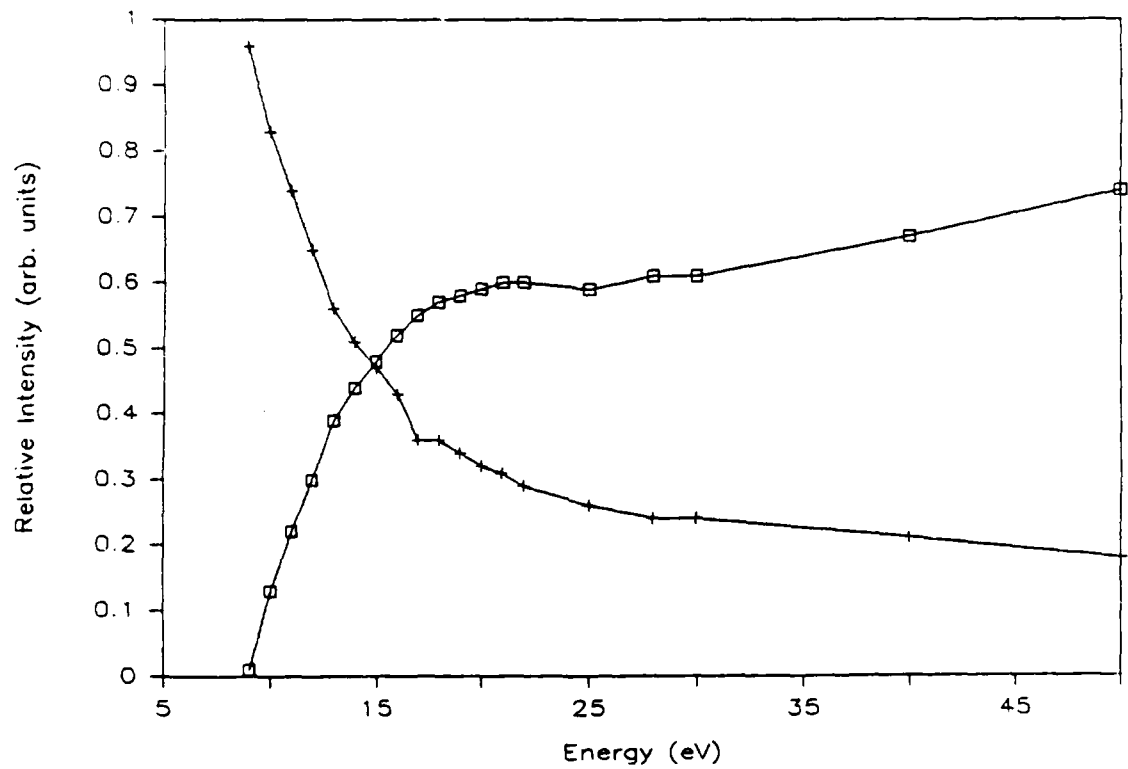


Figure 32. Relative Intensities of $C_7H_8^+(+)$ and $C_7H_7^+(□)$ Ions Produced from Cycloheptatriene as a Function of Electron Impact Energy.

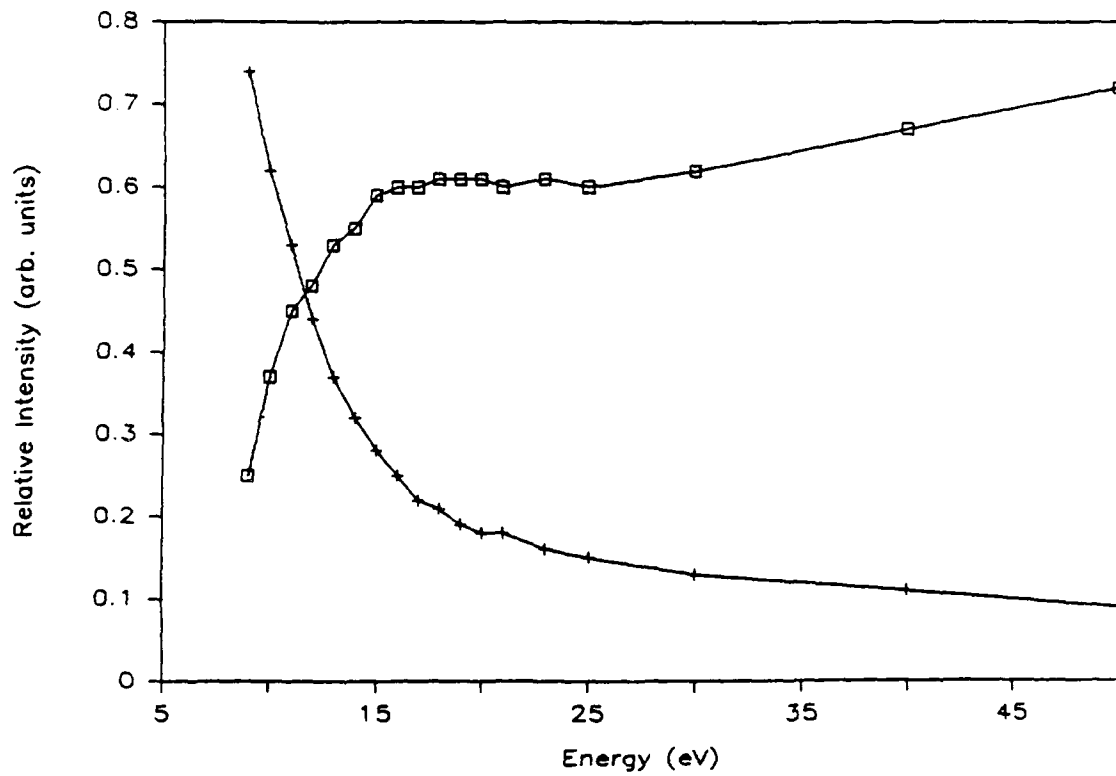


Figure 33. Relative Intensities of $\text{C}_7\text{H}_8^+ (+)$ and $\text{C}_7\text{H}_7^+ (\square)$ Ions Produced from Norbornadiene as a Function of Electron Impact Energy.

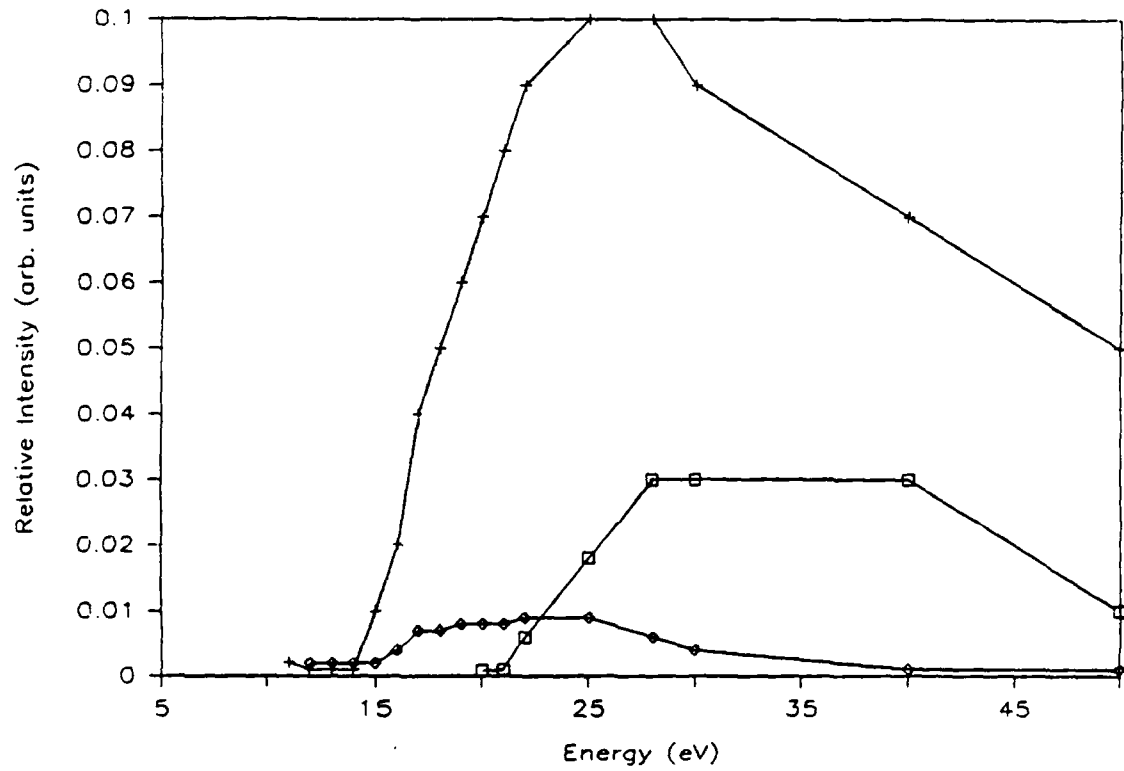


Figure 34. Relative Intensities of $C_5H_6^+$ (◊), $C_5H_5^+$ (+), and $C_3H_3^+$ (□) Ions Produced from Cycloheptatriene as a Function of Electron Impact Energy.

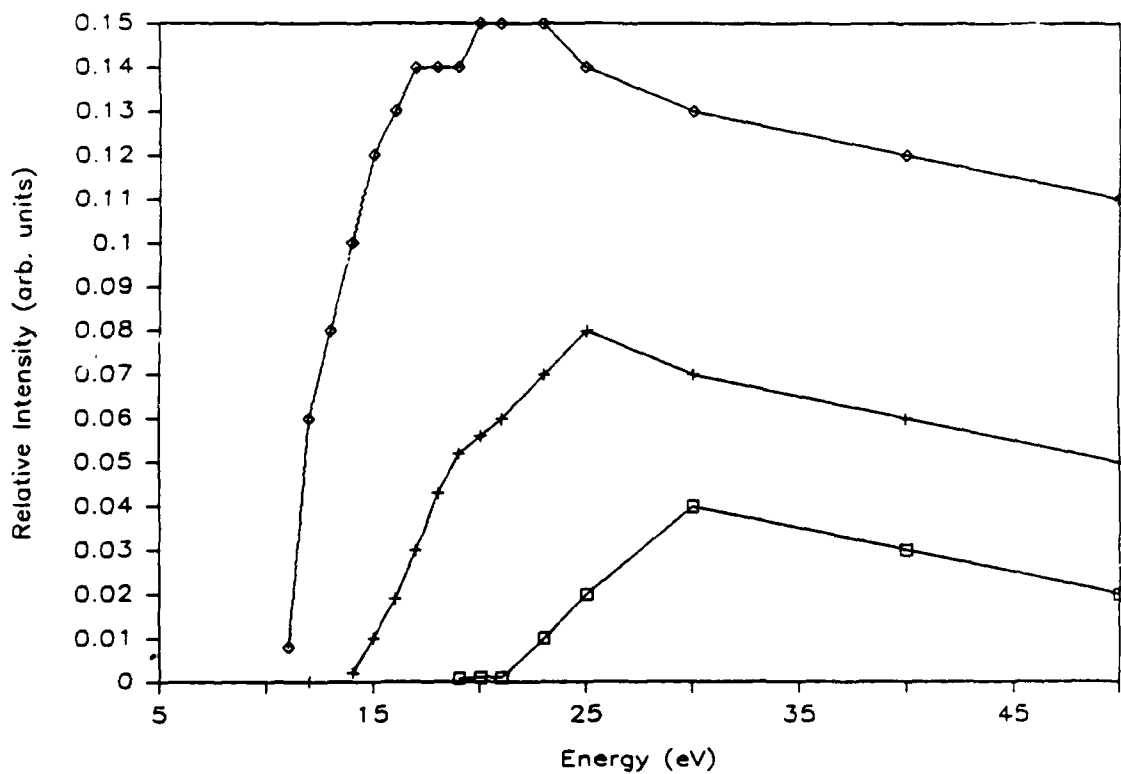


Figure 35. Relative Intensities of C_5H_6^+ (diamond), C_5H_5^+ (plus), and C_3H_3^+ (square) Ions Produced from Norbornadiene as a Function of Electron Impact Energy.

c. $C_5H_5^+$ reactions with diacetylene.

After ejection of all ions except $C_5H_5^+$ following charge transfer chemical ionization of a mixture of diacetylene and a precursor compound, the ion/molecule reactions as a function of time were monitored. Independent of the precursor used, the main reaction was the addition of C_4H_2 to $C_5H_5^+$ to produce the $C_9H_7^+$ ion.



Other minor reactions observed were:



For $C_5H_5^+$ ions produced from cyclopentadiene, the C_2 addition Reaction (87) was not observed with C_4H_2 .

The rate coefficient for the disappearance of $C_5H_5^+$ was calculated as described earlier (42) and the values found for $C_5H_5^+$ ions produced from different precursors are given in Table 27.

d. $C_5H_5^+$ reactions with acetylene.

$C_5H_5^+$ ions formed from four of the five precursors (cyclopentadiene, 1-penten-3-yne, norbornadiene, cycloheptatriene) reacted very slowly with C_2H_2 , producing very small amounts of $C_7H_7^+$ and $C_9H_9^+$.



Rate constants for the $C_5H_5^+ + C_2H_2$ reaction were about one order of magnitude less than those for reactions with C_4H_2 (see Table 28).

TABLE 27. RATE COEFFICIENTS FOR THE REACTION OF $C_5H_5^+$ IONS FROM DIFFERENT PRECURSORS^a WITH DIACETYLENE.

Precursor	Absolute rate coefficient/(10 ⁻¹⁰ cm ³ /s)
cyclopentadiene	1.0 ± 0.5
1-penten-3-yne	2.0 ± 1.0
norbornadiene	2.9 ± 1.4
cycloheptatriene	3.3 ± 1.9
dicyclopentadiene	1.6 ± 0.8

^a $C_5H_5^+$ ions were produced by charge transfer chemical ionization using different gases as shown in Table 25.

TABLE 28. RATE COEFFICIENTS FOR THE REACTION OF ACETYLENE WITH $C_5H_5^+$ IONS PRODUCED FROM DIFFERENT PRECURSORS^a.

Precursor ^b	Absolute rate coefficient/(10 ⁻¹¹ cm ³ /s)
cyclopentadiene	(4.8 ± 1.9)
1-penten-3-yne	(2.7 ± 1.0)
norbornadiene	(3.1 ± 1.3)
cycloheptatriene	(1.8 ± 0.7)

^a $C_5H_5^+$ ions were produced using charge transfer chemical ionization using different gases as shown in Table 25.

^b Ion signal for dicyclopentadiene was too small to produce reproducible results for the rate coefficient.

3. Discussion

a. $C_5H_3^+$.

Two different $C_5H_3^+$ structures have been identified earlier (85,86) by measuring the heats of formation of the $C_5H_5^+$ ions from 1,3-pentadiyne and 2,4-hexadiyne. In the work reported here, $C_5H_3^+$ ions were produced from 2,4-hexadiyne and from reaction of $C_3H_3^+$ with diacetylene. Although $C_5H_3^+$ ions produced either way were reactive toward their precursor neutrals, $C_5H_3^+$ ions produced from 2,4-hexadiyne were unreactive with both C_4H_2 and C_2H_2 , while those formed as ion/molecule reaction products reacted with C_4H_2 with the relatively high rate constant of $(7.79 \pm 3.26) \times 10^{-10} \text{ cm}^3/\text{s}$. Dannacher et al. (85) suggested the structures $CH_3-C\equiv C-C\equiv C^+$ and $HC\equiv C-C\equiv C-CH_2^+$ for the $C_5H_3^+$ ions produced from 2,4-hexadiyne and 1,3-pentadiyne respectively. Experimental values of the heat of formation of these ions showed that the former had a higher heat of formation (1431 kJ/mole) (86) than the latter (1317 kJ/mole) (85). In this study, higher reactivity of $C_5H_3^+$ ions produced by the $C_3H_3^+ + C_4H_2$ reaction, compared to those produced by electron ionization of 2,4-hexadiyne suggests that a higher energy isomer of $C_5H_3^+$ is formed in the former case. It has been found for small hydrocarbon ions that enhanced reactivity often correlates with a higher heat of formation.

b. $C_5H_5^+$ ion structures produced from different precursors.

$C_5H_5^+$ ions produced from different precursors all exhibited at least two populations, one reactive, other unreactive. This behavior for numerous other ionic reactants has been used previously (79,98-100) to argue for the existence of at least two different structural isomers; one reactive and one nonreactive. These results agree with the earlier reactivity study of $C_5H_5^+$ ions from different precursors (88). To distinguish the reactive $C_5H_5^+$ structures, their reaction mechanisms and reaction rates with acetylene and diacetylene were studied. Although they reacted with their precursor neutrals with different rates, they all reacted with acetylene and diacetylene at similar rates (within the experimental error limits), as shown in Tables 27 and 28. Thus no isomeric differentiation based on reactivity can be made. Rate

coefficients for the reaction with acetylene were similar to those determined earlier (87,88), i.e. in the range of 10^{-11} cm³/s. Reaction mechanisms were similar for all C₅H₅⁺ ions with the exception of cyclopentadiene, which didn't give C₂ addition reactions with C₄H₂. More definitive identification of C₅H₅⁺ structures may be forthcoming when better theoretical calculations⁸ have been reported.

To compare the behavior of ions produced from 1,3,5-cycloheptatriene and norbornadiene precursors (both having the formula C₇H₈), relative abundances as a function of electron energy shown in Figures 32-35 were obtained. As shown, the curves for C₇H₇⁺ (Figures 32-33), C₅H₅⁺ and C₃H₃⁺ (Figures 34-35) are very similar both in terms of energetics and of general shape. Slight differences in their relative intensities are probably due to the normalization procedure used in each case. Increase in relative intensity of C₅H₅⁺ ions in both cases in the energy range of 15-25 eV and the fact that the C₇H₇⁺ curve becomes flat in this energy range implies that most of the C₅H₅⁺ ions are produced from C₇H₇⁺. Similar behavior exists for C₃H₃⁺ ions, i.e., the intensity of C₅H₃⁺ increases near 22 eV (on the energy scale shown on Figures 34-35) where the rate of increase in intensity of C₅H₅⁺ lessens. This implies that C₇H₇⁺ formed from these two compounds behaves similarly, i.e., follows the same fragmentation pathways in the same energy range. Similar behavior for C₇H₇⁺ ions from these two compounds has also been reported earlier as a result of a collisional activation study (101). Formation of C₅H₆⁺, both in terms of energetics and relative intensity, is different for cycloheptatriene and norbornadiene, indicating that C₇H₈⁺ ions formed from these compounds by electron impact have different structures. Based on the higher relative intensity of C₅H₆⁺ for norbornadiene, there exists the possibility of formation of C₅H₅⁺ ions from the C₅H₆⁺ channel too. In fact, C₅H₅⁺ ions formed from cycloheptatriene in the energy range of 12 to 50 eV show similar behavior in reactivity, i.e., the percent of unreactive C₅H₅⁺ remains constant at 5 percent while in the norbornadiene case, percent of unreactivity increases to 20 percent, indicating that C₅H₅⁺ formed from the C₅H₆⁺ channel has a high percent of unreactive isomer. This trend is also apparent from the results shown in Tables 25 and 26 for norbornadiene, which indicates that when Ar⁺/N₂⁺ replaces Kr⁺ as the charge donor, the unreactive population of the observed C₅H₅⁺ increases while there is a corresponding decrease in the yield of the C₅H₆⁺ ion.

Similar results have also been reported earlier for norbornadiene (80,102).

In general, a similar trend in ion/molecule reactivity with acetylene and diacetylene has been found for $C_5H_5^+$ ions as was seen (Reference 42 and Section IIIC.) for $C_3H_3^+$ ions: little or no reactivity with acetylene, but extensive and rapid reactivity with diacetylene. The results of bimolecular reactivity studies on both $C_3H_3^+$ and $C_5H_5^+$ suggest that the proposed ion/molecule condensation reactions with diacetylene in the ionic soot formation mechanism are quite credible while the proposed sequential acetylene addition reactions should be reconsidered. These experiments and those reported earlier (42) were carried out at relatively low pressures ($< 5 \times 10^{-5}$ torr). It is thus quite possible that third-body collisions in atmospheric pressure flames can stabilize a larger fraction of the $C_7H_7^+$ reaction complexes and result in increased reactivity with acetylene. In fact, such collisional stabilization of the association complexes for the reactions of $C_3H_3^+$ and $C_4H_4^+$ with C_2H_2 has been shown to occur in higher pressure selected ion flow tube (SIFT) studies (103,104).

E. REACTIONS OF GASEOUS $C_7H_7^+$ IONS

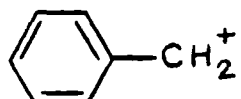
1. Introduction

The $C_7H_7^+$ ion has been proposed as one species involved in the ion/molecule mechanism of soot formation (14a,b). According to the proposed ion/molecule mechanism, $C_5H_5^+$ forms $C_7H_7^+$ in reactions with acetylene. However, work reported in Section IIID. on the reactions of $C_5H_5^+$ with acetylene did not reveal significant formation of $C_7H_7^+$. Much higher concentrations of $C_7H_7^+$ than observed experimentally were predicted (14a) by a simple model which assumed a benzyl structure for the ion. To account for this difference between experiment and theory, it was suggested (14a) that the actual ion in the flame, presumably formed by ion/molecule reactions of $C_3H_x^+$ and $C_5H_x^+$ ions, is some other $C_7H_7^+$ isomer less stable than benzyl. To help understand this question we have extended our earlier studies on hydrocarbon ions which might be important in an ionic mechanism of soot formation⁵ (42,76,96,105) to follow the reactions of $C_7H_7^+$ ions with certain flame neutrals and to try to identify different $C_7H_7^+$ isomers.

There have been a significant number of both theoretical and experimental studies relating to structural characterization of $C_7H_7^+$ ions. Theoretical studies (106,107) which reported heats of formation for $C_7H_7^+$ ions indicated that tropylidium, I ($\Delta H_f = 207.9, 195.6$ kcal/mol) (106,107) and benzyl, II ($\Delta H_f = 217.1, 220.4$ kcal/mol) (106,107) are the most stable structures with an

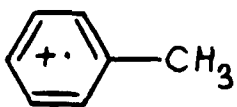


I

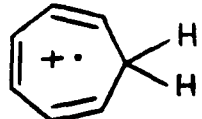


II

activation energy of 32.7 kcal/mol (107) for II \rightarrow I isomerization. Experimental measurements of ionization potentials for tropylidium and benzyl radicals by monoenergetic electron impact gave values of $\Delta H_f = 209$ and 211 kcal/mol (108-110) respectively. Studies of metastable ions (111-113), collisional activation (101,114,115) gas phase radiolysis (116-119), photoionization/photodissociation (95,120-124) photoelectron photoion coincidence (PEPICO) (125,126), and ion/molecule Reactions (79,99,100,127,128) of $C_7H_7^+$ ions from different precursors were used to characterize the different structures. General experimental evidence including the determination of appearance potentials and heats of formation (122-126) supported the idea that these ions exist in the gas phase with at least two structures; tropylidium, I and benzyl, II. Unreactive and reactive $C_7H_7^+$ observed in ion/molecule reactions have been attributed to structures I and II, respectively (79,99,100,127,128). Furthermore, it was proposed that there is an equilibrium between these two structures (114,129) similar to that proposed between the toluene, III and cycloheptatriene, IV (114,80) ions.



III



IV

Several groups studied the effect of internal energy above the $C_7H_7^+$ formation threshold on the predominance of one structure over the other (80,112,121, 128). Their results in general were supportive of the equilibria between different structures mentioned above. Although McLafferty et al. (101,112)

reported evidence for stable tolyl and norbornadienyl structures in earlier collisional activation studies no definitive indication for stable structures other than benzyl and tropylum was provided in later work (79,80,114,115). In this work $C_7H_7^+$ ions were produced from three different precursors using different charge transfer gases. Reaction pathways and the rate coefficients for the reaction of $C_7H_7^+$ ions with precursor neutrals, acetylene and diacetylene near room temperature were investigated. Results are discussed in relation to previous work involving $C_7H_7^+$ structures and the proposed ionic route to soot formation.

2. Results

a. Effect of Precursor Neutrals.

$C_7H_7^+$ ions produced from different precursors were found to have both reactive and unreactive populations. Figures 36, 37, and 38 show normalized ion intensities of $C_7H_7^+$ and product ions vs time for reactions with precursor neutrals: toluene, norbornadiene and cycloheptatriene, respectively. Following an exponential decay indicative of first-order kinetics, a substantial fraction of unreactive ions remains at long reaction times. Table 29 shows the charge transfer agents used to produce $C_7H_7^+$ ions from different precursors, the maximum internal energy imparted to the ions, and the percent of unreactive ions remaining at long reaction times.

The major reaction of $C_7H_7^+$ produced by charge transfer from toluene with the toluene neutral gives $C_8H_9^+$ (Reaction (93)). When norbornadiene is used as a precursor and neutral reactant, Reaction (94) is observed.



$C_7H_7^+$ from norbornadiene also reacts to give small amounts of higher molecular weight products. On the other hand, $C_7H_7^+$ produced from cycloheptatriene reacts with its precursor neutral to give significant amounts of higher molecular weight product ions along with smaller amounts of $C_8H_9^+$ and $C_9H_9^+$ product ions:

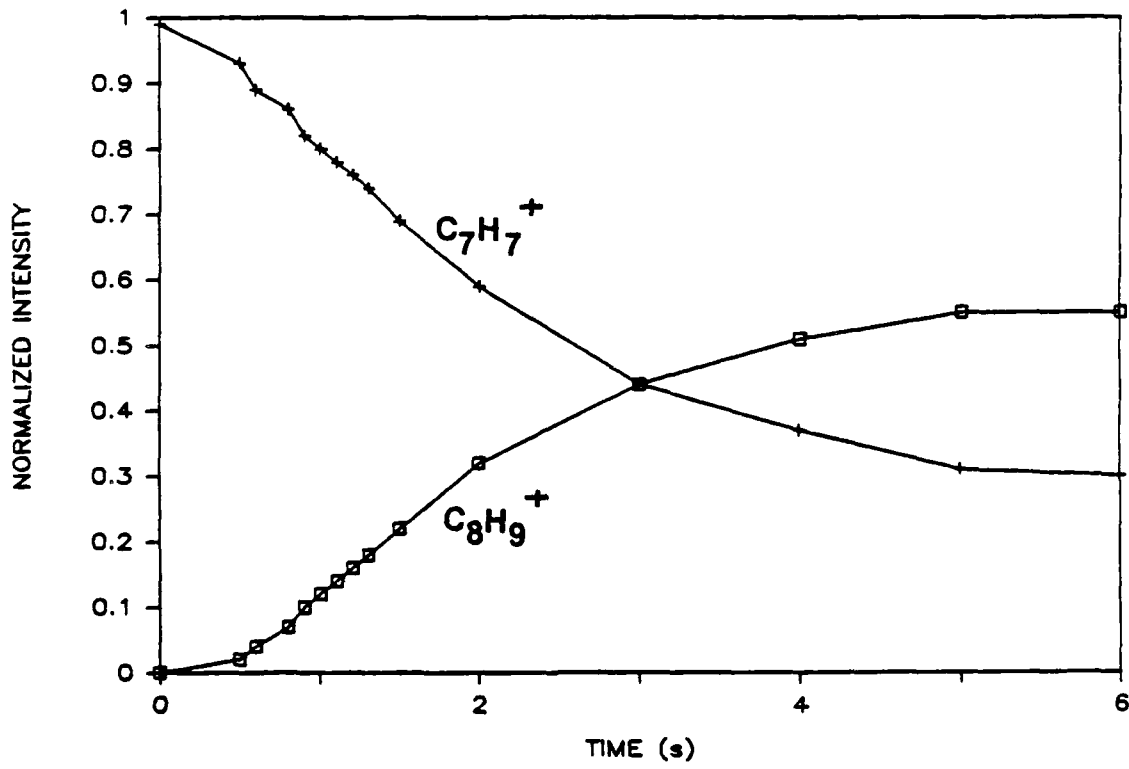


Figure 36. Reaction of $C_7H_7^+$ Produced from Toluene by Kr^+ Charge Transfer with its Precursor Neutral. $P_{toluene} = 1.17 \times 10^{-7}$ torr, $P_{Kr} = 6.3 \times 10^{-6}$ torr. $C_7H_7^+$ (+) and $C_8H_9^+$ (□).

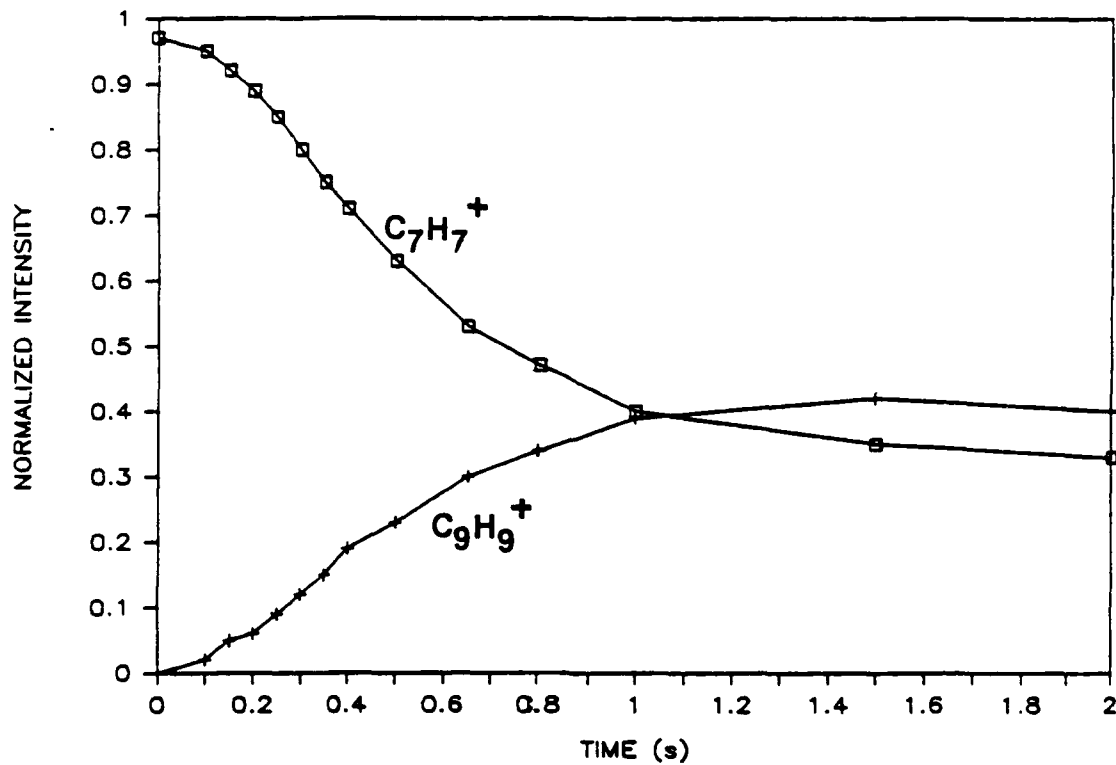


Figure 37. Reaction of $C_7H_7^+$ Produced from Norbornadiene by Xe^+ Charge Transfer with its Precursor Neutral. $P_{\text{norbornadiene}} = 5.4 \times 10^{-7}$ torr, $P_{Xe} = 4.3 \times 10^{-6}$ torr. $C_7H_7^+$ (\square) and $C_9H_9^+$ (\diamond).

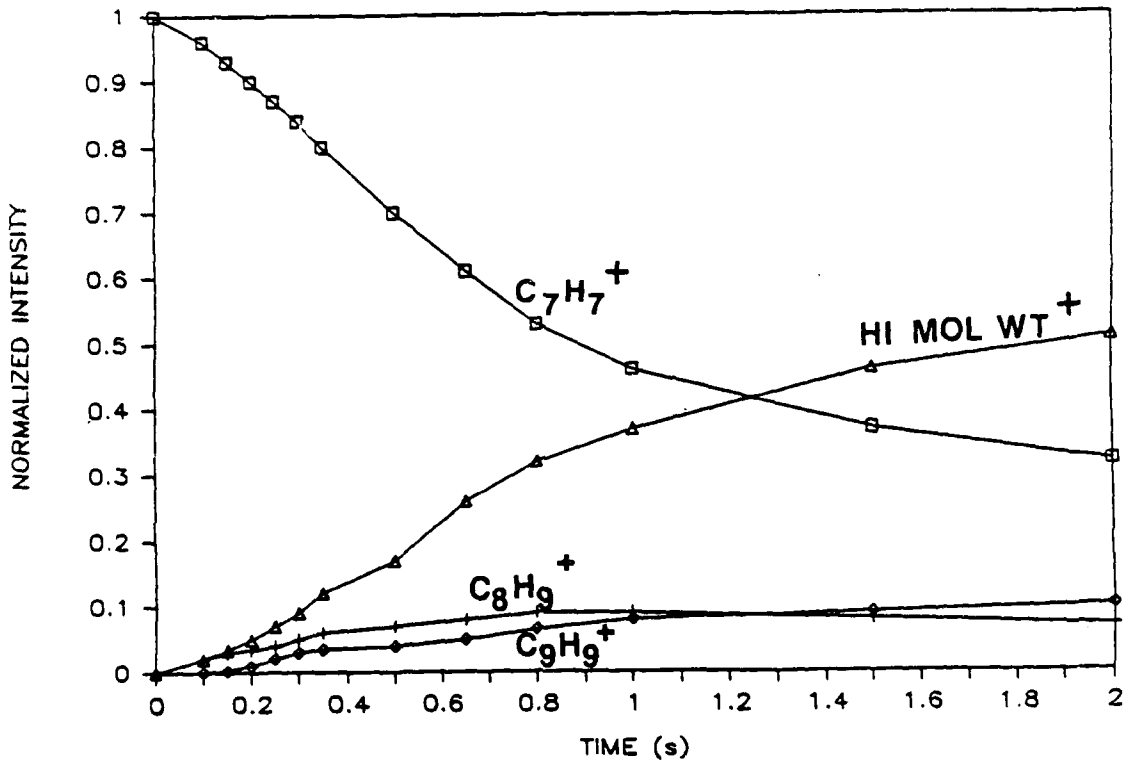


Figure 38. Reaction of $C_7H_7^+$ Produced from Cycloheptatriene by Xe^+ Charge Transfer with its Precursor Neutral. $P_{Cycloheptatriene} = 3.6 \times 10^{-7}$ torr, $P_{Xe} = 4.6 \times 10^{-6}$ torr. $C_7H_7^+$ (□), $C_8H_9^+$ (+), $C_9H_9^+$ (\diamond), and higher molecular weight product ions (Δ).

TABLE 29. PERCENTAGES AND MAXIMUM INTERNAL ENERGIES OF UNREACTIVE $C_7H_7^+$ IONS FORMED FROM VARIOUS PRECURSORS BY DIFFERENT IONIZATION METHODS MONITORED BY OBSERVING REACTION WITH THE PRECURSOR NEUTRAL.^a

Precursor Neutral	Ionizing Charge Transfer Agents	Maximum Internal Energy (eV) ^b	Percent Unreactive
Toluene	Xe ⁺	1.4	45-50
	Kr ⁺	3.3	25-30
	Ar ⁺	5.0	25-30
Norbornadiene	$C_4H_2^+$	0.9	70-75
	Xe ⁺	2.5	30-35
	Kr ⁺	4.4	25-30
Cycloheptatriene	$C_4H_2^+$	1.1	70-75
	Xe ⁺	2.8	35-40
	Kr ⁺	4.6	35-40

^a For those ions produced by $C_4H_2^+$ charge transfer, reactions with both precursor neutral and diacetylene were monitored.

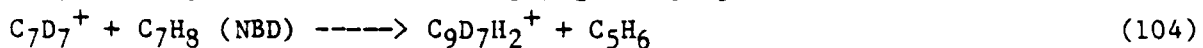
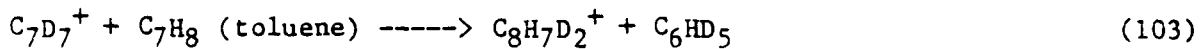
^b Based on $C_7H_7^+$ appearance energies given by Traeger and McLougin (1978).



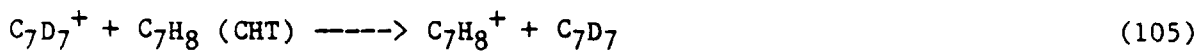
b. Deuteration Studies.

In order to further investigate the mechanisms of some of the reactions shown above, deuterated toluene was used both to produce $C_7D_7^+$ for

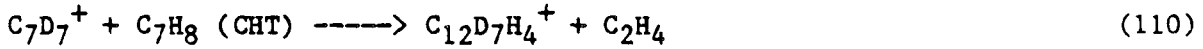
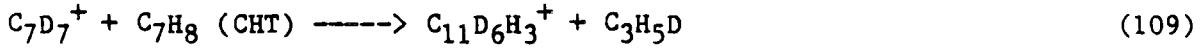
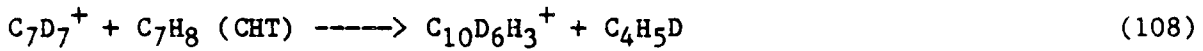
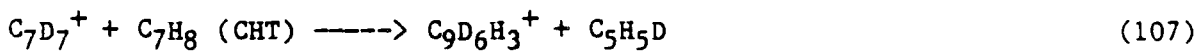
reactions with neutral precursors and as a neutral reactant for reactions of $C_7H_7^+$ produced from different precursors. Reactions of $C_7D_7^+$ with toluene and norbornadiene (NBD) were respectively:



When $C_7D_7^+$ reacted with cycloheptatriene (CHT), the major product observed was unreactive $C_7H_7^+$ due to Reactions (105) and (106).



Other reactions observed were:



$C_7H_7^+$ ions produced from toluene reacted with deuterated toluene as shown by Equation (111):



Very low intensities of $C_3D_7H_2^+$ were also observed in the mass spectra of $C_7H_7^+$ ions produced from cycloheptatriene and norbornadiene. The rate coefficients for the disappearance of $C_7H_7^+/C_7D_7^+$ by reactions with precursor neutrals were calculated as described earlier⁵ (42) and the values are shown in Table 30.

c. $C_7H_7^+$ Reactions with Acetylene.

$C_7H_7^+$ ions produced by Xe^+ dissociative charge transfer of norbornadiene and cycloheptatriene reacted slowly with acetylene to produce very small amounts of $C_9H_9^+$.

TABLE 30. RATE COEFFICIENTS FOR DIFFERENT $C_7H_7^+$ /C₇H₈ REACTION SYSTEMS.

	k/10 ⁻¹⁰ (cm ³ /s)		
	$C_7D_7^+$ from Toluene-d ₈	$C_7H_7^+$ from NBD	$C_7H_7^+$ from CHT
Neutral			
Toluene-d ₈	(3.5 ± 1.0)	(0.8 ± 0.3)	(1.7 ± 0.5)
NBD	(3.2 ± 1.0)	(5.4 ± 1.7)	
CHT	(4.6 ± 1.5)		(8.2 ± 2.6)



The following reaction was also observed with the ions produced from cycloheptatriene:



The rate coefficients for the disappearance of C₇H₇⁺ ions produced from norbornadiene and cycloheptatriene were found to be (1.0 ± 1.0) × 10⁻¹¹ and (3.6 ± 1.3) × 10⁻¹¹ cm³/s, respectively. However, when toluene was used as a precursor for C₇H₇⁺ production by Kr⁺ dissociative charge transfer, no reaction with acetylene was observed.

d. C₇H₇⁺ Reactions with Diacetylene.

C₇H₇⁺ ions from different precursors were reacted with both diacetylene and deuterated diacetylene in order to identify the reaction products from those formed by reaction of C₇H₇⁺ with the precursor neutral (for instance the reactions with diacetylene and cycloheptatriene both give C₁₁H₉⁺). The following reactions of C₇H₇⁺ with diacetylene were observed:





In the toluene case, the following reactions were also observed:

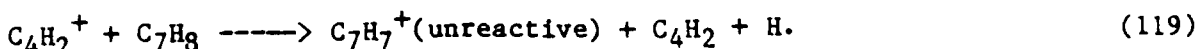


Ion intensity versus time curves of C_7H_7^+ (produced by Kr^+ charge transfer from toluene) and product ions for the reaction with diacetylene are shown in Figure 39. The rate coefficients for the disappearance of C_7H_7^+ by the sum of Reactions (114) and (115) for different precursors are given in Table 31.

TABLE 31. REACTION RATE COEFFICIENTS FOR $\text{C}_7\text{H}_7^+ + \text{C}_4\text{H}_2$ REACTION.

Precursor	$k/10^{-10}(\text{cm}^3/\text{s})$
Toluene	(1.50 \pm 0.50)
Norbornadiene	(0.25 \pm 0.19)
Cycloheptatriene	(0.75 \pm 0.25)

When C_7H_7^+ ions were produced in a 100 ms reaction time by Xe^+ dissociative charge transfer from norbornadiene and cycloheptatriene in the presence of C_4H_2 , production of unreactive C_7H_7^+ was observed by the following reactions:



Thus, to obtain accurate information on reaction kinetics of the $\text{C}_7\text{H}_7^+ + \text{C}_4\text{H}_2$ reaction, the C_4H_2^+ ion was continuously ejected when C_7H_7^+ ions were formed

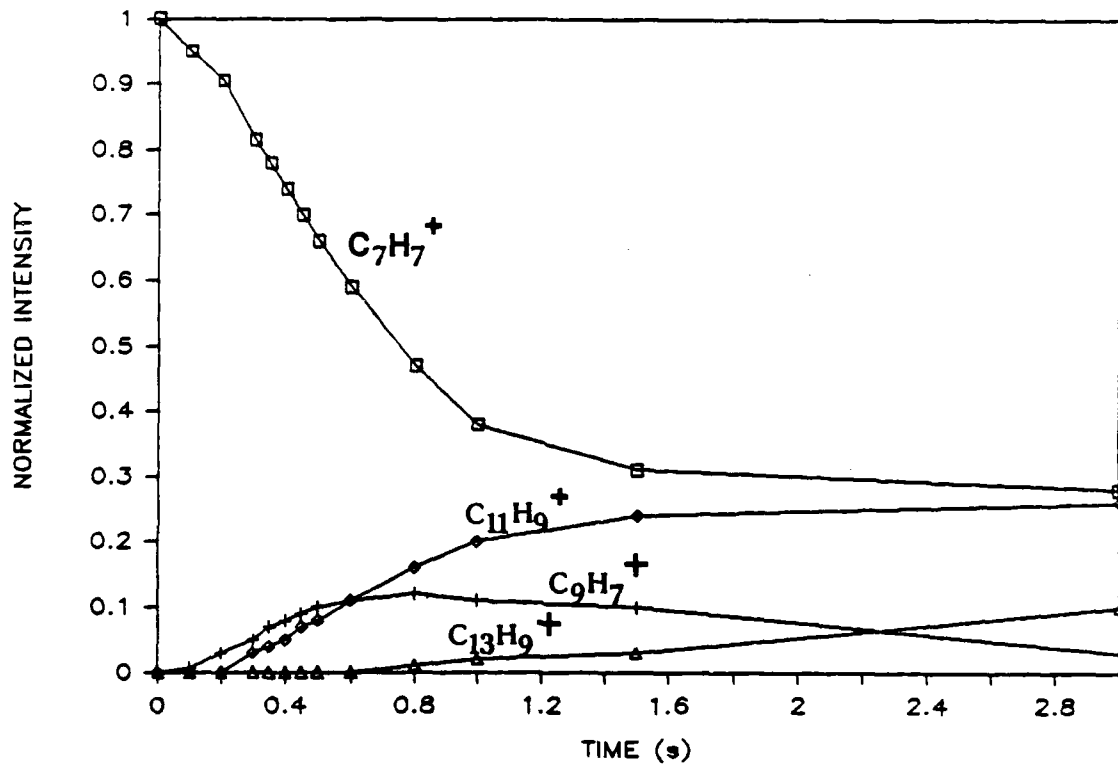


Figure 39. Reactions of $C_7H_7^+$ Produced from Toluene by Kr^+ Charge Transfer with Diacetylene. $P_{toluene} = 1.1 \times 10^{-7}$ torr, $P_{C_4H_2} = 8.6 \times 10^{-7}$ torr, $P_{Kr} = 6.3 \times 10^{-6}$ torr. $C_7H_7^+$ (\square), $C_9H_7^+$ (+), $C_{11}H_9^+$ (\diamond), and $C_{13}H_9^+$ (Δ).

by dissociative charge transfer using Xe^+ .

Also in this study, the relative abundances of the ions produced from toluene as a function of electron impact energy were determined for the purpose of comparison with earlier results obtained for norbornadiene and cycloheptatriene⁵. Relative abundances of C_5H_5^+ and C_3H_3^+ as a function of energy for toluene are shown in Figure 40. Results of the earlier study⁵ for norbornadiene and cycloheptatriene are also included in the figure for comparison.

3. Discussion

Since numerous earlier investigations (79,100,114,121,123) have demonstrated that C_7H_7^+ ions have at least two stable structures, one reactive and the other unreactive, the results of this study are interpreted in terms of the possibility of other stable structure(s).

The nature of the reaction products observed for the reactions of C_7H_7^+ ions with their precursor neutrals, toluene, norbornadiene and cycloheptatriene, were significantly different, as shown in Figures 36, 37 and 38, respectively. In order to determine whether these differences were due to the neutral or ion structures, deuterated toluene was used to monitor the reaction mechanisms with different neutral precursors. As seen in Equations (103-110), C_7D_7^+ ions reacted with the precursor neutrals, producing deuterated analogues of the same product ions observed for each nondeuterated ion/precursor reaction system. This result showed that the differences in reaction products are the result of the different structures of neutral precursors, and not necessarily of different ion structures. Then deuterated toluene was used as a reactant neutral for C_7H_7^+ ions produced from different precursors. As seen from Equation (111), C_7H_7^+ ions produced from all three precursors reacted with C_7D_8 to produce $\text{C}_8\text{D}_7\text{H}_2^+$, although very low ion intensities were produced with cycloheptatriene and norbornadiene precursors. The reaction mechanism which gives this product ion is also operative in Reaction (103) and is believed to be indicative of the benzyl, II, structure for C_7H_7^+ ions (79,95,121,128). This mechanism has also been studied earlier by similar isotopic labeling experiments (79,99). The only important difference in the

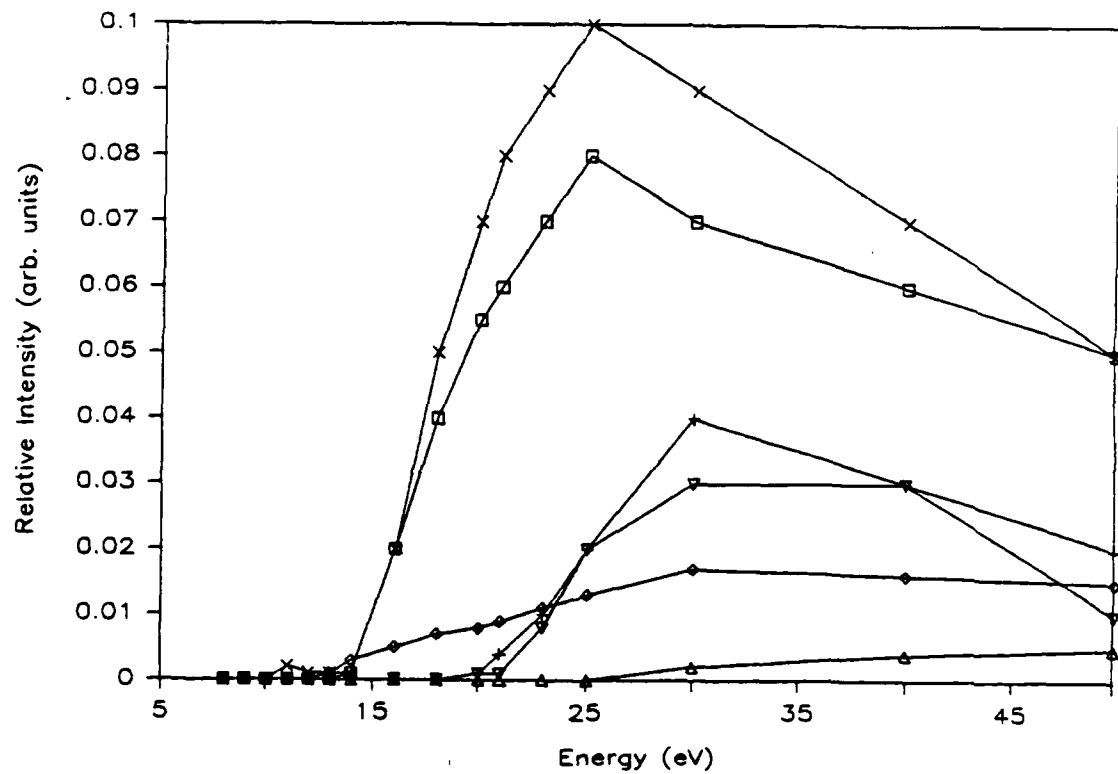


Figure 40. $C_5H_5^+$ and $C_3H_3^+$ Ion Abundances as a Function of Electron Energy.
 $C_5H_5^+$ (X) and $C_3H_3^+$ (V) from Cycloheptatriene, $C_5H_5^+$ (□) and
 $C_3H_3^+$ (+) from Norbornadiene and $C_5H_5^+$ (◇) and $C_3H_3^+$ (Δ) from
Toluene.

behavior of reactive $C_7H_7^+$ ions produced from different precursors was their reaction rates with precursor neutrals. $C_7H_7^+/C_7D_7^+$ ions produced from toluene/deuterated toluene reacted at similar rates with toluene, norbornadiene and cycloheptatriene whereas $C_7H_7^+$ ions produced either from norbornadiene and cycloheptatriene reacted at much slower rates with toluene than with their own precursor neutrals (see Table 30).

Reactions of $C_7H_7^+$ and product ions with diacetylene and deuterodiacetylene are represented by Equations (114-116), independent of the precursor used. An interesting mechanism is observed for C_2 and C_4 addition reactions shown by Equations (114b) and (117b) which is indicative of an ion/molecule complex from which C_2H_2 and H_2 , respectively, rather than C_2D_2 and D_2 are the apparent neutral products. Since complete isotopic scrambling of product ions is not observed, preferential retention of C_2D_2 and D_2 is probably due to a specific structure of the intermediate complex which does not rearrange fast enough to give complete scrambling before falling apart to give the products. Reaction rates with diacetylene followed a different trend than those with precursor neutrals for $C_7H_7^+$ ions from different precursors. In this case, $C_7H_7^+$ ions from toluene reacted faster than those from norbornadiene and cycloheptatriene (see Table 31).

Different behavior was observed when C_2H_2 was used as a reactant neutral. $C_7H_7^+$ from norbornadiene and cycloheptatriene reacted slowly with acetylene as shown by Equations (112) and (113). On the other hand, no reaction products were observed with $C_7H_7^+$ from toluene.

Table 29 shows the percent of unreactive $C_7H_7^+$ as a function of the internal energy of the ion formed from different precursors. At the lowest internal energies above $C_7H_7^+$ formation threshold, $C_7H_7^+$ from toluene had a much smaller percentage of unreactive isomer than $C_7H_7^+$ from norbornadiene and cycloheptatriene. Formation of unreactive $C_7H_7^+$ from all three precursors decreased with increasing internal energy and stayed constant at high enough energy. This behavior is different from that observed previously for toluene and norbornadiene (121,80) in which the unreactive percent first decreased and then increased with internal energy. The previous results were interpreted in terms of the interplay between the two equilibria involving different $C_7H_8^+$

and $C_7H_7^+$ structures (114,118,129,80). The different behavior observed in an earlier ICR study (79), which is similar to that observed in this work, was suggested (114,80) to be the result of the displacement of the equilibrium between two $C_7H_7^+$ structures by the removal of the reactive $C_7H_7^+$ ions through chemical reaction.

In an earlier study⁵, the relative abundances of ions produced from norbornadiene and cycloheptatriene as a function of ionizing electron energy were determined. Similarities of $C_7H_7^+$, $C_5H_5^+$ and $C_3H_3^+$ appearance curves were interpreted to imply that $C_7H_7^+$ formed from these two neutral molecules behaves similarly, i.e., follows the same fragmentation pathways in the same energy range. Differences in the appearance curve of $C_5H_6^+$ for norbornadiene and cycloheptatriene were interpreted as suggesting that $C_7H_8^+$ formed from these compounds by electron impact may have different structures⁵. Extensive fragmentation of $C_7H_8^+$ to give $C_5H_6^+$ was also reported earlier for norbornadiene (80). In this study, the relative abundances of the ions produced from toluene as a function of energy were determined for the purpose of comparison with earlier results obtained for norbornadiene and cycloheptatriene. In contrast to the observed similarity mentioned above between norbornadiene and cycloheptatriene fragment ion appearance curves, those of toluene were significantly different both in terms of energetics and of general shape. For example, the onsets of formation for both $C_5H_5^+$ and $C_3H_3^+$ were different than those values observed for the other two precursors. Furthermore, the relative intensities for $C_5H_5^+$ and $C_3H_3^+$ increased much more slowly with energy relative to those from norbornadiene and cycloheptatriene. The maximum relative intensities for $C_5H_5^+$ and $C_3H_3^+$ ions were 0.017 and 0.005 for toluene and 0.10 and 0.035 for norbornadiene and cycloheptatriene, respectively (see Figure 40). This different behavior in the fragmentation of $C_7H_7^+$ produced from toluene suggests the involvement of a different structure (benzyl⁺, II) for $C_7H_7^+$ in the case of toluene.

Based on the differences in behavior observed in this study of $C_7H_7^+$ ions produced from three precursors, the possibility of structures other than benzyl and tropylum must be considered. The unreactive structure which was observed in all three cases has been shown to be cyclic "tropylum" (I) by a number of previous experimental (79,99,100,122-128) and theoretical (106,107)

studies. Similarly, the reactive isomer produced from toluene was identified as the "benzyl" (II) structure numerous times previously (79,99,100,121-128). However, the results of this study have shown that it behaves somewhat differently than the reactive $C_7H_7^+$ isomers produced from norbornadiene and cycloheptatriene. Although no definitive assignment for reactive $C_7H_7^+$ ion structure(s) produced from norbornadiene and cycloheptatriene can be made at this point, the most probable structures will be discussed considering the energetics of $C_7H_7^+$ ions.

a. Cycloheptatriene.

AM1 calculations for the $C_7H_8^+/C_7H_7^+$ surface¹² suggest the structure produced by hydrogen loss from the bicyclo[3.2.0]heptadiene radical cation (BCH^+) (V), is a possible stable $C_7H_7^+$ isomer, accessible at about



V



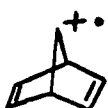
VI

2.8 ev above the appearance potential of tropylium from cycloheptatriene. This structure is in a potential well which is deep enough that it might reasonably be expected to live for an extended time¹². It was also suggested¹² that this structure is most probably formed from cycloheptatriene by isomerization on the radical cation surface followed by hydrogen loss from V. Isomerization of $(BCH-H)^+$, VI ($\Delta H_f = 274.4$ kcal/mol)¹² to tropylium is considered unlikely due to the requirements of orbital symmetry, which imposes no constraints for the odd electron radical parent ion. Although the barrier to form II is lower than that for V, it was suggested¹² that the simplicity of the rearrangement to the latter, compared to the convoluted surface leading to benzyl or toluene radical ion, may make formation of BCH^+ , V, a faster rearrangement at high enough energy. Consistent with these calculations, our experimental results show that the percent of unreactive $C_7H_7^+$ from cycloheptatriene decreases very rapidly with increasing internal energy. This can be interpreted as a result of increased isomerization of the cycloheptatriene cation to V. At high energy, when the equilibrium between these two parent ions is established, the percent of unreactive isomer stays constant due to

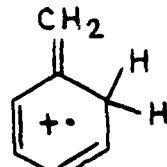
the absence of isomerization between two $C_7H_7^+$ structures with an energy barrier of 14.1 kcal/mol¹². Other experimental evidence for the involvement of different structures for $C_7H_8^+$ ions formed from toluene and cycloheptatriene comes from the strikingly different photodissociation curves of these ions (130).

b. Norbornadiene.

In spite of the general similarity of the behavior of $C_7H_7^+$ ions from cycloheptatriene and norbornadiene, differences in reactivity (see Tables 29 and 30) suggest the formation of a $C_7H_7^+$ structure different from the structure formed from cycloheptatriene. A simple bond breakage in norbornadiene, (VII) can directly form an ipso-protonated benzyl radical,



VII



VIII

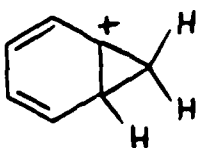
$C_6H_5(H^+)CH_2$ ion, in which a 1,2-hydrogen shift leads to the intermediate, 5-methylene-1,3-cyclohexadiene ion, VIII, with a theoretical $\Delta H_f = 219$ kcal/mol (131). The latter ion was proposed to account for the ring expansion of the toluene ion in the III \rightarrow IV isomerization process (131). The formation of VIII from other precursor cations at least with a transitory existence has been indicated by previous experimental evidence (132). After the availability (133) of 5-methylene-1,3-cyclohexadiene, experimental determination of its ionization potential indicated a heat of formation 18 kcal/mol higher than that of the toluene ion (134).

Once this intermediate ion is formed, it can rearrange to another structure or decompose directly to the $C_7H_7^+$ ion. In fact, it was suggested that direct decomposition of this ion is in competition with rearrangement to other structures, cycloheptatriene cation being the most probable rearrangement product (135). The competition between these two processes is believed to depend on the internal energy with rearrangement being favored at lower energies (136). Thus at low energies, fragmentation to $C_7H_7^+$ after rearrangement

to the cycloheptatriene ion is expected due to the lower activation barrier for fragmentation of the cycloheptatriene ion (121). This is consistent with our results, which indicate a high percent of unreactive $C_7H_7^+$ (tropylium $^+$, I) formed from norbornadiene at low energy (see Table 28). Studies of the photodissociation of $C_7H_8^+$ ions suggested about half of the norbornadiene cations convert to cycloheptatriene cations (130). On the other hand, it has been reported that there is no rearrangement of this ion to the toluene ion on a time scale of 10^{-2} s (137).

Photodissociation spectra of n-butylbenzene and 2-phenylethanol ions which are believed to form VIII were studied to identify any possible rearrangement products (136). The results were consistent with the retention of the VIII structure. Although there was not any evidence for ready interconversion among $C_7H_8^+$ structures for nondecomposing methylenecyclohexadiene ions, it was suggested that the more energetic, decomposing VIII ions may interconvert to other structures. In this study, the decrease in the percent of tropylium structure with an increase in energy is interpreted as a result of the fact that decomposition of VIII becomes competitive with rearrangement to IV. Thus, we suggest the $C_7H_7^+$ structure formed by hydrogen loss from VIII as the reactive isomer formed from norbornadiene.

ICR studies (134) involving the formation of VIII from its precursor neutral at 30 eV electron energy indicated ion/molecule chemistry different from that of toluene. $C_7H_7^+$ produced from VIII was reported to have a different rate coefficient and reaction efficiency for the formation of $C_8H_9^+$. It is interesting to note that the rate coefficient reported ($0.6 \times 10^{-10} \text{ cm}^3/\text{s}$) (134) for this reaction agrees very closely with the value ($0.8 \pm 0.3 \times 10^{-10} \text{ cm}^3/\text{s}$) found in this work for the reaction of $C_7H_7^+$ formed from norbornadiene with toluene (see Table 30). Although a definitive structure can not be assigned to $C_7H_7^+$ formed from VIII, one possible structure is the norcaradienyl ion, IX, which was calculated as a stable structure with $\Delta H_f = 235.9 \text{ kcal/mol}$ (107).



IX

Supporting experimental evidence for the existence of stable $C_7H_7^+$ structures other than benzyl and tropylium comes from a UV absorption study of $C_7H_7^+$ ions in solid argon (129). A trend in reactivity was observed for reactions of $C_7H_7^+$ ions from norbornadiene and cycloheptatriene with precursor neutrals, acetylene, and diacetylene. In all three cases, the reactive structure formed from norbornadiene reacted more slowly than that formed from cycloheptatriene. This is consistent with the general observation that less reactive structures of small hydrocarbon ions have lower heats of formation since $C_7H_7^+$ structure formed from VIII has a higher heat of formation than that formed from V.

Finally, in relation to the ionic soot formation mechanism, the existence of a different $C_7H_7^+$ ion less stable than benzyl in flames would account for the low $C_7H_7^+$ concentration found in flames (14a). As with $C_5H_5^+$ and $C_3H_3^+$ (42), $C_7H_7^+$ also reacts rapidly with diacetylene, but does not react with acetylene. Furthermore, in this study, product ions with increased C:H ratios having as many as 13 carbon atoms have been observed in the reaction of $C_7H_7^+$ with diacetylene. There is, however, still the possibility of stabilization of a larger fraction of the $C_9H_9^+$ reaction complexes by the greater number of third-body collisions in atmospheric pressure flames. In fact, such collisional stabilization for $C_5H_5^+$ and $C_6H_6^+$ reaction complexes has been observed in higher pressure SIFT studies (103,104).

SECTION IV

KINETIC MODELING OF THE REACTIONS OF $C_3H_3^+$ WITH ACETYLENE, DEUTEROACETYLENE, AND DIACETYLENE

A. INTRODUCTION

The energetics of small hydrocarbon ions such as $C_3H_3^+$, $C_5H_3^+$, $C_5H_5^+$, and $C_7H_7^+$ and their reactions with a variety of neutral hydrocarbons, particularly acetylene and diacetylene, have been reported in Sections II and III.

As reported in Section IIIC, bimolecular reactions of the propargylium form of $C_3H_3^+$ with acetylene most often result in an isomerization to the cyclopropenylidene isomer. To help understand this isomerization process, $C_3H_3^+$ reactions with deuterated acetylene were investigated (42). These studies showed that the isomerization proceeds via the $C_5H_5^+$ ion/molecule reaction complex, which is sufficiently long-lived under the experimental conditions employed that deuterium exchange, as well as isomerization, takes place. Thus with time the reactive, propargylium $C_3H_3^+$ isomer is converted to both reactive and unreactive species containing one, two, and three deuterium atoms.

To better understand the isomerization which converts the reactive to the unreactive form of $C_3H_3^+$, kinetic modeling studies of the ion intensity versus time curves reported earlier (42) were carried out. It was also hoped that fitting procedures would produce improved ion/molecule reaction rate coefficients. Quantum mechanical calculations on $C_3H_3^+$ and $C_5H_5^+$ structures and reactivity, reported in Sections IID-IIIF, were used to guide the modeling effort.

B. METHODOLOGY

Nonlinear least-squares fitting routines employing Marquardt's algorithm (138), implemented on two different computers¹³, were used for kinetic modeling. Complete analytical solutions were obtained from the chemical models developed below for the systems $C_3H_3^+ + C_2H_2$ and $C_3H_3^+ + C_4H_2$. A

complete analytical solution was not possible when an isotope effect was included in the chemical model for the $C_3H_3^+ + C_2D_2$ system. Numerical integrations used the finite difference method (138). The independent variable step size for the numeric portion was generally set to 0.001 s. Increasing the step size to 0.002 s had negligible effect on the results.

C. THEORY

In studying reactions it is desirable to have knowledge of the internal energy distribution, $P(E)$, and the microcanonical rate constants, $k(E)$. With this information the time-dependent expression for the j th rate constant, $k_j(t)$, can be written as:

$$k_j(t) = \int_{E_0}^E P(E) k_j(E) \exp\left\{-\sum_i k_i(E)\right\} t dE, \quad (119)$$

in which E_0 is the threshold energy for the j th reaction and the summation in the exponential term is over all competing reactions, including the j th reaction (139,140). In fast unimolecular ionic decomposition reactions $P(E)$ might not be characterized by a Boltzmann distribution.

The reactions studied here are bimolecular addition reactions followed by unimolecular decomposition. Given the ionization potential of Xe (12.1 eV) and the reported (44) appearance potential of the propargylum ion from C_3H_3I (10.5 eV), 1.6 eV of excess energy is available. Much of this excess energy will be converted into translational motion of the heavy Xe and I neutrals resulting from the charge transfer in the collision process. Under typical experimental conditions (ca. $2 - 3 \times 10^{-6}$ torr total pressure), about 125 ms was allowed for the charge transfer process and for ejecting intermediates. For these conditions the $C_3H_3^+$ ions collided a number (10-15) of times with the excess Xe present in the FTICR cell, leading to near thermalization of internal energy before the ion/molecule reactions were monitored. Since the reaction time scale was on the order of seconds, we believe that any slight initial deviation from Boltzman behavior presents no serious error.

The long reaction time, due to the bimolecular nature of the process, allows for energy randomization very early within the time scale of the

reactions. Therefore simple rate constants and rate expressions can be used in lieu of detailed applications of Equation (119).

D. RESULTS

1. Models of $C_3H_3^+$ + C_2H_2

As reported earlier (42), collision of the propargylium cation, $\ell-C_3H_3^+$, with acetylene forms the cyclopropylium cation, $c-C_3H_3^+$, which is unreactive on the time scale of the experiments, given the pressures attainable in the FTICR cell. Experiments with C_2D_2 showed that an encounter complex which allows for isotopic scrambling is formed. Hence, whatever the isomeric form of this complex, a structure having the chemical formula $C_5H_5^+$ can be postulated. Since no species of m/z 65 is observed in the mass spectrum, the $C_5H_5^+$ species must be in steady-state and of low concentration. The simplest scheme which takes into account this information is:



Applying steady-state kinetics to scheme (120) yields

$$I(t) = I^0 - k'_p I_\ell^0 (1 - e^{-\theta t})/\theta, \quad (121)$$

in which I^0 and $I(t)$ are ion intensities initially and as a function of time, respectively, I_ℓ^0 refers only to the linear form, $k'_p = k_p P_{C_3H_3I}$, and

$$\theta = [k_f k_c P_{C_2H_2} / (k_\ell + k_c)] + k'_p. \quad (122)$$

Equation (121) was fitted to several kinetic runs reported earlier (42). Table 32 shows results of these fits. A plot of θ versus $P_{C_2H_2}$ should be linear, as implied by Equation (122), and this is demonstrated in Figure 41. Results yield $k_f k_c / (k_\ell + k_c) = (2.3 \pm 0.2) \times 10^6 \text{ torr}^{-1} \text{ s}^{-1}$ and $k'_p = (1.4 \pm 0.2) \text{ s}^{-1}$.

TABLE 32. RESULTS OF FITS OF EQUATION (121) TO KINETIC DATA FOR THE $C_3H_3^+ + C_2H_2$ REACTION.^a

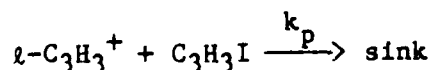
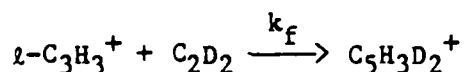
$P_{C_2H_2}$ / torr	$k_p' I^0 / \text{Arb units} \cdot s^{-1}$	θ/s^{-1}
0	1.53(.06)	1.58(.08)
4.4×10^{-7}	1.65(.20)	2.40(.31)
1.0×10^{-6}	1.74(.12)	3.60(.24)
1.6×10^{-6}	1.71(.08)	4.82(.23)
2.0×10^{-6}	1.71(.11)	6.33(.38)

^a The standard error of estimate computed by the fitting program is shown in parentheses.

2. Models of $C_3H_3^+ + C_2D_2$.

Reaction of $C_3H_3^+ + C_2D_2$ is complicated by the observation that isotopic scrambling occurs and isotope effects are possible. Several models have been tried, including those which allow for complete isotopic scrambling and those which allow only partial scrambling. The simplest model allows for complete scrambling and no isotope effects¹⁴.

Complete scrambling occurs when fragmentation of the complex, $C_5L_5^+$ ($L = H, D$), yields precursors having a statistical distribution of hydrogen and deuterium atoms. $C_5H_3D_2^+$ will then yield the following ratios of precursors: $C_3H_3^+:C_3H_2D^+:C_3HD_2^+ = 1:6:3$. Using these statistics for obtaining the isotopic distribution in the $C_3L_3^+$ precursors, we find:



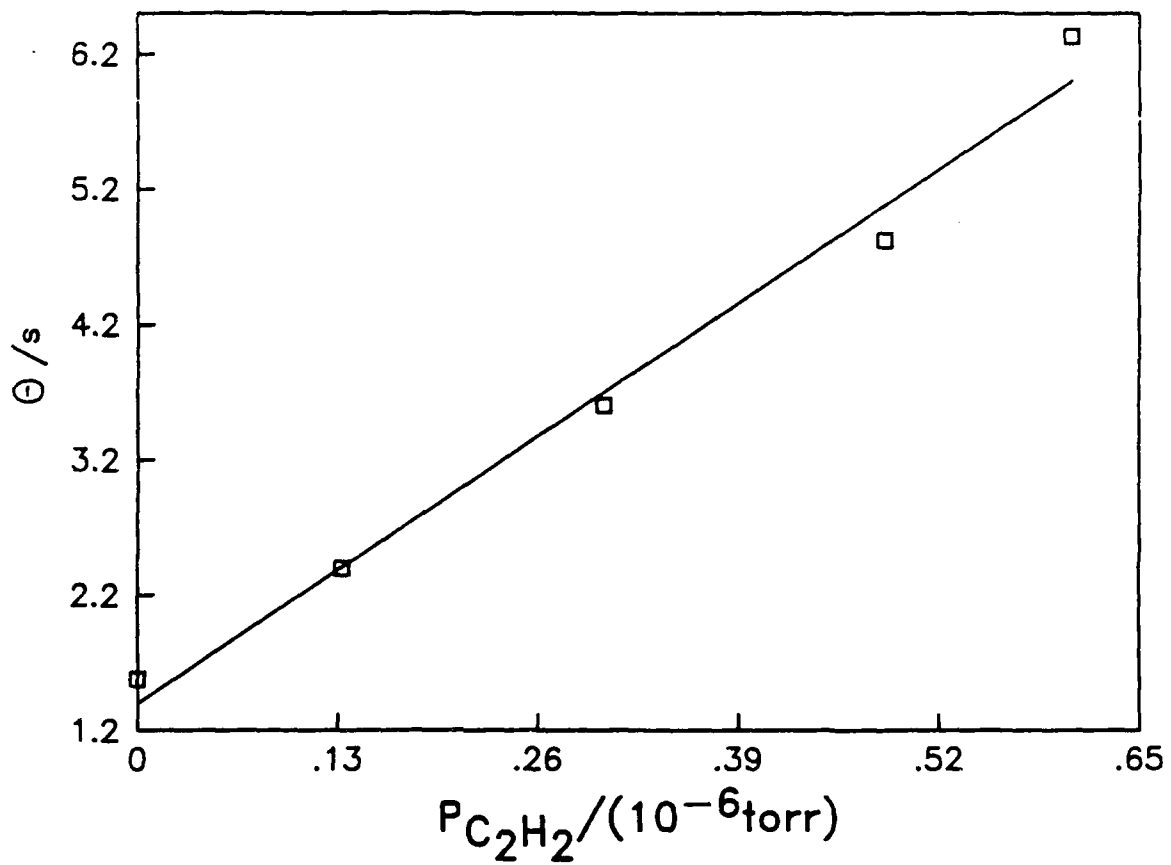
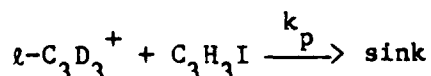
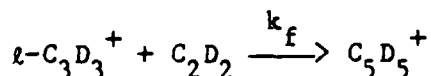
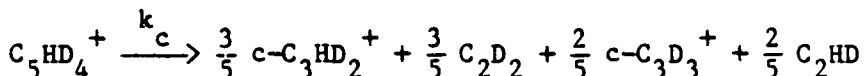
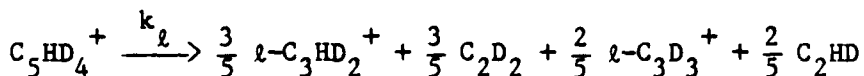
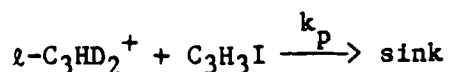
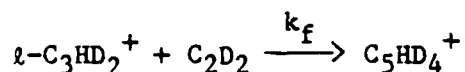
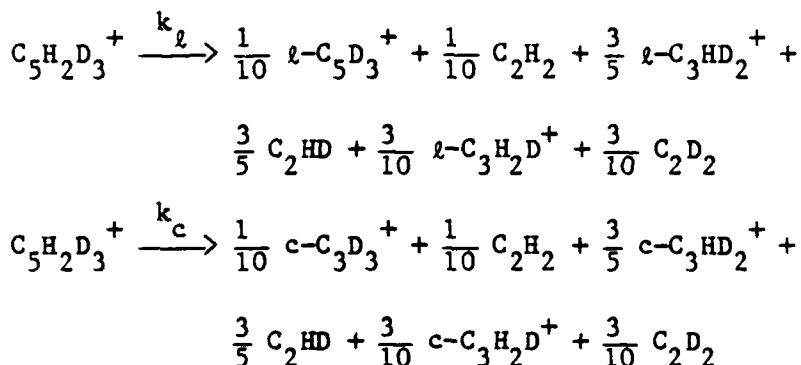
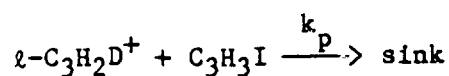
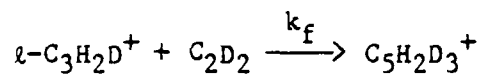
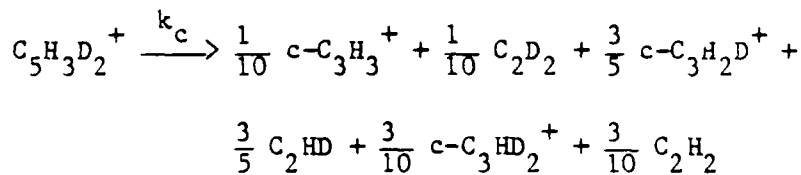
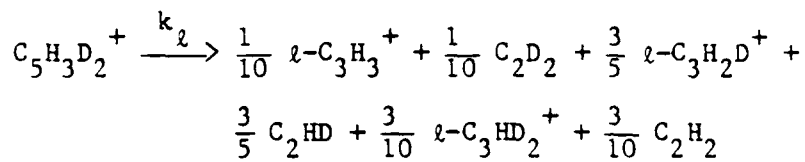


Figure 41. Plot of θ versus $P_{C_2H_2}$ (Equation (122)), Showing Best Fit Line.

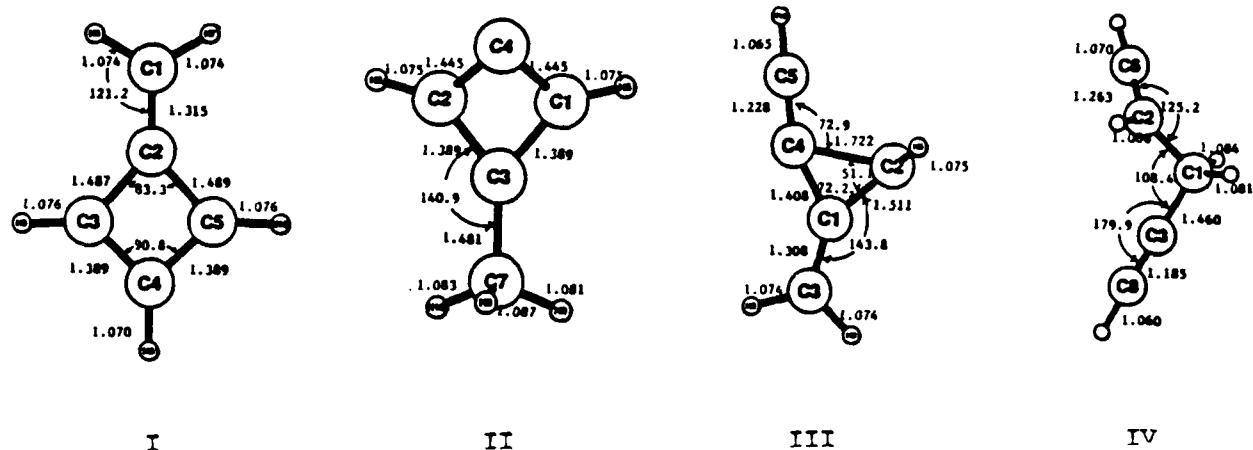




With the assumption again that all four $C_5L_5^+$ complexes are in steady-state a full analytical solution is possible for the set of kinetic differential rate equations. The solutions to the set of equations are given in Appendix B. Figure 42 shows the best fit curves to a typical data set. Table 33 shows the fitted parameters, errors, and residual sum of squares from fits of a typical data set: these results are labelled $F = 1$.

An examination of Figure 42 shows that the model given in scheme (123) does not adequately explain the production of $C_3HD_2^+$. In an attempt to examine this, incomplete, or partial isotopic scrambling was next assumed. To do this correctly requires a detailed knowledge of the chemistry of the system, which is not available. A somewhat crude application of isotope effects applies multiplicative factors to the individual rate constants and this procedure requires but a nominal knowledge of the structure of the species involved¹⁵. We apply this simple scheme as described below.

Quantum mechanical calculations^{8,9} indicate that C_2H_2 does not react with the cyclopropenyl cation, but does react with the propargylic cation ($\ell-C_3H_3^+$) without barrier with formation of the following four possible products:



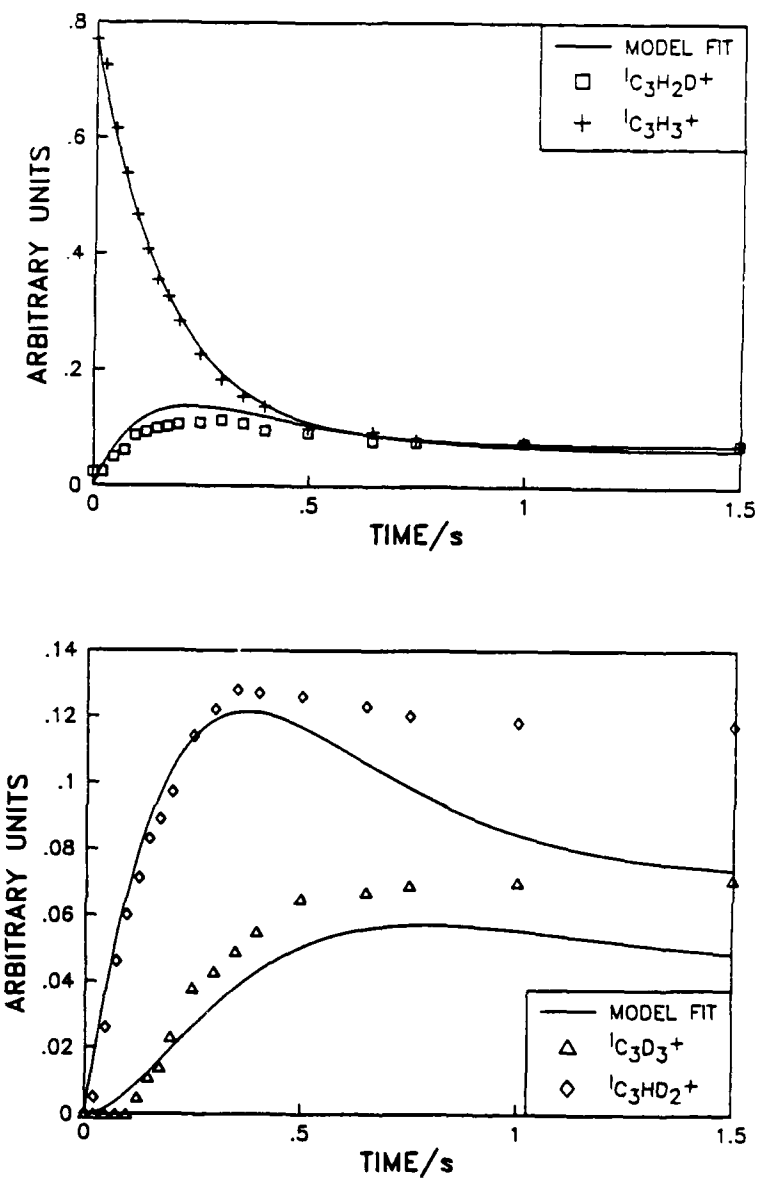


Figure 42. Model Fit (scheme (123)) to Typical Data Set for $\text{C}_3\text{H}_3^+ + \text{C}_2\text{D}_2$ Reactions.

TABLE 33. RESULTS OF MODEL FITS (SCHEMES 123 AND 124) FOR THE SYSTEM $C_3H_3^+ + C_2D_2$ UNDER VARIOUS EXPERIMENTAL CONDITIONS.

Pressures (torr) (P_{Xe} for all runs = 6×10^{-6} torr)	$k_f P_{C_2D_2}$	k_c/k_x	F	$k_p P_{C_3H_3I}$	I_g^0	I_c^0	SOS*
				(s^{-1})	(arb units)	(arb units)	
$P_{C_2D_2} = 1.2 \times 10^{-6}; P_{C_3H_3I} = 1.1 \times 10^{-7}$	4.17(.15)	.212(.030)	1(fixed)	2.03(.10)	.707(.007)	.063(fixed)	.017
$P_{C_2D_2} = 1.2 \times 10^{-6}; P_{C_3H_3I} = 1.1 \times 10^{-7}$	1.11(.14)	.308(.026)	1.86(.11)	2.16(.08)	.703(.005)	.067(fixed)	.0069
$P_{C_2D_2} = 7.8 \times 10^{-7}; P_{C_3H_3I} = 1.1 \times 10^{-7}$.920(.098)	.318(.032)	1.71(.08)	2.20(.09)	.671(.007)	.057(.008)	.0023
$P_{C_2D_2} = 6.2 \times 10^{-7}; P_{C_3H_3I} = 1.1 \times 10^{-7}$	1.30(.12)	.389(.026)	1.53(.06)	2.74(.07)	.881(.006)	.100(.006)	.0038
$P_{C_2D_2} = 1.1 \times 10^{-6}; P_{C_3H_3I} = 1.3 \times 10^{-7}$	1.86(.34)	.363(.034)	1.58(.13)	2.18(.11)	.856(.007)	.061(fixed)	.024

* Sum of squares.

Thermodynamically, only I is stable with respect to decomposition to $\alpha\text{-C}_3\text{H}_3^+ + \text{C}_2\text{H}_2$. However, since the $\alpha\text{-C}_3\text{H}_3^+ + \text{C}_2\text{H}_2 \rightarrow \text{I}$ reaction is at least 60 kcal/mol exothermic,⁸ in the absence of stabilizing collisions this energy then permits many different isomeric forms to be sampled before decomposition back to $\text{C}_3\text{H}_3^+ + \text{C}_2\text{H}_2$. If the sampling of all isomers is fast, complete isotopic scrambling is expected. Given the uncertainty in C_5H_5^+ structures, total equivalence of carbon atoms in the complex is assumed. For ease of understanding, a cyclic C_5H_5^+ complex, in which all C atoms are sp^2 hybridized, might be visualized. With these assumptions, it is a simple matter to determine which carbon atoms undergo hybridization changes during the reaction. For instance, in the attack of C_2H_2 on $\alpha\text{-C}_3\text{H}_3^+$, three carbon atoms change from sp to sp^2 hybridization. Upon fragmentation, some carbon atoms remain sp^2 hybridized; others become sp hybridized.

In general, for α -secondary isotope effects, an increase in hybridization in going from the reactant state to the transition state yields an inverse isotope effect ($k_{\text{H}} < k_{\text{D}}$), whereas a decrease in hybridization yields a normal isotope effect ($k_{\text{H}} > k_{\text{D}}$) (142). In our system the bimolecular addition reaction will have an inverse isotope effect, and the fragmentation reaction should have a normal isotope effect. Figure 43 shows the energetics for the reaction of $\alpha\text{-C}_3\text{H}_3^+ + \text{C}_2\text{L}_2$ and how the isotope effects for the elementary reactions can arise. For the forward addition reaction, $E_{\text{FH}} > E_{\text{FD}}$ and for the fragmentation reaction, $E_{\text{RH}} < E_{\text{RD}}$, in which the subscripts "F" and "R" refer to forward and reverse, respectively. Since the bimolecular addition is very exothermic for the formation of most C_5L_5^+ isomers^{8,9} it might be expected that the "average" transition state structure might closely resemble the reactants and not any of the C_5L_5^+ isomers. This in turn implies that $E_{\text{RD}} - E_{\text{RH}} > E_{\text{FH}} - E_{\text{FD}}$ (zero-point effects). However, the excess energy in the reaction will allow longer sampling times for the more energetic C_5L_5^+ isomers. The less energetic isomers which are sampled will undoubtedly be in higher rotational and vibrational levels. The overall effect is to lessen the normal isotope effects expected in the fragmentation of the C_5L_5^+ isomers, unless there are sufficient collisions to stabilize the isomers prior to fragmentation.

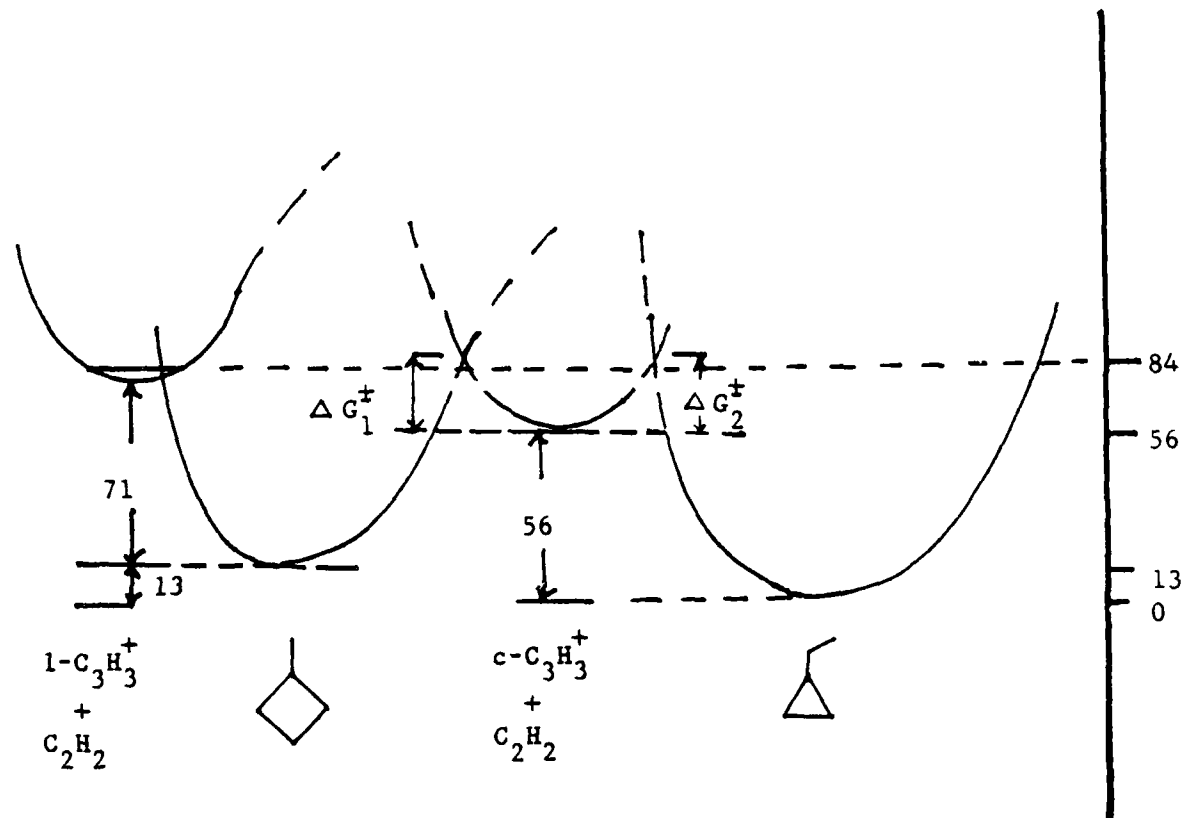


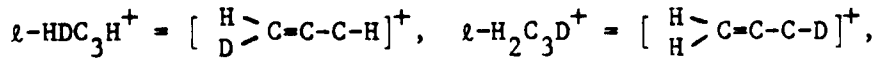
Figure 43. A Schematic Diagram of the Reaction of $i\text{-C}_3\text{H}_3^+$ with C_2H_2 . The values given in the Figure are kcal/mol. Since experiments indicate that $c\text{-C}_3\text{H}_3^+$ can be found, ΔG_1^\ddagger cannot be much greater than 28 kcal/mol. ΔG_2^\ddagger is unknown as the studied reaction leads to no stable C_5H_5^+ species in the absence of collisions.

In the model development outlined below, only α -secondary isotope effects will be considered important. β -secondary isotope effects, arising predominantly from hyperconjugation, can sometimes be important (143), but will be assumed here to be minor compared to the α -effects. It is also possible that hydride/deuteride shifts may be occurring in the transition-state. However, hydride transfers often exhibit small isotope effects (144), and hydride shifts, if they occur at all, will be assumed here to give negligible contributions to the isotope effects.

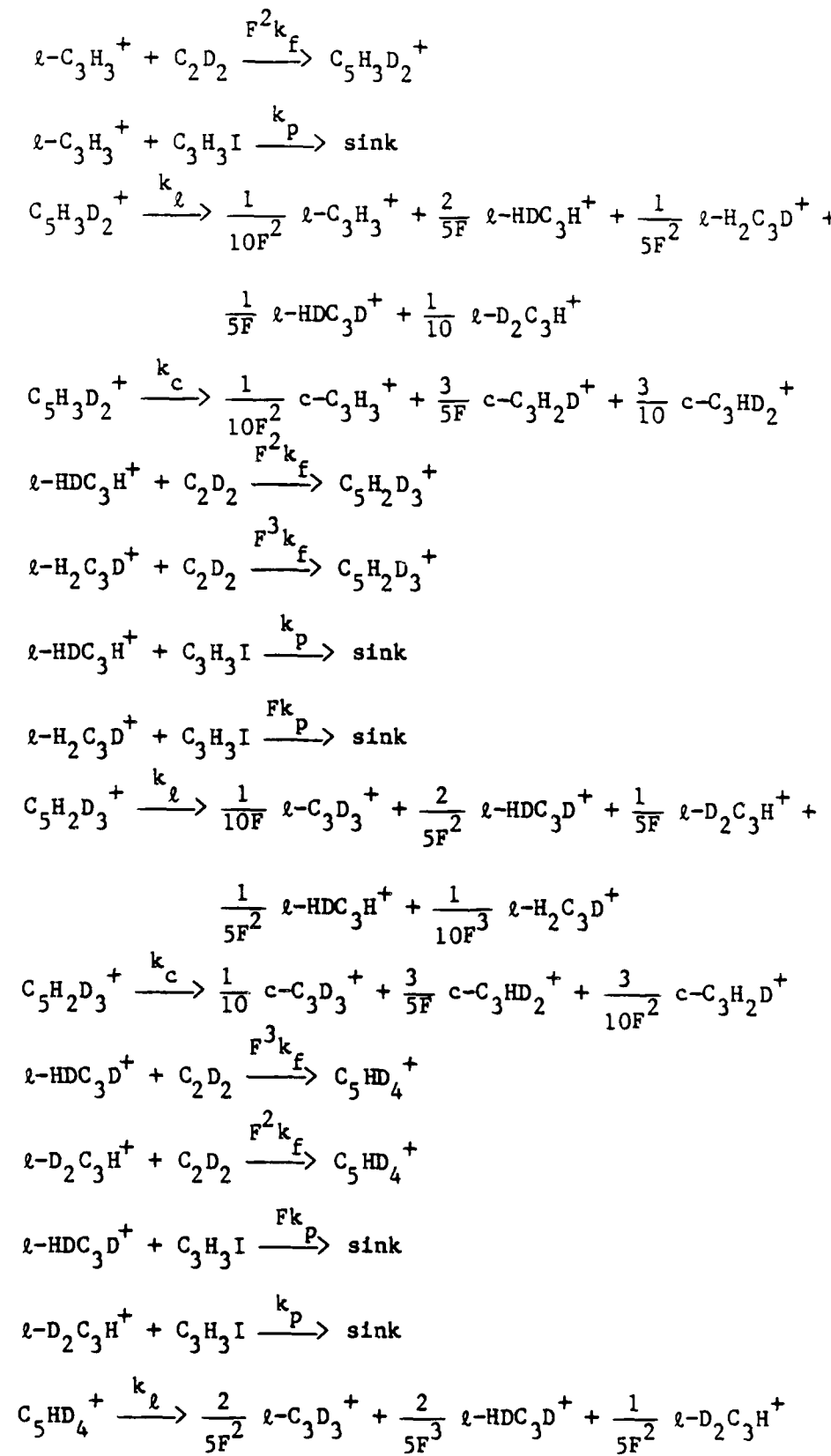
Even though the different reactions represented by Equations (113) will have different isotope effects, the introduction of an independent fitting parameter for each reaction is not justified. Though crude, only one additional parameter is introduced into the model to account for all potential α -secondary isotope effects. The method for introducing this parameter is outlined as follows.

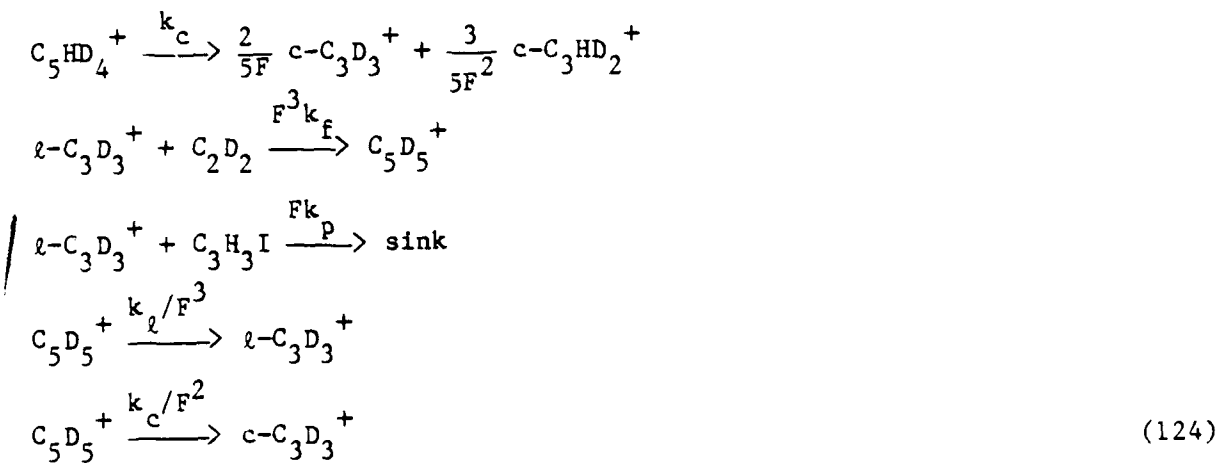
If a carbon atom bearing a deuterium atom undergoes a hybridization change from sp to sp^2 (force field becoming stronger), the "isotope effect factor", F, is introduced as a multiplicative factor in the rate constant. For two deuterium atoms, F^2 is the multiplicative factor, etc. If the deuterium atom is attached to an atom changing from sp^2 to sp hybridized, the rate constant is divided by F, for two deuteriums, F^2 , etc. Introducing the same factor for both addition and fragmentation reactions implies a constraint which is at best only qualitatively correct. Applied in the numerator the factor corrects for a single deuterium atom (F^2 for two, etc.) attached to a center undergoing hybridization change from sp to sp^2 in the transition-state complex. Applied in the denominator, it corrects for a change from sp^2 to sp hybridization. Since the transition-state complex has a stronger force field than the reactant state ($\ell\text{-C}_3\text{L}_3^+ + \text{C}_2\text{L}_2$) at these centers, the α -secondary isotope effect should be "inverse" and F should therefore be greater than unity.

Using the structural notation,



the full kinetic scheme is:





The neutral fragmentation products, C_2H_2 , C_2HD , and C_2D_2 , have not been included for brevity. It is assumed that $l-C_3L_3^+$ undergoes the same kind of hybridization changes when reacting with C_3H_3I as it does with C_2L_2 . Earlier work (42,76) has shown that the products of the $l-C_3L_3^+ + C_3H_3I$ reaction are of higher mass and do not enter further into the kinetic schemes modeled here.

Steady-state conditions are applied for all $C_5L_5^+$ isotopic species as before (without regard for isomeric differentiation) and the differential rate Equations which represent Equations (124) are given in Appendix B. Table 33 shows fitting results for several data sets using Equations (124). Figure 44 shows plots of the best fit of this model to the same data set as fitted in Figure 42.

Using FTICR double resonance techniques (69) some experiments were conducted where certain ions were ejected from the analyzer cell as they formed. Among the ions ejected were $C_3H_2D^+$ and $C_3^{HD_2}^+$. Without further fitting, this model was used to predict the behavior of the kinetic system if there were ejected. Figure 45 shows predicted results and data points.

3. Models for $C_3H_3^+ + C_4H_2$.

The reaction of $C_3H_3^+$ with C_4H_2 (diacetylene) is kinetically more complicated than that of $C_3H_3^+$ with C_2H_2 . There are more isomeric possibilities, and ion/molecule reaction products of higher m/z are detected. Several models were tried in attempts to fit the experimental data, and the best of these made the assumptions that $C_7H_5^+$ and the excited forms of

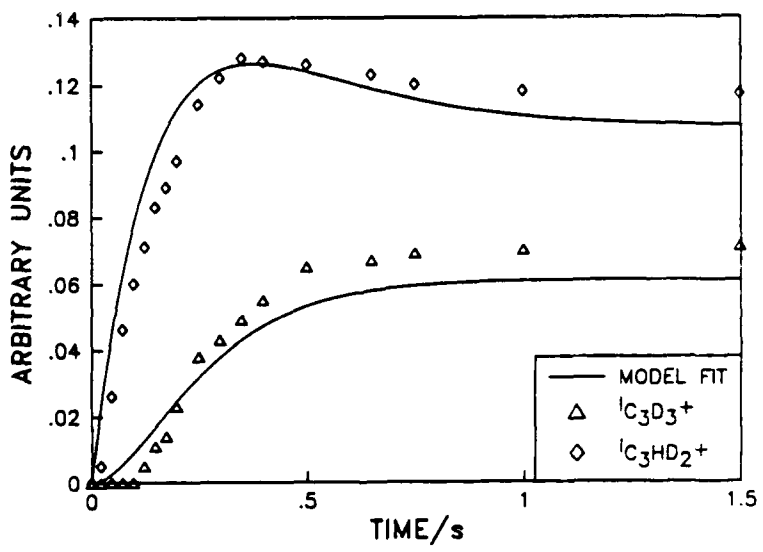
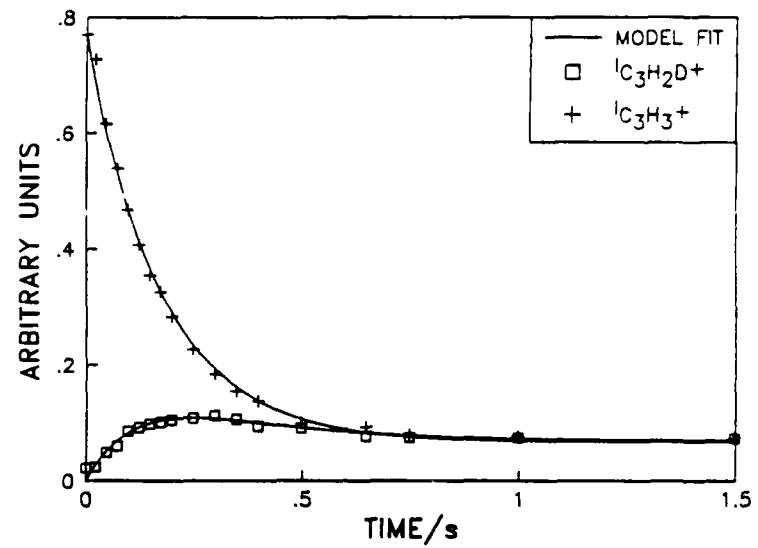


Figure 44. Model Fit (scheme (124)) to Typical Data Set for C_3H_3^+ + C_2D_2 Reactions.

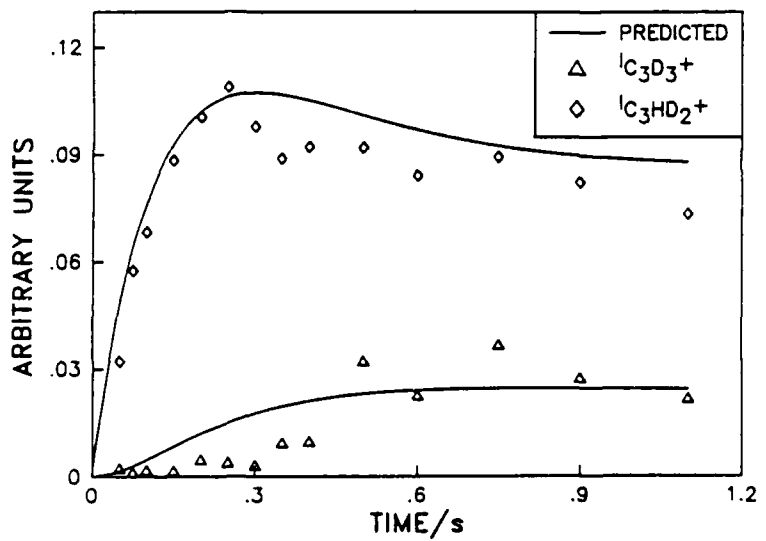
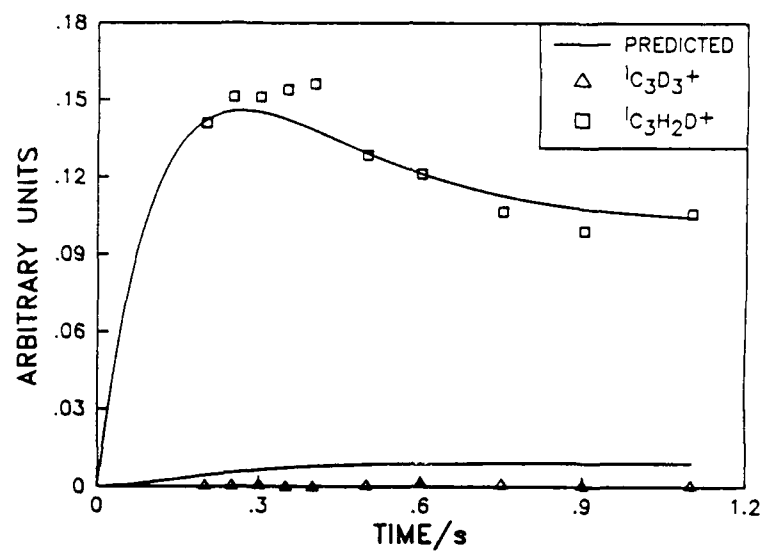
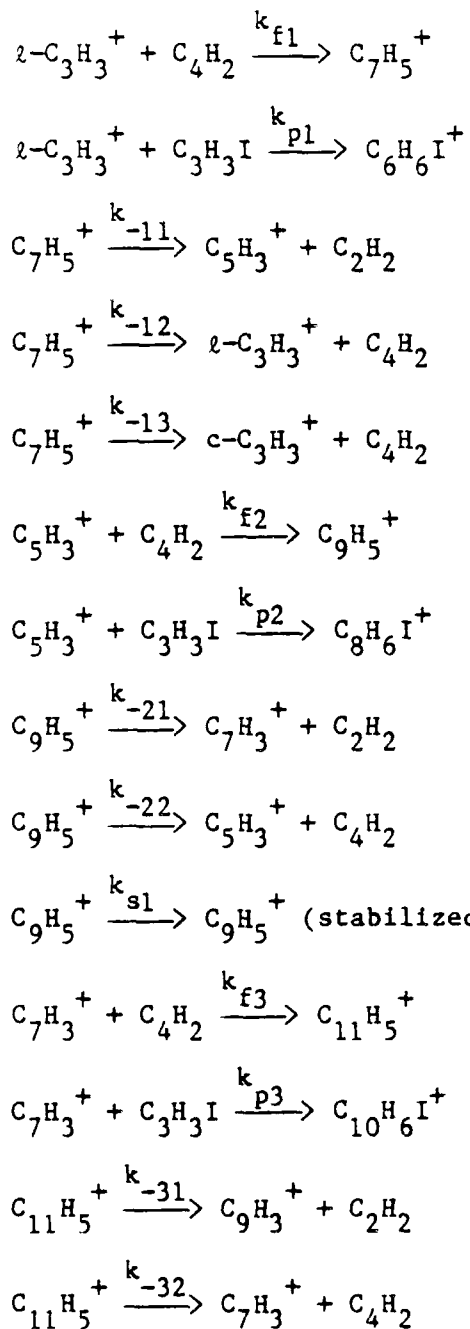
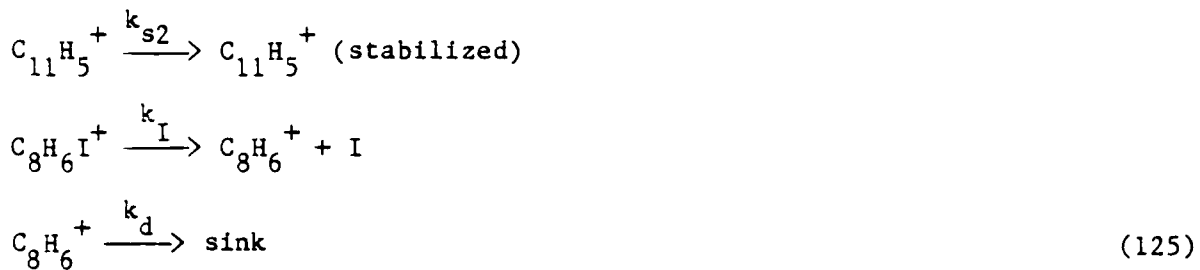


Figure 45. Data from Ejection Studies (C_3H_3^+ + C_2D_2 reaction) and Model Prediction (C_3HD_2^+ ejected - top; $\text{C}_3\text{H}_2\text{D}^+$ ejected - bottom).

$C_9H_5^+$ and $C_{11}H_5^+$ are in steady state, while $C_5H_3^+$ and $C_7H_3^+$ are not. In order to account for the build-up of $C_9H_5^+$ and $C_{11}H_5^+$ ions, it was necessary to include collision-induced stabilization steps for the excited forms of these ions. A further assumption was made that the stabilized forms of $C_9H_5^+$ and $C_{11}H_5^+$ are not reactive within the time frame (2s) of the experiments.

The resulting scheme is:





Reactions involving $C_8H_6I^+$ are included because $C_8H_6^+$ is detected in the ICR experiments. Applying steady-state assumptions to the $C_7H_5^+$, $C_9H_5^+$, $C_{11}H_5^+$, and $C_8H_6^+$ ions yields a model with a full analytical solution (Appendix B). Figure 46 shows results of the model fit to a typical data set. The kinetic parameters have been grouped as exponential and pre-exponential terms in the equations, yielding 9 fitting parameters. Table 34 shows results of model fits of two data sets. The term $k_{p2}P_{C_3H_3I}$ is $-(\theta_2 + k_{-21}\phi_2 + k_{S1}\phi_2)$, and hence can be calculated from the parameters. The results of the first data fit yield in Table 34 yield $k_{p2}P_{C_3H_3I} = (1.2 \pm 0.3) s^{-1}$ and those from the second data fit, $k_{p2}P_{C_3H_3I} = (1.3 \pm 0.2) s^{-1}$.

E. DISCUSSION

1. $C_3H_3^+ + C_2H_2/C_2D_2$

Several insights into the mechanism of the $C_3H_3^+ + C_2H_2/C_2D_2$ reactions are obtained from these modeling studies. First, a value of $(1.4 \pm 0.2) s^{-1}$ is obtained for k_p' from the intercept of Figure 41 (values for k_p' are a little higher from model fits shown in Table 33). Assuming a cell temperature of 363 K (3) and given that $P_{C_3H_3I} = 3.3 \times 10^{-8}$ torr (after system factor correction), $k_p = (1.6 \pm 0.2) \times 10^{-9} \text{ cm}^3 \cdot \text{s}^{-1}$, in good agreement with previous work in these laboratories. Second, the model gives branching ratios for the complex $C_5L_5^+$. The ratio, k_c/k_ℓ , is ca. 0.34 (.03) (Table 33), implying that $C_5L_5^+$ fragments to $\ell-C_3H_3^+$ at a rate three times that of fragmentation to $c-C_3H_3^+$. $c-C_3H_3^+$ is thermodynamically more stable than $\ell-C_3H_3^+$ by ca. 25 kcal mol⁻¹ (16); however, only I can decompose to $c-C_3H_3^+$. Apparently, there is enough "sampling time" for I to allow $c-C_3H_3^+$ to be formed in significant amounts. Any factor affecting the internal energy of $C_5L_5^+$, such a collisional stabilization, will undoubtedly affect the ratio k_c/k_ℓ . Hence, k_c/k_ℓ is probably very sensitive to experimental conditions (method of

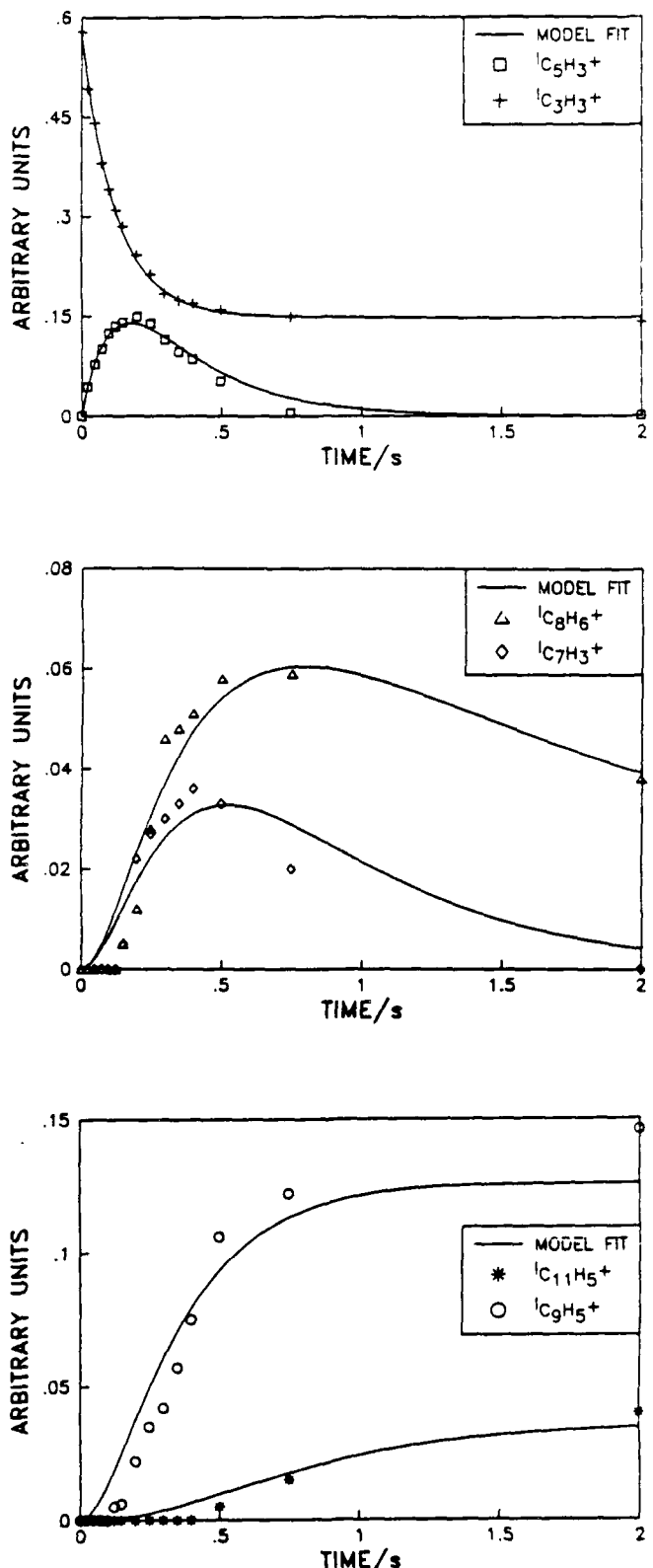


Figure 46. Model Fit (scheme (125)) to a Typical Data Set for $\text{C}_3\text{H}_3^+ + \text{C}_4\text{H}_2$ Reactions.

TABLE 34. RESULTS OF MODEL FITS (SCHEME 125) FOR THE SYSTEM $C_3H_3^+ + C_4H_2$ UNDER VARIOUS EXPERIMENTAL CONDITIONS. a

Pressures (torr)	$\theta_1(s^{-1})^b$	$\theta_2(s^{-1})^b$	$\theta_3(s^{-1})^b$	$(1-k_{-31}\phi_1/\theta_1)^{1/2}^b$ (Arb units)	$k_{-11}\phi_1^{1/2}/\theta_{12}$ (Arb units)
$P_{C_3H_3I} = 1.1 \times 10^{-7};$ $P_{C_3H_3} = 4.8 \times 10^{-7};$ $P_{C_4H_2} = 6.2 \times 10^{-6};$ $P_{X_e} = -8.1(.2)$					
			$-3.9(.2)$	$-1.9(.7)$	$.743(.007)$
					$-0.93(.07)$
$P_{C_3H_3I} = 1.4 \times 10^{-7};$ $P_{C_3H_3} = 5.7 \times 10^{-7};$ $P_{C_4H_2} = 5.3 \times 10^{-6};$ $P_{X_e} = -8.4(.2)$			$-3.9(.1)$	$-3.4(.7)$	$.829(.007)$
					$-1.23(.08)$
$k_{-21}\phi_2(s^{-1})^{\#}$	$k_{s1}\phi_2(s^{-1})^{\#}$	$k_{s2}\phi_3(s^{-1})^{\#}$	$k_d(s^{-1})$	SOS	
1.0(.1)	1.79(.07)	1.0(.3)	.5(.1)	.0051	
1.2(.1)	1.45(.05)	.7(.2)	.2(.2)	.015	

a Initial readings were scaled to one arbitrary unit for comparison.

b $\theta_1 = -(k_{-11} + k_{-13})k_{f1} P_{C_4H_2} / (k_{-11} + k_{-12} + k_{-13}) - k_{p1} P_{C_3H_3I}; \theta_2 = -(k_{-21} + k_{s1})k_{f2} P_{C_4H_2} / (k_{-21} + k_{-22} + k_{s1}) - k_{p2} P_{C_3H_3I}; \theta_3 = -(k_{-31} + k_{s2})k_{f3} P_{C_4H_2} / (k_{-31} + k_{-32} + k_{s2}) - k_{p3} P_{C_3H_3I}; \phi_1 = k_{f1} P_{C_4H_2} / (k_{-11} + k_{-12} + k_{13}); \theta_{12} = \theta_1 - \theta_2; \phi_2 = k_{f2} P_{C_4H_2} / (k_{-21} + k_{-22} + k_{s1}); \phi_3 = k_{f3} P_{C_4H_2} / (k_{-31} + k_{-32} + k_{s2}).$

ionization, total pressure, and temperature). Finally the "direction" and magnitude of F (1.67 (.10)) suggest not only that the model is reasonable, but that the isotope effect plays an important part in the overall kinetics.

It should be remembered that F is not an overall isotope effect; isotope effects are ratios of rate constants. The magnitude of F does, however, indicate the kinetic contribution of replacing one hydrogen atom with a deuterium atom on a hydrogenic site undergoing a hybridization change in the transition-state structure. F^{-1} is the α -secondary kinetic isotope effect for the elementary bimolecular addition reactions per hydrogenic site (only those sites giving rise to α -secondary effects are included). F is the isotope effect for the elementary fragmentation reactions (to $\alpha\text{-C}_3\text{H}_3^+$ and $\text{c-C}_3\text{H}_3^+$) per hydrogenic site (again only those sites giving rise to α -secondary effects are included). Because of the complexity of scheme (124), overall isotope effects cannot be gleaned by determining product ratios, as is often done in isotopic studies of more elementary ion/molecule reactions. However, F can be compared to isotope effects found in elementary ion/molecule reactions.

α -secondary kinetic isotope effects can be quite large (145,146). The larger effects found in ion/molecule reactions are due to a narrow (non-Boltzmann) energy distribution centered close to the threshold energy (147). Even though the secondary isotope effects for the elementary reactions are fairly large in our system, they are not nearly as large as in some of the other systems studied at low pressure in ICR experiments. The magnitude of the isotope effect factor, F, indicates a fair amount of bond rearrangement in the transition state structures. Due to the number of assumptions and the indirect method for obtaining F, we have not attempted to calculate isotope effects from molecular models and calculated vibrational frequencies.

2. $\text{C}_3\text{H}_3^+ + \text{C}_4\text{H}_2$

Kinetic data and modeling of this system reveal some insight into the mechanism for the reaction of C_3H_3^+ and C_4H_2 . Although scheme (125) does not account for specific isomeric reactivities, the scheme does account reasonably well for the data. The signal-to-noise ratios of the available data do not warrant further refinements of the model. Several crude models were at-

tempted, and the model reported here may not be the best or only model which can adequately explain the results. However, of the variations of scheme (125) which were tried, the one reported here gave the best fitting results. In particular, a scheme was tried in which stable forms of $C_9H_5^+$ and $C_{11}H_5^+$ were formed from the corresponding bimolecular additions reactions rather than requiring stabilization steps of "hot" $C_9H_5^+$ and $C_{11}H_5^+$ ions. This scheme did not fit the data. Apparently, only in the ions larger than $C_7H_5^+$ are there enough internal vibrational modes to give rise to an ion/molecule collision complex of sufficient lifetime to allow collisional stabilization at these pressures.

Scheme (125) does not show $C_5H_3^+$ and $C_7H_3^+$ fragmenting to any products. Undoubtedly any isomers of $C_5H_3^+$ and $C_7H_3^+$ which form are all resonance-stabilized. Any fragmentation product would be highly energetic and unlikely to form, even at the energy levels available in these reacting systems. Hence, once $C_5H_3^+$ and $C_7H_3^+$ ions are formed, they will react only in bimolecular addition reactions, which are orders of magnitude slower than the unimolecular fragmentation reactions of $C_7H_5^+$, $C_9H_5^+$, and $C_{11}H_5^+$. Hence, there is a non-steady-state build up of $C_5H_3^+$ and $C_7H_3^+$ ions at the first part of the reaction.

SECTION V

CONCLUSIONS AND RECOMMENDATIONS

A. CONCLUSIONS

The experimental and theoretical work reported here contributes significantly to an understanding of the reactivity, energetics, and structures of small hydrocarbon ions. However, it does not prove or disprove an ionic mechanism of soot formation. It does lead to several clarifications of the ionic mechanism, which will be discussed below.

The low bimolecular reactivity of acetylene with all of the small hydrocarbon ions studied indicates that it may not be as important as postulated in soot nucleation. On the other hand, as reported in Sections IIIB, IIIC, and IIID, diacetylene reacts at rates approaching the Langevin limit with all of the small hydrocarbon ions studied, producing larger ions with high carbon-to-hydrogen ratios. The general reaction



appears to occur in a facile manner and could be quite important in soot nucleation.

The experimental studies carried out here were at significantly lower temperatures and pressures than those found in most combustion environments. Studies of selected rate constants over a limited range found no significant temperature dependence. At high pressures, significant collisional stabilization of ion/molecule collision complexes can occur. Thus, the complexes formed by reaction of acetylene with small hydrocarbon ions might be stabilized, leading to significant termolecular reactivity, even though no bimolecular reactivity was observed in the work reported here.

B. RECOMMENDATIONS

Continuation of this work in several directions could have a major impact

on assessing the importance of an ionic mechanism of soot formation. First, experiments should be carried out at higher pressures, using a high pressure source for the FTICR mass spectrometer, to assess the importance of third-body stabilization of ion/molecule collision complexes. Actual sampling of ions from flames into the FTICR mass spectrometer, in order to probe their structures and reactivity, would extend the isolated studies done here to an actual combustion environment.

A crucial argument in favor of an ion/molecule soot nucleation route is the ease with which cyclic ions, which could lead to polycyclic aromatic hydrocarbons, are formed. Yet the work reported here did not identify definitively when the first cyclic ions were formed. The predicted spectra from theoretical calculations on $C_5H_5^+$ ions were obtained after the end of the contract period, and similar data which can be calculated using the same methodology for $C_5H_3^+$ and $C_7H_x^+$ ions should be combined with laser spectroscopic studies on these ions to determine which, if any, have cyclic structures. Also, theoretical studies which probe the geometries of the ion/molecule collision complexes, such as those carried out here for $C_3H_3^+ +$ acetylene, should be extended to other important reactions, e.g. with diacetylene, and the nature of the proposed chemi-ionization reaction which forms the $C_3H_3^+$ ion (see the Introduction Section) should be investigated.

REFERENCES

1. Gaydon, A. G. and Wolfhard, H. G., Flames, Their Structure, Radiation and Temperature, Wiley, N.Y. 1979.
2. Miller, W. J., Fourteenth Symposium (International) on Combustion, The Combustion Institute, 1973, p. 307.
3. Calcote, H. F., Kurzius, S. C., and Miller, W. J., Tenth Symposium (International) on Combustion, The Combustion Institute, 1965, p. 605.
4. Miller, W. J., Oxidation and Combustion Reviews, Vol. 3, p. 98, 1968.
5. Michaud, R. S. Tse, and Delfau, J. L., Nature, 1978, p. 153.
6. Hayhurst, A. N. and Kittelson, D. B., Combustion and Flame, Vol. 31, p. 37, 1978.
7. Goodings, J. M., Bohme, D. K., and Ng, Chun-Wai, Combustion & Flame, Vol. 36, p. 27, 1979.
8. Goodings, J. M., Bohme, D. K., and Ng, Chun-Wai, Combustion & Flame, Vol. 36, p. 45, 1979.
9. Michaud, P., Delfau, J. L., and Barassin, A., Eighteenth Symposium (International) on Combustion, Combustion Institute, 1981, p. 443.
10. Olson, D. B., and Calcote, H. F., ibid, p. 453.
11. Calcote, H. F., Eight Symposium (International) on Combustion, Combustion Institute, Pittsburgh, 1967, p. 311.
12. Vinckier, C., J. Phys. Chem., Vol. 83, p. 1234, 1979.
13. Messing, I., Carrington, T., Filseth, S. V., and Sudoski, C. M., "Absolute Rate Constants for the Reaction of CH with N and O." Sixth International Symposium on Gas Kinetics, Southampton, England, July 1980.
14. a. Olson, D. B. and Calcote, H. F., in Particulate Carbon: Formation During Combustion, Siegla, D. C. and Smith, G. W., Eds., Plenum, N.Y., 1981, p. 177.
b. Calcote, H. F., "Mechanisms of Soot Nucleation in Flames - a Critical Review", Combustion and Flame, Vol. 42, p. 215, 1981.
15. Prado, G. P., and Howard, J. B., Evaporation-Combustion of Fuels, Advances in Chemistry Series #166, Ed. Zung, J. T. (American Chemical Society, Washington, 1978), Ch. 10.
16. Bulewicz, E. M., Evans, D. G., and Padley, P. J., 15th Symposium (International) on Combustion, (The Combustion Institute, Pittsburgh,

- 1975), p. 1461.
17. Heinsohn, R. J. and Becker, P. M., "Effects of Electric Fields in Flames", in Combustion Technol. Some Mod. Dev., Palmer , H. B. and Beer, J. M., eds., (Academic Press, N.Y., 1974).
 18. Vinckier, C., Gardner, M. P., and Bayes, K. D., 16th Symposium (International) on Combustion, (The Combustion Institute, Pittsburgh, 1977), p. 881.
 19. Wagner, H. G., 17th Symposium (International) on Combustion, (The Combustion Institute, Pittsburgh, PA, 1979), p. 3.
 20. Delfau, J. L., Michaud, P., and Barassin, A., Combustion Sci., and Tech., Vol. 20, p. 165, 1979.
 21. Frenklach, M., Clary, D. W., Gardiner, Jr., W. C., and Stein, S. E., in "Twentieth Symposium (International) on Combustion", The Combustion Institute, Pittsburgh, 1985.
 22. Olson, D. B., Keil, D. G., Calcote, H. F., "The Mechanism of Soot Formation", Aerochem Report #TP-445, Aerochem Research Laboratories, Inc. Princeton, NJ 08542.
 23. Murtagh, B. A. and Sargent, R. W. H., Comp. Jour., Vol. 13, p. 185, 1970.
 24. McIver, I. W. and Komornicki, A., J. Amer. Chem. Soc., Vol. 94, p. 2625, 1972.
 25. Broyden, C. G., J. Inst. Maths. Appl., Vol. 6, p. 76, 1970.
 26. Fletcher, R., Comp. Jour., Vol. 13, p. 317, 1970.
 27. Goldfarb, D., Math. Comp., Vol. 24, p. 23, 1970.
 28. Shanno, D. F., Math. Comp., Vol. 24, p. 647, 1970.
 29. Fletcher, R., in: Practical Methods of Optimization, Vol. 1 (Wiley, New York, 1980).
 30. Head, J. D. and Zerner, M. C., Chem. Phys. Lett., Vol. 131, p. 359, 1986.
 31. Fogarsi, G. and Pulay, P., Ann. Rev. Phys. Chem., Vol. 35, p. 191, 1984.
 32. Geometrical Derivatives of Energy Surfaces and Molecular Properties, Eds. Jorgensen, P. and Simons, J., Reidel, D., Holland, 1986.
 33. a. Pulay, P., in Modern Theoretical Chemistry, Vol. 4, ed. Schaeffer, III, H. F., (Plenum Press, New York, 1977).
b. Pulay, P., Adv. Chem. Phys., 1986.
c. Schlegel, H. B., in Chem. Phys., Vol. 67, p. 249, 1987.

34. Head, J. D. and Zerner, M. C., *Adv. Quantum Chem.*, Vol. 20, p. 1, 1988.
35. Head, J. D. and Zerner, M. C., *Chem. Phys. Lett.*, Vol. 122, p. 264, 1985.
36. Simons, J., Jorgensen, P., Taylor, H., and Ozment, J., *J. Phys. Chem.*, Vol. 87, p. 2745, 1983, O'Neal, D., Taylor, H., and Simons, J., *J. Phys. Chem.*, Vol. 88, p. 1510, 1984.
37. Cerjan, C. J. and Miller, W. H., *J. Chem. Phys.*, Vol. 75, p. 2800, 1981.
38. Taylor, H. and Simons, J., *J. Phys. Chem.*, Vol. 89, p. 6841, 1985.
39. Nguyen, D. T. and Case, D. A., *J. Phys. Chem.*, Vol. 89, p. 4020, 1985.
40. Baker, J., *J. Comput. Chem.*, Vol. 7, p. 385, 1986.
41. Karelson, M. M., Katritzky, A. R., and Zerner, M. C., *Int. J. Quan. Chem. Symp.*, Vol. 20, p. 521, 1986.
42. See, for example, Ozturk, F., Baykut, G., Moini, M., and Eyler, J. R., *J. Phys. Chem.*, Vol. 91, p. 4360, 1987.
43. Smyth, K. C., Lias, S. G., and Ausloos, P., *Combust. Sci. Technol.*, Vol. 28, p. 147, 1982.
44. Lossing, F. P., *Can. J. Chem.*, Vol. 50, p. 3973, 1972.
45. Radom, L., Hariharan, P. C., Pople, J. A., and Schleyer, P. V. R., *J. Amer. Chem. Soc.*, Vol. 98, p. 10, 1976.
46. Bacon, A. D. and Zerner, M. C., *Theoret. Chim. Acta*, Vol. 53, p. 21, 1979.
47. See, for example, Hehre, W. J., Radom, L., Schleyer, P. V. R., and Pople, J. A., Ab-Initio Molecular Orbital Theory, John Wiley and Sons, New York, 1986.
48. Head, J. D. and Zerner, M. C., in *Geometric Derivatives of Energy Surfaces and Molecular Properties*, NATO ASI Series C, Reidel, Dordrecht, 1985.
49. Pople, J. A., Krishnan, R., Schlegel, H. B., and Binkley, J. S., *Intern. J. Quantum. Chem.*, Vol. 13, p. 225, 1979.
50. Pople, J. A., Krishnan, R., Schlegel, H. B., Binkley, J. S., *Intern. J. Quantum Chem.*, Vol. 14, p. 545, 1978.
51. Ridley, J. E. and Zerner, M. C., *Theoret. Chim. Acta (Berl)* Vol. 32, p. 111, 1973.
52. Zerner, M. C., Loew, G. H., Kirchner, R. F., Muller-Westerhoff, U. T., *J. Amer. Chem. Soc.* Vol. 102, p. 589, 1980.
53. Holmes, J. L. and Lossing, F. P., *Can. J. Chem.*, Vol. 57, p. 249, 1979.

54. Takada, T. and Ohno, K., Bull. Chem. Soc. Jpn., Vol. 52, p. 334, 1979.
55. Eyler, J. R., Oddershede, J., Sabin, J. R., Diercksen, G. H. F., and Gruner, N., J. Phys. Chem., Vol. 88, p. 3121, 1984.
56. Oddershede, J., Adv. Quantum Chem., Vol. 11, p. 275, 1978.
57. See, for example, McQuarrie, D., Statistical Mechanics, Harper and Row, New York, 1976.
58. Dupuis, M., Spangler, D., Wendoloski, J. J., NRCC Program QC01 (1980); Dupuis, M., Rys., J. and King, H. F., HONDOS QCPE, Vol. 13, p. 401, 403, 1981; Guest, M. F. and Kendrick, J., Computational Science Groups, Daresbury, Laboratories. This version of GA,,ES was obtained from Michael Schmidt, North Dakota State University.
59. Stohrer, W. D. and Hoffmann, R., J. Am. Chem. Soc., Vol. 94, p. 1661, 1972.
60. Hehre, W. J. and Schleyer, P. V. R., J. Am. Chem. Soc. Vol. 95, p. 5837, 1973.
61. Kollmann, H., Smith, H. O., and Schleyer, P. V. R., J. Am. Chem. Soc., Vol. 95, p. 5834, 1973.
62. Dewar, M. J. S. and Haddon, R. G., J. Am. Chem. Soc., Vol. 95, p. 5836, 1973.
63. Köhler, H.-J. and Lischka, H., J. Am. Chem. Soc., p. 7863, 1979.
64. Masamune, S., Sakai, M. and Ona, H., J. Am. Chem. Soc., Vol. 94, p. 8955, 1972; Masamune, S., Sakai, M., Ona, H., and Jones, A. J., J. Am. Chem. Soc., Vol. 94, p. 8956, 1972.
65. Hart, H. and Kuzuya, M., J. Am. Chem. Soc., Vol. 94, p. 8958, 1972.
66. Gross, M. L. and Rempel, D. L., Science, Vol. 226, p. 261, 1984.
67. Baykut, G. and Eyler, J. R., Trends in Anal. Chem., Vol. 5, p. 44, 1986.
68. Laude, Jr., D. A., Johlman, C. L., Brown, R. S., Weil, D. A., and Wilkins, C. L., Mass Spectrom. Rev., Vol. 5, p. 107, 1986.
69. Comisarow, M. B., Grassi, V., and Parisod, G., Chem. Phys. Let., Vol. 57, p. 413, 1978.
70. Le Breton, P. R., Williamson, A. D., Beauchamp, J. L. and Huntress, W. T., J. Chem. Phys., Vol. 62, p. 1623, 1975.
71. Warneck, P., Ber. Bunsen Gesellschaft, Vol. 76, p. 421, 1972.
72. Sieck, W. and Ausloos P. J., Res. Natl. Bur. Stand. A, Vol. 76, p. 253, 1972.
73. Gross, M. L. and Norbeck, J., J. Chem. Phys., Vol. 54, p. 3651, 1971.

74. Herod, A. A. and Harrison, A. G., Int. J. Mass Spectrom. Ion Phys., Vol. 4, p. 415, 1970.
75. March, J., Advanced Organic Chemistry, Reactions, Mechanisms and Structure, 1977, 2nd Ed. New York: Plenum, 177.
76. Baykut, G., Brill, F. W. and Eyler, J. R., Combust. Sci. and Tech., Vol. 45, p. 233, 1986.
77. Snow, A. W., J. Macrom. Sci., Vol. A22, p. 1429, 1985.
78. Organic Syntheses, Coll. Vol. IV, p. 238, 1963.
79. Jackson, J-A. A., Lias, S. G. and Ausloos, P., J. Am. Chem. Soc., Vol. 99, pp. 7515-21, 1977.
80. Ausloos, P., J. Am. Chem. Soc., Vol. 104, pp. 5259-65, 1982.
81. Holmes, J. L. and Lossing, F. P., Can. J. Chem., Vol. 57, p. 249, 1979.
82. Ausloos, P. J. and Lias, S. G., J. Am. Chem. Soc., Vol. 103, p. 6505, 1981.
83. Anicich, V. G., Huntress, Jr., W. T. and McEvan, M. J., J. Phys. Chem., Vol. 90, p. 2446, 1986.
84. Jarrold, M. F., Wagner-Redeker, W., Illies, A. J., Kirchner, N. J., and Bowers, M. T., Int. J. Mass Spectrom. Ion Phys., Vol. 58, p. 63, 1984.
85. Dannacher, J., Heilbronner, E., Stadelmann, J.-P. and Vogt, J. Helvetica Chimica Acta, Vol. 62, p. 2186, 1979.
86. Baer, T., Willett, G. D., Smith, D. and Phillips, J. S., J. Chem. Physics, Vol. 62, p. 2186, 1979.
87. Buckley, T. J., Ph.D. Dissertation, Univ. of Florida, 1982.
88. Brill, F. W., Ph.D. Dissertation, Univ. of Florida, 1983.
89. Dorman, F. H., J. Chem. Phys., Vol. 43, p. 3507, 1965.
90. Occolowitz, J. L. and White, G. L., Aust. J. Chem., Vol. 21, p. 997, 1968.
91. Harrison, A. G., Haynes, P., McLean, S. and Meyer, F., J. Am. Chem. Soc., Vol. 87, p. 5099, 1965.
92. Franklin, J. L. and Carroll, S. R., J. Am. Chem. Soc., Vol. 91, p. 6564, 1969.
93. Tajima, S. and Tsuchiya, T., Bull. Chem. Soc. Japan, Vol. 46, p. 3291, 1973.
94. Lossing, F. P. and Traeger, J. C., J. Am. Chem. Soc., Vol. 97, p. 1579, 1975.
95. McCreary, D. A. and Freiser, B. S., J. Am. Chem. Soc., Vol. 100, p.

2902, 1978.

96. Eyler, J. R. Reactivities and structures of some hydrocarbon ions and their relationship to soot formation. In "The Chemistry of Combustion Processes", T. M. Sloane (Ed.). American Chemical Society Series, Washington, D.C., p. 49, 1984.
97. Borden, M. J. and Haddon, R. C., J. Am. Chem. Soc., Vol. 101, p. 3771, 1979.
98. Gross, M. L., Russell, D. H., Aerni, R. J. and Bronczyk, S. A., J. Am. Chem. Soc. Vol. 99, p. 3603, 1977.
99. Ausloos, P., Jackson, J.-A. A. and Lias, S. G., Int. J. Mass Spectrom. Ion Phys., Vol. 33, p. 269, 1980.
100. Sharma, D. K. S. and Kebarle, P., Can. J. Chem., Vol. 59, pp. 1592-601, 1981.
101. Winkler, J. and McLafferty, F. W., J. Am. Chem. Soc., Vol 95, p. 7533, 1973.
102. Davidson, R. A. and Skell, P. S., J. Am. Chem. Soc., Vol. 95, p. 6843, 1973.
103. Smith, D. and Adams, N. G., Int. J. Mass Spectrom. Ion Phys., Vol. 76, p. 307, 1987.
104. Knight, J. S., Freeman, C. G., McEwan, M. J., Anicich, V. G. and Huntress, Jr., W. T., J. Phys. Chem., Vol. 91, p. 3898, 1987.
105. Brill, F. W. and Eyler, J. R., J. Phys. Chem., Vol. 85, p. 1091, 1981.
106. Abbaund, J. L. M., Hehre, W. J., and Taft, R. W., J. Am. Chem. Soc., Vol. 98, p. 6072-3, 1976.
107. Cone,C., Dewar, M. J. S. and Landman, D., J. Am. Chem. Soc., Vol. 99, pp. 372-6, 1977.
108. Thrush, B.A. and Zwolenik, J.J., Discuss. Faraday Soc., Vol. 35, p. 196, 1963.
109. Elder, F.A. and Parr, A.C., J. Chem. Phys., Vol. 50, p. 1057, 1969.
110. Lossing, F.P., Can. J. Chem., Vol. 49, p. 357, 1971.
111. Cooks, R. G., Beynon, J. H., Bertrand, M. and Hoffman, M. K., Org. Mass Spectrom., Vol. 7, pp. 1303-12, 1973.
112. McLafferty, F. W. and Winkler, J., J. Am. Chem. Soc., Vol. 96, pp. 5182-9, 1974.
113. Grotzmeyer, J. and Grueitzmacher, H. F., Curr. Top. Mass Spectrom. Chem. Kinet., Proc. Symp., 1981, Beynon, J. H., McGlashan, M. L., Eds.;

- Heyden:London, UK, 1982, pp. 29-59.
114. McLafferty, F. W. and Bockhoff, F. M., J. Am. Chem. Soc., Vol. 101, pp. 1783-6, 1979.
 115. Koeppel, C., Dymerski, P. P., Bockhoff, F. M., and McLafferty, F. W., Adv. Mass Spectrom., Vol. 7A, pp. 295-6, 1978.
 116. Takamuku, S., Sagi, N., Nagaoka, K. and Sakurai, H., J. Am. Chem. Soc., Vol. 94, pp. 6217-18, 1972.
 117. Takamuku, S., Nakamura, K., Nagaoka, K. and Sakurai, H., Chem. Lett., Vol. 12, pp. 1303-6, 1973.
 118. Sagi, N., Yamamoto, Y., Nagaoka, K., Takamuku, S. and Sakurai, H., Bull. Chem. Soc. Jap., Vol. 47, pp. 1387-92, 1974.
 119. Yamamoto, Y., Takamuku, S. and Sakurai, H., J. Am. Chem. Soc., Vol. 91, pp. 7192-4, 1969.
 120. Yaroslavtsev, V. T., Abakumov, G. A., and Simonov, A. P., Kuantovaya Electron., Vol. 11, pp. 752-6, 1984.
 121. Dunbar, R. C., J. Am. Chem. Soc., Vol. 97, pp. 1382-4, 1975.
 122. Traeger, J. C. and McLoughlin, R. G., J. Am. Chem. Soc., Vol. 99, pp. 7351-2, 1977.
 123. Traeger, J. C. and McLoughlin, R. G., Int. J. Mass Spectrom. Ion Phys., Vol. 27, pp. 319-33, 1978.
 124. McLoughlin, R. G., Morrison, J. D., and Traeger, J. C., Org. Mass Spectrom., Vol. 14, pp. 104-8, 1979.
 125. Bombach, R., Dannacher, J., and Stadelmann, JP., J. Am. Chem. Soc., Vol. 105, pp. 4205-11, 1983.
 126. Bombach, R., Dannacher, J., and Stadelmann, JP., Chem. Phys. Lett., Vol. 95, pp. 259-61, 1983.
 127. Jackson, J-A. A., Diss. Abstr. Int. B, Vol. 38, p. 2691, 1977.
 128. Shen, J., Dunbar, R. C., and Olah, G. A., J. Am. Chem. Soc., Vol. 96, pp. 6227-9, 1974.
 129. Andrews, L. and Keelan, B. W., J. Am. Chem. Soc., Vol. 103, pp. 99-103, 1981.
 130. Dunbar, R. C. and Fu, E. W., J. Am. Chem. Soc., Vol. 95, p. 2716, 1973.
 131. Dewar, M. J. S. and Landman, D., J. Am. Chem. Soc., Vol. 99, pp. 2446-53, 1977.
 132. Levsen, K., McLafferty, F. W., and Serina, D. M., J. Am. Chem. Soc., Vol. 95, p. 6332, 1973.

133. Gajewski, J. J. and Gortva, A. M., J. Am. Chem. Soc., Vol. 104, p. 334, 1982.
134. Bartmess, J. E., J. Am. Chem. Soc., Vol. 104, p. 335, 1982.
135. Bursey, J. T., Bursey, M. M., and Kingston, D. G. I., Chem. Rev., Vol. 73, p. 191, 1973.
136. Dunbar, R.C. and Klein, R., J. Am. Chem. Soc., Vol. 99, p. 374, 1977.
137. Bursey, M.M., Hoffman, M.K. and Benezra, S.A., J. Chem. Soc. D, 1971, p. 1417.
138. Annino, R. and Driver, R., "Scientific and Engineering Applications with Personal Computers", John Wiley and Sons, Inc., New York, 1986.
139. Rosenstock, H. M., Wallenstein, M. B., Wahrhaftig, A. L., and Eyring, H., Proc. Natl. Acad. Sci. U.S.A., Vol. 38, p. 667, 1952.
140. Forst, W., "Theory of Unimolecular Reactions", Academic Press, New York.
141. Streitweiser, Jr., A., Jagov, R. H., Fahey, R. C., and Suzuki, S., J. Am. Chem. Soc., Vol. 80, p. 2326, 1958.
142. Dreuth, W. and Kwart, H., "Kinetics Applied to Organic Reactions", Marcel Dekker, Inc., 1980.
143. Melander, L., "Isotope Effects on Reaction Rates", Ronald Press, New York, 1960.
144. Melander, L. and Saunders, Jr., W. H., "Reaction Rates of Isotopic Molecules", John Wiley and Sons, New York, 1980.
145. Tumas, W., Foster, R. F., Pellerite, M. J., and Brauman, J. I., J. Am. Chem. Soc., Vol. 109, p. 961, 1987.
146. Mead, P. T., Douchi, K. F., Traeger, J. C., Christie, J. R., and Derrick, P. J., J. Am. Chem. Soc., Vol. 102, p. 3364, 1980.
147. Derrick, P. J., Mass Spec. Rev., Vol. 2, p. 285, 1983.

APPENDIX A

- ¹ If internal coordinates y are used, this choice of G¹ = l for cartesian coordinates x corresponds to Gy² = (B⁻¹)⁺B⁻¹ where y = Bx and B⁻¹ = (B⁺mb)⁻¹B⁺m where m is an arbitrary (3N - 6) x (3N - 6) matrix; see, for example, E. B. Wilson, J. C. Decius and P. C. Cross, in: Molecular Vibrations (McGraw-Hill, New York, 1955).
- ² Quantum Chemistry Interactive Program Utility (QUIPU), Quantum Theory Project, Departments of Chemistry and Physics, 362 Williamson Hall, University of Florida, Gainesville, FL 32611.
- ³ J. S. Binkley, M. J. Frisch, D. J. Defrees, K. Raghavachari, H. B. Whiteside, H. B. Schlegel, E. M. Fulder and J. A. Pople, Carnegie Mellon Univ. Pg, PA 15213.
- ⁴ F. Wiseman, F. Ozturk, J. R. Eyler and M. C. Zerner, see Section IV.
- ⁵ F. Ozturk, M. Moini, F. Brill, J. R. Eyler, T. J. Buckley, S. G. Lias and P. J. Ausloos, submitted.
- ⁶ A. Cameron, J. Leszczynski, M. C. Zerner and B. Weiner, submitted.
- ⁷ F. L. Wiseman, F. Ozturk, M. C. Zerner and B. Weiner, submitted.
- ⁸ J. Feng, J. Leszczynski and M. C. Zerner, submitted.
- ⁹ J. Leszczynski, M. C. Zerner and F. Wiseman, submitted.
- ¹⁰ The uncertainty given is the 95 percent confidence limit of the mean of 5 determinations. Reported uncertainties for the correction factor and rate coefficients throughout this Section are also 95 percent confidence limits.
- ¹¹ The large uncertainties reported for the correction factor and rate coefficients calculated using it in this work are primarily due to the wide

range of reported values for the $C_2H_4^+ + C_2H_4$ reaction used to determine the correction factor. The even more widely studied "standard" calibration reaction of CH_4^+ with CH_4 could not be employed because the lowest mass-to-charge ratio accessible to the FTMS-1000 instrument is m/z 18.

¹² Bartmess, J. E. private communication.

¹³ Tektronix Model 4054 and Hewlett Packard Model 150.

¹⁴ Lampe and Field (F. W. Lampe, and F. H. Field, Tetrahedron, 7, 189 (1959)) studied the reaction of $CD_4^+ + C_2H_4$, and observed the following yields: $C_3HD_4^+$: 1/10, $C_3H_3D_2^+$: 3/5, $C_3H_2D_3^+$: 2/5, and $C_3HD_4^+$: 1/10 (+L₁ + L₂). Statistical yields with no isotope effect would have been: $C_3H_4D^+$: 1/14, $C_3H_5D_2^+$: 3/7, $C_3H_2D_3^+$: 3/7, and $C_3HD_4^+$: 1/14, very close to the observed values. Hence, since the $C_3L_8^+$ complex exhibited almost complete scrambling, it is reasonable to expect the $C_5L_5^+$ complex modeled here to undergo complete, or nearly complete, scrambling.

¹⁵ Although somewhat crude, applying a multiplicative factor to the rate constant for each deuterated site is in keeping with experimental evidence. For instance, in the acetolysis of some identical tosylates, each deuterium atom substitution changed the rate constant by ca. 0.84 (Reference 141).

APPENDIX B

ANALYTICAL EXPRESSIONS FOR KINETIC MODELING IN SECTION IV.

1. Scheme (123) in Section IV.

$$\begin{aligned}
 I_{C_3H_3^+} &= I_{C_3H_3}^0 + I_{\ell-C_3H_3}^0 [1 + \beta\phi/(10\theta_1)] [\exp(\theta_1 t) - 1] \\
 I_{C_3H_2D^+} &= 3I_{\ell-C_3H_3}^0 [\exp(\theta_2 t) - \exp(\theta_1 t)] - \frac{3}{10} \beta\phi I_{\ell-C_3H_3}^0 \{[\exp(\theta_1 t) \\
 &\quad - 1]/\theta_1 - 3[\exp(\theta_2 t) - 1]/\theta_2\} \\
 I_{C_3HD_2^+} &= 3I_{\ell-C_3H_3}^0 [\exp(\theta_1 t) - 2\exp(\theta_2 t) + \exp(\theta_3 t)] + \\
 &\quad \frac{3}{10} \beta\phi I_{\ell-C_3H_3}^0 \{[\exp(\theta_1 t) - 1]/\theta_1 - 6[\exp(\theta_2 t) - 1]/\theta_2 \\
 &\quad + 6[\exp(\theta_3 t) - 1]/\theta_3\} \\
 I_{C_3D_3^+} &= I_{\ell-C_3H_3}^0 [3 \exp(\theta_2 t) + \exp(\theta_4 t) - \exp(\theta_1 t) - 3 \exp(\theta_3 t)] \\
 &\quad - \beta\phi I_{\ell-C_3H_3}^0 \{[\exp(\theta_1 t) - 1]/(10\theta_1) - 9[\exp(\theta_2 t) - \\
 &\quad 1]/(10\theta_2) + 9[\exp(\theta_2 t) - 1]/(5\theta_3) - [\exp(\theta_4 t) - 1]/\theta_4\},
 \end{aligned}$$

in which $\beta = k_c/k_\ell$, $\phi = k_\ell k_f P_{C_2D_2}/(k_\ell + k_c)$, $\theta_1 = k_\ell \phi/10 - k_f P_{C_2D_2} - k_p P_{C_3H_3} I$, $\theta_2 = 3k_\ell \phi/10 - k_f P_{C_2D_2} - k_p P_{C_3H_3} I$, $\theta_3 = 3k_\ell \phi/5 - k_f P_{C_2D_2} - k_p P_{C_3H_3} I$, and $\theta_4 = k_\ell \phi - k_f P_{C_2D_2} - k_p P_{C_3H_3} I$. The fitting parameters for this model are $I_{\ell-C_3H_3}^0$, β , $k_f P_{C_2D_2}$, and $k_p P_{C_3H_3} I$. $I_{C_3H_3}^0$ is fixed at its experimental value if the initial point is at $t = 0$; otherwise it is also a fitting parameter.

2. Differential Rate Equations for Scheme (124) in Section IV.

$$\frac{dI}{\ell-C_3H_3^+}/dt = \theta I \ell-C_3H_3^+$$

$$\frac{dI}{c-C_3H_3^+}/dt = \beta I \ell-C_3H_3^+/(10F^2)$$

$$\frac{dI}{\ell-HDC_3H^+}/dt = - (F^2 k_f + k_p) I \ell-HDC_3H^+ + \phi_2 (I \ell-HDC_3H^+ +$$

$$FI \ell-H_2C_3D^+)/(5F^2) + 2\phi_1 I \ell-C_3H_3^+/(5F)$$

$$\frac{dI}{\ell-H_2C_3D^+}/dt = -F(F^2 k_f + k_p) I \ell-H_2C_3D^+ + \phi_2 (I \ell-HDC_3H^+ +$$

$$FI \ell-H_2C_3D^+)/(10F^3) + \phi_1 I \ell-C_3H_3^+/(5F^2)$$

$$\frac{dI}{c-C_3H_2D^+}/dt = 3\beta [\phi_2 (I \ell-HDC_3H^+ + FI \ell-H_2C_3D^+)/(2F) +$$

$$\phi_1 I \ell-C_3H_3^+]/(5F)$$

$$\frac{dI}{\ell-HDC_3D^+}/dt = -F(F^2 k_f + k_p) I \ell-HDC_3D^+ + 2\phi_3 (FI \ell-HDC_3D^+ +$$

$$I \ell-D_2C_3H^+)/(5F^3) + 2\phi_2 (I \ell-HDC_3H^+ +$$

$$FI \ell-H_2C_3D^+)/(5F^2) + \phi_1 I \ell-C_3H_3^+/(5F)$$

$$\frac{dI_{\ell-D_2C_3H^+}}{dt} = -(F^2 k_f' + k_p') I_{\ell-D_2C_3H^+} + \phi_3(FI_{\ell-HDC_3D^+}) +$$

$$I_{\ell-D_2C_3H^+})/(5F^2) + \phi_2(I_{\ell-HDC_3H^+}) +$$

$$FI_{\ell-H_2C_3D^+})/(5F) + \phi_1 I_{\ell-C_3H_3^+}/10$$

$$\frac{dI_{c-C_3HD_2^+}}{dt} = 3\beta [\phi_3(FI_{\ell-HDC_3D^+}) + I_{\ell-D_2C_3H^+})/F^2 + \phi_2(I_{\ell-HDC_3H^+})$$

$$+ FI_{\ell-H_2C_3D^+})/F + \phi_1 I_{\ell-C_3H_3^+}/2]/5$$

$$\frac{dI_{\ell-C_3D_2^+}}{dt} = [\phi_4/F^2 - F(F^2 k_f' + k_p')] I_{\ell-C_3D_2^+} + 2\phi_3(FI_{\ell-HDC_3D^+}) +$$

$$+ I_{\ell-D_2C_3H^+})/(5F^2) + \phi_2(I_{\ell-HDC_3H^+}) + FI_{\ell-H_2C_3D^+})/(10F)$$

$$\frac{dI_{c-C_3D_3^+}}{dt} = \beta[\phi_4 I_{\ell-C_3D_3^+}/F^2 + 2\phi_3(FI_{\ell-HDC_3D^+}) +$$

$$I_{\ell-D_2C_3H^+})/(5F) + \phi_2(I_{\ell-HDC_3H^+}) + FI_{\ell-H_2C_3D^+})/10,$$

in which $\theta = \phi_1/(10F^2) - F^2 k_f' - k_p'$, $k_f' = k_f P_{C_2D_2}$, $k_p' = k_p P_{C_3H_3} I$, $\phi_1 = F^2 k_f' / (\lambda_1 + \beta \lambda_2)$,

$\phi_2 = F^2 k_f' / (\lambda_3 + \beta \lambda_1)$, $\phi_3 = F^2 k_f' / (\lambda_4 + \beta \lambda_5)$, $\phi_4 = F^6 k_f' / (1 + F\beta)$, and the λ 's are given as:

$$\lambda_1 = (1 + 6/F + 3/F^2)/10$$

$$\lambda_2 = (3 + 6/F + 1/F^2)/10$$

$$\begin{aligned}\lambda_3 &= \lambda_2/F \\ \lambda_4 &= (3 + 2/F)/5F^2 \\ \lambda_5 &= (2 + 3/F)/(5F).\end{aligned}$$

The fitting parameters for this model are $I_{\text{C}_3\text{H}_3}^0$, β , k_f , k_p , and F .

$I_{\text{C}_3\text{H}_3}^0$ is fixed if the initial point is at $t = 0$; otherwise it is also a fitting parameter.

3. Analytical Expressions for Scheme (125) in Section IV.

$$I_{\text{C}_3\text{H}_3}^+ = I_{\text{C}_3\text{H}_3}^0 + I_{\text{C}_3\text{H}_3}^0 [1 + k_{-31}\phi_1/\theta_1] [\exp(\theta_1 t) - 1]$$

$$I_{\text{C}_5\text{H}_3}^+ = k_{-11}\phi_1 I_{\text{C}_3\text{H}_3}^0 [\exp(\theta_1 t) - \exp(\theta_2 t)]/\theta_{12}$$

$$I_{\text{C}_7\text{H}_3}^+ = k_{-11}k_{-21}\phi_1\phi_2 I_{\text{C}_3\text{H}_3}^0 [\exp(\theta_1 t)/\theta_{13} - \exp(\theta_2 t)/\theta_{23} +$$

$$(1/\theta_{23} - 1/\theta_{13})\exp(\theta_3 t)]/\theta_{12}$$

$$I_{\text{C}_9\text{H}_5}^+(s) = k_{-11}k_{-21}\phi_1\phi_2 I_{\text{C}_3\text{H}_3}^0 \{ [\exp(\theta_1 t) - 1]/\theta_1 - [\exp(\theta_2 t) -$$

$$1]/\theta_2 \}/\theta_{12}$$

$$I_{\text{C}_{11}\text{H}_5}^+(s) = k_{-11}k_{-21}k_{-21}\phi_1\phi_2\phi_3 I_{\text{C}_3\text{H}_3}^0 \{ [\exp(\theta_1 t) - 1]/(\theta_1\theta_{13}) -$$

$$[\exp(\theta_2 t) - 1]/(\theta_2\theta_{23}) - (1/\theta_{23} - 1/\theta_{13})[\exp(\theta_3 t) -$$

$1]/\theta_3\}/\theta_{12}$,

$$I_{C_8H_6^+} = k_{-11} k'_{p2} \theta_1 I^0_{l-C_3H_3} + [\exp(\theta_1 t)/\theta'_1 - \exp(\theta_2 t)/\theta'_2 + (1/\theta'_2$$

$$-1/\theta'_1) \exp(-k_2 t)]/\theta_{12},$$

in which $\phi_1 = k_{f1} P_{C_4H_2}/(k_{-11} + k_{-12} + k_{-13})$, $\phi_2 = k_{f2} P_{C_4H_2}/(k_{-21} + k_{-22} + k_{s1})$, $\theta_3 = k_{f3} P_{C_4H_2}/(k_{-31} + k_{-32} + k_{s2})$; $-\theta_1$, $-\theta_2$, and $-\theta_3$ are parameters (1), (2), and (3), in that order, in Equations (125), $\theta_{12} = \theta_1 - \theta_2$, $\theta_{13} = \theta_1 - \theta_3$, $\theta_{23} = \theta_2 - \theta_3$, $\theta'_1 = \theta_1 + k_d$, and $\theta'_2 = \theta_2 + k_d$. The fitting parameters are θ_1 , θ_2 , θ_3 , $I^0_{l-C_3H_3} + (1 + k_{-31}\phi_1/\theta_1)$, $k_{-11}\phi_1 I^0_{l-C_3H_3} + / \theta_{12}$, $k_{-21}\phi_2$, $k_{s1}\phi_2$, $k_{s2}\phi_3$, and k_d .

It can be seen that $k'_{p2} = -\theta_1 - k_{-21}\phi_2 - k_{s1}\phi_2$, in which $k'_{p2} = k_{p2} P_{C_3H_3} I^0$.